Department of Oncology-Pathology,
Karolinska Institutet, Stockholm, Sweden

MODELLING AND CALCULATION OF DNA DAMAGE AND REPAIR IN MAMMALIAN CELLS INDUCED BY IONIZING RADIATION OF DIFFERENT QUALITY

Reza Taleei

Stockholm 2013

Published by Karolinska Institutet. Printed by Universitets service US-AB

ISBN 978-91-7549-189-9

To my family

Doctoral thesis submitted to the department of Oncology-Pathology, Karolinska Institutet

Modelling and calculation of DNA damage and repair in mammalian cells induced by ionizing radiation of different quality (June, 2013)

Reza Taleei	PhD Candidate

Professor Hooshang Nikjoo, Karolinska Institutet	Supervisor
Professor Mats Harms-Ringdahl, Stockholm University	Co-supervisor
Professor Michael Weinfeld, University of Alberta	Co-supervisor

Examination Committee

Professor Penelope Jeggo, University of Sussex	Opponent
Professor Bo Stenerlöw, Uppsala University	Examination committee (Chair)
Professor Anders Brahme, Karolinska Institutet	Examination committee
Professor Andrea Ottolenghi, Pavia University	Examination committee

ABSTRACT

Recent experimental data have revealed a wealth of information that provides an exceptional opportunity to construct a mechanistic model of DNA repair. The cellular response to radiation exposure starts with repair of DNA damage and cell signalling that may lead to mutation, or cell death. The purpose of this work was to construct a mechanistic mathematical model of DNA repair in mammalian cells. The repair model is based on biochemical action of repair proteins to examine the hypotheses regarding two or more components of double strand break (DSB) repair kinetics.

The mechanistic mathematical model of repair proposed in this thesis is part of a bottom-up approach that assumes the cell is a complex system. In this approach radiation induces DNA damage, and the cellular response to radiation perturbation was modelled in terms of activating repair processes. A biochemical kinetic method based on law of mass action was employed to model the repair pathways. The repair model consists of a set of nonlinear differential equations that calculates and explains protein activity on the damage step by step. The model takes into account complexity of the DSB, topology of damage in the cell nucleus, and cell cycle.

The solution of the model in terms of overall kinetics of DSB repair was compared with pulsed-field gel electrophoresis measurements. The repair model was integrated with the track structure model to calculate the damage spectrum and repair kinetics for every individual DSB induced by monoenergetic electrons, and ultrasoft X-rays. For this purpose we proposed a method to sample the protein repair actions for every individual DSB, and finally calculate the total repair time for that specific DSB. The DSB-repair kinetics for the number of DSB induced by 500 tracks of monoenergetic electrons and ultrasoft X-rays were calculated and compared with experimental results for cells irradiated with Al_K, C_K, and Ti_K ultrasoft X-rays.

The results presented here form the first example of mechanistic modelling and calculations for NHEJ, HR and MMEJ repair pathways. The results, for the first time, quantitatively confirm the hypothesis that the complex type double strand breaks play a major role in the slow kinetics of DSB repair. The results also confirm that simple DSB located in the heterocromatin delay the repair process due to a series of processes that are required for the relaxation of the heterochromatin. The repair model established in this work provides a unique opportunity to continue this study of cellular responses to radiation further downstream that may have important implications for human risk estimation and radiotherapy.

LIST OF PUBLICATIONS

I. Taleei R, Nikjoo H (*2013)* Biochemical DSB-Repair Model for Mammalian Cells in G1 and Early Phases of the Cell Cycle, Mutation Research, (In press)

II. Taleei R, Nikjoo H (*2013)* The Nonhomologous End-Joining (NHEJ) Pathway for the Repair of DNA Double-Strand Breaks: I- A Mathematical Model, Radiation Research 179: 530-539

III. Taleei R, Girard P M , Sankaranarayanan K, Nikjoo H (*2013)* The Nonhomologous End-Joining (NHEJ) Mathematical Model for the Repair of Double-Strand Breaks: II- Application to Damage Induced by Ultrasoft X-Rays and Low Energy Electrons, Radiation Research, 179: 540-548

IV. Taleei R, Nikjoo H (*2012)* Repair of the Double-Strand Breaks Induced by Low Energy Electrons: A Modelling Approach. International Journal of Radiation Biology 88 (12) : 948-53

V. Taleei R, Weinfeld M, Nikjoo H. (*2011)* A Kinetic Model of Single-Strand Annealing for the Repair of DNA Double-Strand Breaks. Radiation Protection Dosimetry 143(2-4): 191-195

RELATED PUBLICATIONS

VI. Taleei R, Weinfeld M, Nikjoo H (*2012)* Single strand Annealing Mathematical Model for Double Strand Break Repair. Molecular Engineering & Systems Biology 1:1

VII. Taleei R, Hultqvist M, Gudowska I, Nikjoo H (*2012)* Monte Carlo Evaluation of Carbon and Lithium Ions Dose Distributions in Water. International Journal of Radiation Biology 88(1-2)**:** 189-194

VIII. Sankaranarayanan K, Taleei R, Rahmanian S, Nikjoo H *(2013)* Ionizing Radiation and Genetic Risks - Bridging the Gap Between Radiation Induced DNA Double-Strand Breaks and the Origin of DNA Deletions. Mutation Research Reviews (In press)

CONTENTS

List of Abbreviations

53BP1	P53-binding protein 1
APE	Apurinic/Apyrimidinic endonuclease
AP	Apurinic/Apyrimidinic
ATM	Ataxia telangiectasia mutated
ATR	Ataxia telangiectasia and Rad3-related protein
BER	Base Excision Repair
BL	Base Lesion
BLM	Bloom Syndrome Helicase
bp	base pair
BRCA1	Breast cancer type 1 susceptibility protein
B RCA2	Breast cancer type 2 susceptibility protein
BRCT	BRCA1 C terminal
CDF	Cumulative Distribution Function
CDK	Cyclin-Dependent Kinase
CFGE	Constant-field gel electrophoresis
D	Dose
D-loop	Displacement loop
DNA-PKcs	DNA-dependent protein kinase catalytic subunit
dRP	Deoxyribose Phosphate
DSB	Double Strand Break
DSBR	Double Strand Break Repair
dsDNA	double stranded DNA
EC	Euchromatin
Exo	Exonuclease

FANCM	Fanconi Anemia Complementation Group M
FAR	Fraction of activity released
FEN	Flap Endonuclease
GFP	Green Fluorescent Protein
HC	Heterochromatin
HR	Homologous Recombination
IR	Ionizing Radiation
ITS	Inverse Transform Sampling
KAP	Krüppel-associated protein
LET	Linear Energy Transfer
Lig	Ligase
LQ	Linear-Quadratic
LPL	Lethal Potentially Lethal
MBD	Methyl-CpG binding domain protein
MDC	Mediator of DNA check point
MLQ	Modified Linear Quadratic
MMEJ	Microhomology-Mediated End-Joining
MPG	N-Methylpurine DNA glycosylase
MRN	Mre11-Rad50-Nbs1
NAHR	Non-Allelic Homologous Recombination
NHEJ	Nonhomologous End-Joining
OGG	8-Oxoguanine glycosylase
OxoG	Oxoguanine
PARP	Poly(ADP-Ribose) Polymerase
PCNA	Proliferating Cell Nuclear Antigen

PDB	Protein Data Bank
PDF	Probability Density Function
PFGE	Pulsed-field gel electrophoresis
PNKP	Polynucleotide Kinase/Phosphatase
Pol	Polymerase
RCR	Repairable and potentially Conditionally Repairable damage
RMR	Repair-MisRepair
RIF	Radiation Induced Foci
SDSA	Synthesis-Dependent Strand Annealing
SMUG	Single-strand selective monofunctional uracil DNA glycosylase
SR	Saturable Repair
SSA	Single Strand Annealing
SSB	Single Strand Break
ssDNA	single stranded DNA
TDG	Thymine DNA Glycosylase
TLK	Two Lesion Kinetics
Topo	Topoisomerase
UDG	Uracil-DNA glycosylase
XLF	XRCC4-like factor
XRCC	X-ray repair cross-complementing group

1 INTRODUCTION

Ionizing radiation (IR) is a potential carcinogen, and also widely used for cancer therapy [1]. Exposure to IR induces a variety of biological effects [2]. The main target of IR is the cell nucleus DNA [3]. Activation of the DNA repair and the cell signalling pathways are among the initial steps of the molecular and cellular protective processes as illustrated in Figure 1.1. Inaccurate repair of the damage may lead to mutation and consequently cancer. The cell may avoid the adverse consequences by activating cell death pathways. Mechanism of radiation action and effects is complex and not yet fully understood. However, recent advances in experimental technologies have provided unprecedented opportunity for bottom up mathematical modelling to study the mechanism of radiation action. DNA repair plays the central role in cellular response to radiation insult.

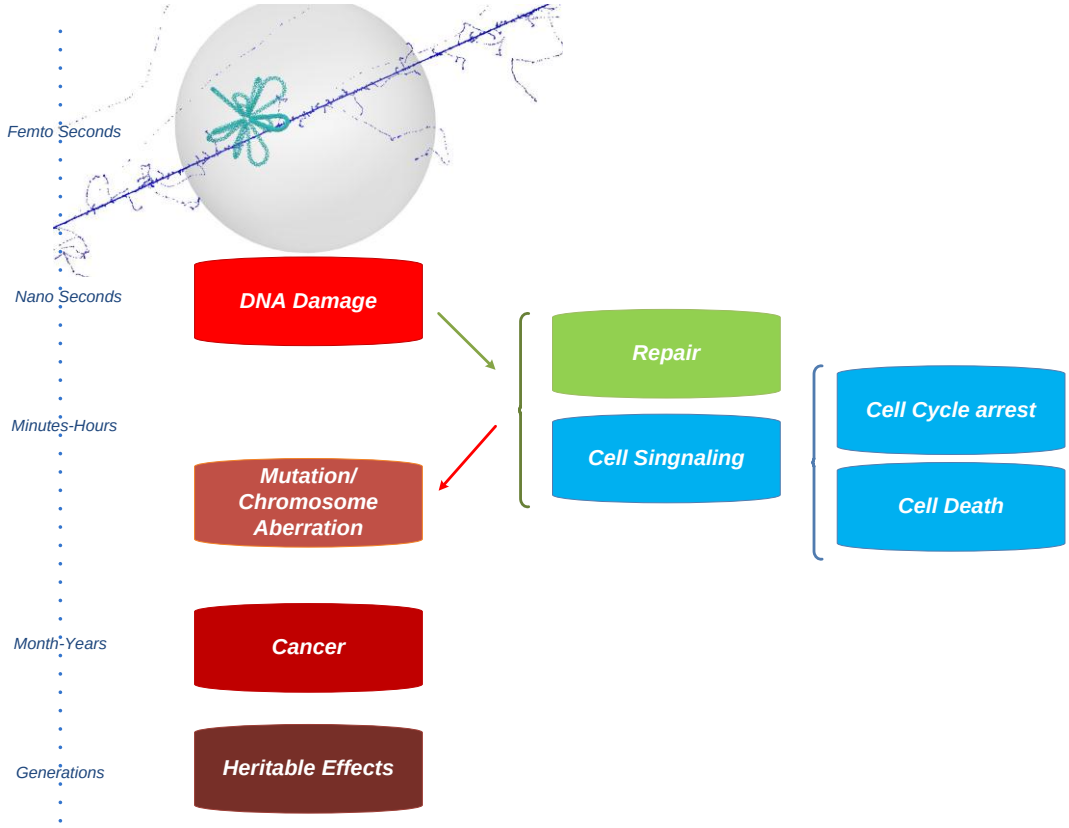

Figure 1.1 Sequential events and effects that follows after ionizing radiation insult in a cell nucleus. The time scale of initial damage induction and biological effects may range from a few nanoseconds to several years. The physical and chemical stages of radiation action are very fast and damage is formed in less than a fraction of second. Damage is induced by direct and indirect interaction of radiation with the DNA molecule. Damage activates repair and signalling pathways within seconds to minutes. If the damage is not correctly repaired it may lead to mutation and chromosome aberration. Signalling pathways may activate cell cycle arrest or cell death pathways to avoid detrimental consequences such as cancer and heritable effects that could develop within years of radiation incident

The damage induced in the DNA is classified as single strand break (SSB), base lesion (BL) and double strand break (DSB). The damage spectrum is influenced by dose, dose rate and type of the radiation exposure. The most cytotoxic type of damage is DSB. Figure 1.2 illustrates specific repair pathways are summoned for repair of BL, SSB, and DSB. There are several DSB-repair pathways that could fix the damage. The choice of DSB repair pathway is dependent upon the cell cycle, type of damage, and damage topography (damage induced in the Heterochromatin (HC) versus Euchromatin (EC)). In this work DSB-repair was studied mechanistically using computational modelling. Basic questions regarding repair kinetics of DSB have been addressed. It is known that DSB repair kinetics have at least two components. It is hypothesised that the repair kinetics is affected by DSB complexity and topography. The complexity of the DSB is defined by the proximity of DSB to other lesions such as DSB or SSB within 10 base pairs (bp) [4]. It has been shown that the complexity of the DSB increases with linear energy transfer (LET), using Monte Carlo track structure simulation [5-8]. LET is a parameter that is generally used to characterise radiations of different quality. However, LET is an average macroscopic quantity and does not account for the stochastic nature of radiation interaction [9, 10]. Topography of the damage relates to the DSB positioned in the HC or EC [11-13]. HC is the condensed region of the chromatin in contrast to EC that is transcriptionally active. It is assumed that both complexity and topography of the DSB affect the repair kinetics through activating slower repair processes [14, 15].

By using a computational approach, both assumptions (complexity and topography of DSB) were tested in this work. For this purpose, details of mechanism of action of the repair proteins were applied in the repair model to identify and explain the components of DSB repair kinetics. The mechanism of protein actions and DSB repair were derived from various sources including molecular, biochemical, biophysical, and structural studies. Figure 1.2 shows a schematic representation of the ideas involved in the aforementioned studies. The protective biological responses to DNA damage include DNA repair and cell signalling. The signalling pathways involve sequential protein translational modifications. The cascades of the signalling protein modifications may lead to cell cycle arrest, and cell death. The first response to DNA damage is sensing the damage by a set of proteins including Ku70/80, the MRN complex, PARP-1, ATR and ATM. Following this, other proteins such as histone H2AX become involved in amplifying the response. Consequently, a large number of signalling and repair proteins are recruited to retain genome integrity. Different types of DNA damage are processed sequentially by certain proteins. In general, DNA repair processes have been classified in terms of base excision repair (BER) [16] for the repair of base damage and SSB; while for the repair of DSB, several pathways including homologous recombination repair (HR) [17, 18], nonhomologous end-joining (NHEJ) [19, 20], single strand annealing (SSA) [17, 21], and microhomology-mediated end-joining (MMEJ) [22, 23] are involved. The choice of the DSB-repair pathway depends on several criteria such as type of damage, position of the damage in the nucleus and cell cycle. In mammalian cells NHEJ repair is the prevalent pathway for repairing DSB, however it is still not definitely known in which circumstances other repair pathways, such as HR or MMEJ, are activated. To this end, there are two main ideas circulating in the field. The first argument is that the position of the DSB in the cell nucleus influences the repair

kinetics [11-14, 24-26]. It is suggested that DSB in the heterochromatin require opening of the compact chromosome structure and therefore could result in a longer repair process [12]. It is also suggested that the damage in the heterochromatin undergo resection that leads to HR repair [14, 25, 26]. The second argument suggests that the complexity of the DSB is the main reason for biphasic repair kinetics [15, 27, 28]. It is proposed that increase of LET, and consequently the complexity of damage, changes the repair kinetics in favour of slowing down of the repair process by involving HR or MMEJ [6, 29]. DNA repair processes are cell cycle dependent. HR and SSA are mainly active in late S and G_2 phases of the cell cycle, while NHEJ is active throughout the whole cell cycle. DSB repair is not always conservative and may lead to various types of mutations or chromosome aberrations. The HR repair pathway is error-free, while NHEJ, MMEJ and SSA show different sizes of deletion or addition related to their biochemical DNA catalysis. Non-allelic homologous recombination (NAHR) is a special variant of HR repair which may lead to large deletions in the case of finding the wrong intact template pair. Recent advances in DNA experimental techniques have revealed a plethora of information regarding repair processes in mammalian cells. Nonrepaired and misrepaired DNA lesions could also lead to cell death. Cell death is one the cellular protective responses that could avoid development of mutations, cancer or heritable diseases. Cell death is classified by morphologic appearance as apoptosis, necrosis, autophagy, and mitotic catastrophe [30]. Cell survival is usually measured by clonogenic assays.

Mathematical models of biological processes have been used to improve our understanding of the mechanism of biological processes and quantification of the qualitative experimental observations. The first models to describe radiation effects were phenomenological models describing the cell survival curves. Typical cell survival curves are presented graphically on a log-linear scale. Cell survival as a measure of absorbed dose has been used to propose phenomenological models with different degrees of complexity. To this end, target theory is used to explain exponential dose response survival curves. Target theory proposes that for inactivating a cell, a number of critical targets in turn should be inactivated. Target theory, which accounts for the behaviour of a population of cells, is based on a simple exponential formula to explain the cell survival curve [31]. Among many models, the Linear-Quadratic (LQ) model is the most common one used to study cell survival response to radiation exposure [32, 33]. The LQ model in its simplest form is based on exponential expression with two unknown parameters of α and β. Although the LQ model surprisingly describes rather accurately the cell survival curves in the classical fractionation region (1.5-4 Gy), it does not consider low dose hypersensitivity and shows overestimation at high doses [34]. Other models such as RMR (Repair-MisRepair) [35, 36], LPL (Lethal Potentially Lethal) [37], SR (saturable repair) [38], MLQ (Modified Linear Quadratic) [39] and RCR (Repairable and potentially Conditionally Repairable damage) [40] have been proposed to overcome the shortcomings of the LQ model. Among the models, the RMR [40], biexponential [41], and Two Lesion Kinetics (TLK) [42] models proposed a simple equation to describe DSB repair kinetics. The phenomenological models have shown successful contribution in improving treatment planning for radiation therapy, however mechanistic details of radiation action is complex and sophisticated mathematical

models are required. The phenomenological models do not consider molecular interactions involved in DSB repair. Furthermore some of the assumptions of phenomenological models such as DSB saturation in the shoulder region of the dose or nonlinearity of DSB induction in low doses have not been observed by biological experiments [43].

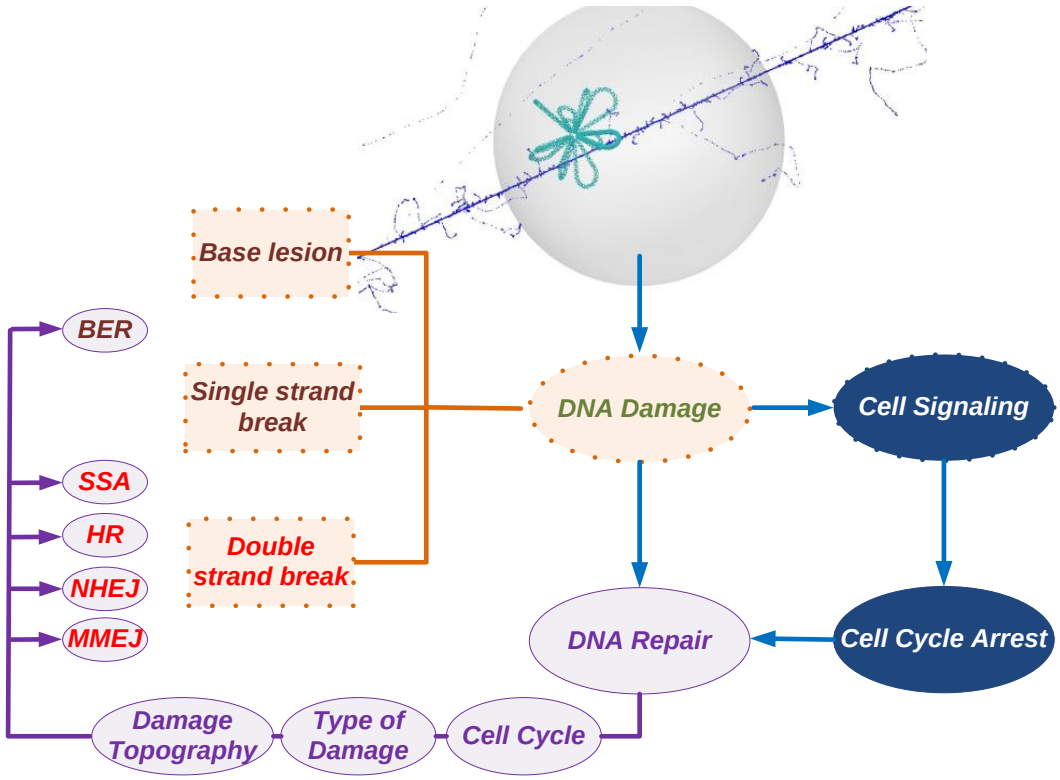

Figure 1.2 DNA repair and initial signalling processes that are activated by radiation exposure to cell. The Damage is in the form of base lesion, single strand break and double strand break. Base lesions and single strand breaks are repaired by the base excision repair (BER) pathway. Double strand breaks are repaired by nonhomologous end-joining (NHEJ), homologous recombination (HR), microhomology-mediated end-joining (MMEJ), and single strand annealing (SSA) repair pathways. The repair of DSB depends on the type of damage, cell cycle, and damage topography.

The link from repair to mutation and cell death is still not clear. Nonrepaired/misrepaired DNA lesions could lead to cell death but the mechanism in which DNA repair may lead to deletions and subsequently to mutation/cell death has yet to be understood. To this end, Sankaranarayanan and colleagues [44] proposed a computational solution to bridge the gap and solve a long standing problem in genetic risk estimation [45]. In the absence of human data, part of the solution to genetic risk estimation in human is computational modelling of the cellular processes using mechanistic models [45, 46]. Cell cycle is one of the cellular processes that has been extensively studied using computational kinetic models [46-50]. More recently, similar approaches have been employed to study the kinetics of DNA repair pathways. These approaches include the Michaelis-Menten kinetics method to study BER kinetics [51-

54]; use of biochemical kinetics model to study DSB repair and γ-H2AX foci formation [55-57], and Monte Carlo method to study DSB spatial-temporal modifications [58-61]. Most of the models used to date are based on some simplifying assumptions, which require further modifications and development to mimic the cellular responses to DNA damage. The advantage of the stochastic method (Monte Carlo) is to take the spatial movements of the DSB ends into consideration. However, the stochastic method is not an easy approach to study protein repair kinetics. The difficulty of using the stochastic method arises from the large number of proteins involved in the repair processes.

In this study, we used three mathematical approaches to model the repair kinetics or characterise the repair kinetics. The first mathematical approach used in this work was a phenomenological model (two exponential method) to describe the repair curves. The two exponential model is a simple method to characterise the repair half time and fraction of repair by slow and fast kinetics, but cannot describe the mechanism of repair. The second method is biochemical kinetic rate modelling. The law of mass action is used to translate the schematic model of repair explained in Chapter 2 into a mathematical formalism explained in Chapter 4. The mathematical model consists of a set of non-linear differential equations, in which the solution of the equations provides the overall repair and protein action kinetics. The biochemical method is a mechanistic approach that explains every step of repair with a separate equation. This model has many unknown parameters that should be carefully devised. In comparison to other mechanistic methods such as the Michaelis-Menten model, it is a simple approach with fewer unknown parameters. The third mathematical model used in this work is inverse transform sampling method (ITS). This method is used to integrate the repair model with the damage model (simulated by Track Structure Monte Carlo method) and calculate the kinetics of every stage of repair for every DSB separately. The overall repair time for a single DSB is calculated with this method. The calculated DSB repair kinetics were tested by comparison to pulsed-filed gel electrophoresis (PFGE) data for electrons and ultrasoft X-rays. The comparison allowed us to explain the mechanisms involved in repair of DSB. In the following section, summary descriptions of paper I to paper V explain how complexity of DSB and distribution of DSB in the heterochromatin affect the repair kinetics of DSB induced by radiation of different quality.

1.1 SUMMARY OF PAPERS

This section provides a short summary of the published papers for the thesis. The papers are presented according to the course of the development of the DSB repair model, from the most recent to the earliest one. The development of the DSB repair model also reflects the level of complexity of the model and availability of the experimental data for benchmarking.

Paper I:

Title: Biochemical DSB-Repair Model for Mammalian Cells in G1 and Early S Phases of the Cell Cycle (2013, Mutation Research)

Paper I presents a model of repair in G1 and early S phases of the cell cycle. In this period of the cell cycle HR is not active. NHEJ and MMEJ are the two candidates to repair the damage. The simple DSB is repaired by NHEJ, the complex DSB is repaired by MMEJ and DSB in the heterochromatin undergoes further end processing for chromatin remodelling that is mediated by ATM and Artemis. The initial steps of the end modifications before synapsis are common for slow, fast and heterochromatin DSB-repair. The model was translated into a system of nonlinear equations. The solution of the model was compared to experimental DSB repair kinetics to derive the rate constants for photon irradiated cells. The model overall DSB-repair kinetics are compared with the experimental DSB-repair kinetics of V79 cells irradiated with 45 Gy of ^{60}Co γ-rays and primary human dermal fibroblasts irradiated with 250 kV_P X-rays. In order to further prove the hypotheses in this work (repair kinetics are delayed by the distribution of DSB in the heterochromatin and the complexity of DSB), comparison with experimental results for cells irradiated with different quality radiation is required. For this purpose the repair model could be integrated with simulation of damage for radiation of different quality to predict the DSB-repair kinetics.

1.1.1 Paper II, Paper III, and Paper IV

Title (paper II): The Nonhomologous End-Joining (NHEJ) Pathway for the Repair of DNA Double-Strand Break: I- Mathematical Model (2013, Radiation Research)

Title (paper III): The Nonhomologous End-Joining (NHEJ) Pathway for the Repair of DNA Double-Strand Break: II- Application to Damage Induced by Ultrasoft X-rays and Low Energy Electrons (2013, Radiation Research)

Title (paper IV): Repair of the Double-Strand Breaks Induced by Low Energy Electrons: a Modelling Approach (2012, Int. J. Radiation Biology)

Collectively, papers II-IV describe different aspects of the development of the NHEJ repair model.

Paper II presents a model that describes the NHEJ repair pathway. The NHEJ model was developed by taking into consideration the biological DSB end processing in the absence of homologous recombination. The model considers separate treatment for simple and complex DSB. However the initial steps of the end modifications before synapsis is common for slow and fast repair. The biochemical end modifications explained in the schematic model were translated to a set of nonlinear equations. In the absence of experimental data for rate constants we determined the rate constants for a sample dose of 20 Gy. The same rate constants proved to be predictive for higher doses up to 80 Gy and several different mammalian cell lines. The initial recruitment kinetics of DNA-PKcs and Ku heterodimer were compared with experimental data measured by green fluorescent protein tagged DNA-PKcs and Ku.

In papers III and IV, the NHEJ mathematical model of DSB repair was used to test the repair capability of the model when applied to computer simulated radiation induced damage by low energy electrons and ultrasoft X-rays. In this work, the Monte Carlo track structure code system KURBUC, which can generate interaction of electron tracks in the environment of a cell including those on DNA from direct interactions and reactions of OH radicals, was used. All types of DSB were subjected to the NHEJ

model for repair. For this purpose, an inverse transform sampling method was used to derive the time required for biochemical catalysis at the ends of every individual DSB. This approach provides details of repair timing that otherwise are not easily measured for protein activities on the DSB ends. The time required for the repair of DSB induced by single tracks of low energy electrons was calculated. The overall repair kinetics of DSB induced by 500 tracks of mono energetic electrons and ultrasoft X-rays were computed. The overall repair kinetics showed good agreement with ultrasoft X-rays experimental measurements. The average times calculated for the repair of the complex DSB were longer than the simple DSB.

1.1.2 Paper V

Title: A Kinetic Model of Single-Strand Annealing for the Repair of DNA Double-Strand Breaks (2011, Radiation Protection Dosimetry)

Paper V presents a mathematical model that describes the SSA repair pathway. The model is based on the biochemical modifications of the DSB ends to rejoin the ends by the SSA pathway. In order to be able to concentrate on the repair exclusively performed by the SSA pathway, cells that are mutated in both HR and NHEJ are chosen for comparison. Comparison of DSB-repair kinetics based on the assumption that the entire repair is performed by SSA is made. The description of the model was translated to a set of equations. The solution of the equations gives the information regarding individual repair protein activity kinetics and the total DSB rejoining kinetics. The rate constants were derived by comparing the DSB repair kinetics of a 20-Gy experiment to the model solutions. Applying the same rate constants it was possible to predict the DSB repair kinetics of 80-Gy irradiated chicken DT40 cells.

2 DNA REPAIR PATHWAYS

Ionizing radiation induces a variety of different types of damage in genomic DNA including base lesions, single strand breaks, and double strand breaks. Cells employ different series of proteins to repair the damage. These specific pathways are BER for the repair of base lesions and single strand breaks, and nonhomologous end-joining, homologous recombination, single strand annealing and microhomology-mediated end-joining for the repair of double strand breaks. The repair pathways and protein functions are explained in this section.

2.1 BASE EXCISION REPAIR

Base Excision Repair (BER) is involved in repairing base damages, Apurinic/Apyrimidinic (AP) sites, and SSB [62-65]. It is estimated that the rate of induction of base and strand lesions per day per mammalian cell is around 10^4 lesions [66, 67]. Figure 2.1 illustrates a simplified model of BER by short and long patch pathways. Base lesions are initially recognized and processed by a DNA glycosylase. The glycosylase hydrolyses the N-glycosidic bond and removes the base resulting in an AP site. The AP site is then cleaved by the AP nuclease. The kinetics of removal of damaged bases by a glycosylase depends on the damaged base [68, 69]. UNG, SMUG1, TDG, MBD4 and MPG (AAG) are human monofunctional glycosylases. Another class of glycosylases, including OGG1, NEIL1 and NEIL2, possess both glycosylase and AP lyase activity [70, 71]. AP endonucleases like APE form 3'-hydroxyl and 5'-abasic deoxyribose phosphate (5'-dRP). The repair of the AP site can proceed by long patch (where 2-13 nucleotides are replaced) or short patch (where 1 nucleotide is replaced) BER pathways. Most of the bifunctional glycosylases activate the short patch repair pathway since DNA polymerase β (pol β) excises the 5'-dRP moiety and replaces the missing nucleotide [72]. XRCC1 and DNA ligase III perform the strand ligation. Long patch BER initial repair steps are similar to that of short patch, starting with DNA glycosylase and AP lyase. Polymerase δ or ε together with proliferating cell nuclear antigen (PCNA) synthesizes a DNA patch up to 13 bases long. PCNA then stimulates Flap endonuclease I (FEN-1 to remove the resulting oligonucleotide flap. The nick is sealed by DNA ligase I. Single strand breaks are first recognized by poly(ADP-ribose) polymerase (PARP) protein and then processed by APE1 or polynucleotide kinase/phosphatase (PNKP) [73]. PNKP restores both 5′-phosphate and 3′-hydroxyl termini. The repair then proceeds either by short patch repair using pol β, XRCC1 and ligase III proteins or by long patch repair using FEN-1, Pol δ or ε, and ligase I proteins.

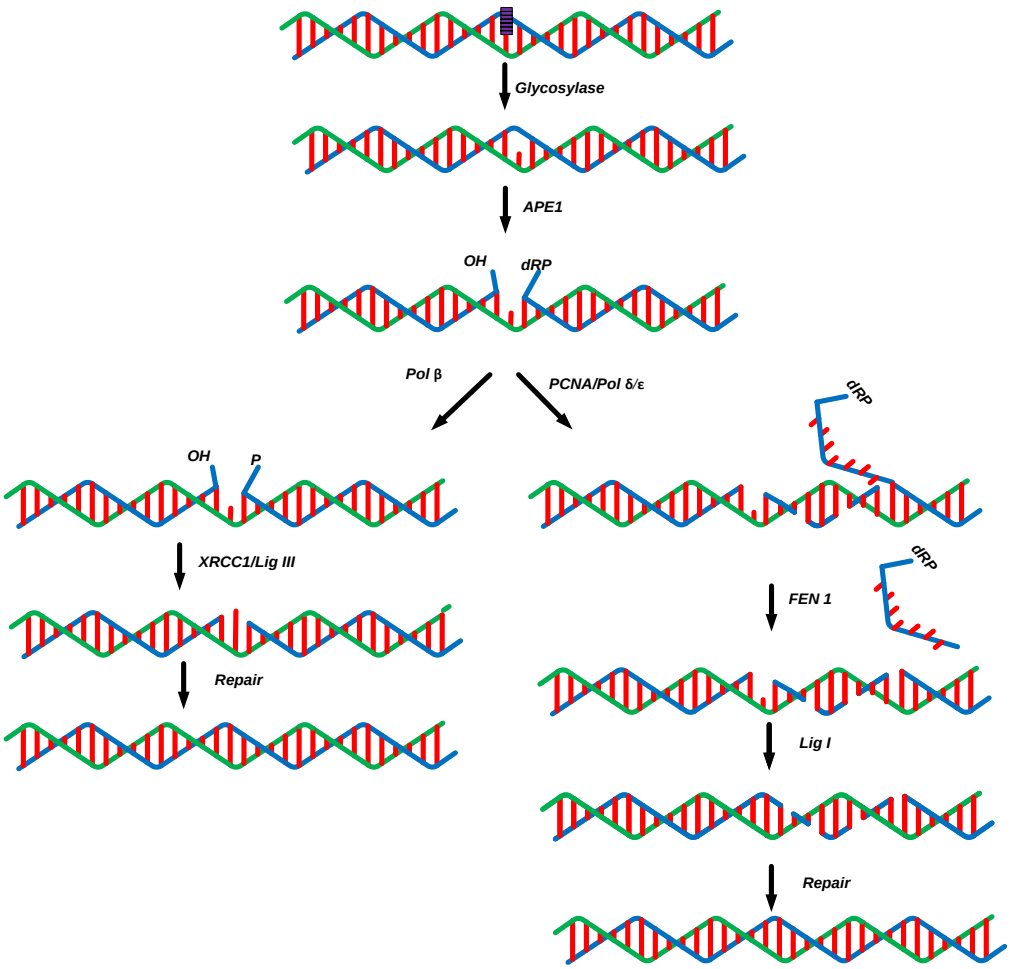

Figure 2.1 BER starts with damage recognition and removal of the damaged base by a DNA glycosylase. APE1 cleaves the abasic site. The repair could proceed by short patch BER with Pol β replacing the damaged nucleotide and XRCC1/Lig III proteins sealing the nick. The other option could be long patch BER that introduces from 2-13 nucleotides. Proteins such as PCNA, Pol δ or ε, FEN-1, and Lig I are involved in long patch BER.

Damage induced by ionizing radiation may contain tandem or bi-stranded base and sugar phosphate backbone lesions. Synthesized or enzymatically-induced lesions have been used to study the effect of closely positioned base lesions and strand breaks of different types [74-82]. It has been observed that closely positioned lesions could slow down the repair. Bi-stranded lesions may lead to DSB in the process of repair, since base lesions are modified to abasic sites in the process of repair [75]. The ability of BER to repair a bi-stranded lesion depends on the juxtaposition of the lesions, and the nature of the second damage [29, 65, 80, 82-98]. Bi-stranded base damage leads to SSB for the first lesion which starts the repair irrespective of the relative position of the lesions [83]. There might be no preference for BER processes to start with either of the base lesions. BER of the second lesion depends on the position of the other damage in the opposite strand. If the other lesion is more than one base pair away, the incision creates a DSB (up to three base pairs), however if the distance between the opposite lesion is just one nucleotide away the repair of the second lesion will be stalled to avoid the DSB [85], and the lesions will be repaired sequentially. Other studies on bistrand

damage BER suggest that a second base lesion has no or little effect on the glycosylase detection and excision of the parallel strand, however lesions in proximity of an AP lesion or SSB compromises the excision of the base lesions on the parallel strand [99]. Tandem lesions can also inhibit the repair of the lesions. 8-OxoG adjacent to a tandem AP site can affect the AP site repair. The direction of the two lesions could affect the repair kinetics. If the AP site is present at -1, -3, -5 positions relative to 8-OxoG, the missing base will be inserted while the ligation cannot be completed causing a lost 8-OxoG. If the AP site is at +1 position relative to 8-OxoG the missing base won't be inserted resulting in a lost 8-OxoG. If the AP site is at either +3, or +5 positions relative to 8-OxoG the missing base will be inserted, the ligation will be complete in +5 position and the repair of the AP site is unaffected by 8-OxoG, while at +3 position ligation may not be complete [100].

2.2 DSB REPAIR PATHWAYS

To date, there are four known main DSB repair pathways namely nonhomologous end-joining, homologous recombination, single strand annealing and microhomology-mediated end-joining. These pathways are dissimilar in terms of repair and proteins and have different characteristics that are summarized in this chapter.

2.2.1 Nonhomologous End-joining

Figure 2.2 presents a schematic description of the repair processes involved in NHEJ as far as known to date. NHEJ is the main pathway in mammalian cells for the repair of DSB. The repair by NHEJ is relatively fast and error prone. Ku70/Ku80 heterodimer is the first protein to bind to the DSB. Ku heterodimer has a toroidal configuration, and translocate inward after binding to DSB ends. This process provides space for other proteins such as DNA-dependent protein kinase catalytic subunit (DNA-PKcs) to bind to the Ku-DNA complex [101].The affinity of DNA-PKcs for DNA increases 100-fold in the presence of Ku heterodimer [102]. DNA-PKcs functions as a gatekeeper of the DSB ends [103]. The synapsis is formed with Ku heterodimer and DNA-PKcs complex. DNA-PKcs autophosphorylation at ABCDE and PQR clusters regulates the NHEJ repair process [104]. DNA-PKcs regulates access to the damage ends by autophosphorylation [105]. ABCDE autophosphorylation is required for efficient ligation by the XLF/XRCC4/LIG IV complex. It is proposed that the non-phosphorylated DNA-PKcs remains bound to the termini rendering the ends inaccessible to the alternative repair pathways. Therefore, cells that are deficient in DNA-PKcs autophosphorylation of the ABCDE site are more radiosensitive than cells that lack DNA-PKcs. In contrast, cells deficient in PQR autophosphorylation are more radioresistant than cells that lack DNA-PKcs. Inhibition of PQR autophosphorylation renders the ends more accessible for repair by the HR pathway. In conclusion autophosphorylation of the ABCDE site and not the PQR site is required to open up the ends for the alternative pathways of repair, while autophosphorylation at both ABCDE and PQR sites allows NHEJ to complete the repair. Based on laser-induced damage

experiments, it is proposed that DNA-PKcs is only required for the complex type repair [106]. Other proteins that are involved in the slow repairing types of DSB are Artemis and ATM [26]. Artemis is an endonuclease [107], and DNA-PKcs phosphorylates Artemis to facilitate its endonuclease activity [108, 109]. Artemis is involved in the repair of the DSB that require end-processing before ligation [110-112]. XRCC4 plays a key role in the recruitment and activation of the end processing enzyme polynucleotide kinase/phosphatase (PNKP) and DNA ligase IV. PNKP possesses a kinase and phosphatase activity to convert 5'-OH to 5'-phosphate and 3'-phosphate to 3'-OH, which is required for efficient ligation [113]. XLF mediates the activity of XRCC4 [114]. The DNA ligase complex composed of XLF/XRCC4/LIG IV could be sufficient for some end ligation. However, some end configurations require additional nucleotide addition by DNA polymerase μ or λ before the ligation process can seal the nick.

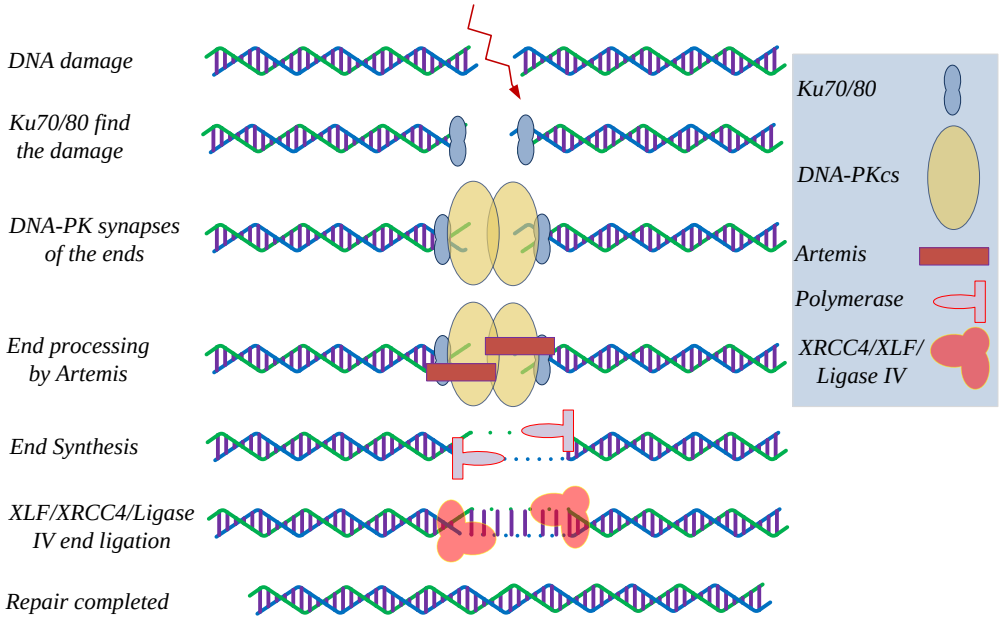

Figure 2.2 Biochemical end processing performed by NHEJ to repair the DSB. The repair starts with Ku70/80 and continues with DNA-PKcs recruitment to the ends. DNA-PKcs together with Ku70/80 forms the DNA-PK complex which acts as a gatekeeper. The repair continues with end processing by Artemis and polymerase μ or λ if required. Finally the XLF/XRCC4/LIG IV complex completes the ligation and repair.

2.2.2 Homologous Recombination

A schematic description of the biochemical end modifications during HR repair is illustrated in Figure 2.3. The HR repair is employed by the cells for different types of complications including radiation induced DSB repair, repair of stalled replication fork (during first meiotic division by repairing the deliberately induced DSB), and telomere maintenance with elongation of the shortened telomeres [115]. HR repair starts with resection of the damaged DSB ends. Ku heterodimer protects the ends in G_1 and blocks

resection, while in the absence of Ku, MRN (Mre11-Rad50-Nbs1) can resect the ends. CtIP mediates the end resection by MRN protein. For this purpose CDK which is a cell cycle protein phosphorylates CtIP in late S and G_2 phases of the cell cycle [116]. BRCA1 can also mediate the resection process [117]. The damage induced by radiation is dirty damage in comparison to clean damage or resected damage. The clean ends result in 3'hydroxyl or 5'phosphate group ends and require no further end processing for DNA polymerases or ligation. Resection of clean ends could be easily processed without MRN while dirty ends require MRN for resection. In the absence of MRN, Exo1 could be a candidate for resection. The average length of resection with and without Exo1 is respectively 270 and 850 nucleotides long for meiotic cells [118]. The average length of resection increases to 2-4 kilobases for mitotic cells [119]. The resection length in the absence of Ku in G_1 phase could extend to 5 kb [120]. The length of resection suggests that for long resections Exo1 collaborates with MRN to facilitate long resection [121]. This is called a two stage model in which MRN starts the resection and the resection is either extended by Exo 1 or BLM helicase activity. The length of resection can be restricted by signalling proteins like ATM to avoid chromosome rearrangement. After resection, RPA binds very strongly to the single-stranded DNA (ssDNA). RPA has a very high affinity for ssDNA and removes all secondary structures and proteins, which facilitates Rad51 recruitment to the ssDNA. Rad51 assembles a filament along the ssDNA. Rad52 and BRCA2 mediate the filament assembly on the ssDNA that is covered by RPA [116, 122]. CDK phosphorylation of BRCA2 in G_0 and G_1 phases precludes filament formation by Rad51. The Rad51 filament has a pitch of 10 nm that includes 18 nucleotides of DNA that is about 6 protein monomers per helical turn [115]. Up to this stage the biochemical modifications of the ends constitute the pre-synapsis steps of repair. The synapsis forms after searching the homologous pair by Rad51-ssDNA filament. The motor protein Rad54 mediates the complementary pair searching, invasion of the intact strands, and formation of a displacement loop (D-loop). Rad54 is capable of bidirectional ATP-dependent translocation along the double-stranded DNA (dsDNA) at a speed of 300 bp/s [123]. Rad54 also mediates dissociation of the Rad51 filament from the intact strand to allow synthesis of the ends. After the synapsis is completed, the HR repair continues with either of the two main sub-pathways namely synthesis-dependent strand annealing (SDSA), and double strand break repair (DSBR). The SDSA sub-pathway involves elongation of the single strand end by polymerase η. The elongation process involves D-loop migration. The dissociation of the D-loop is performed by displacement of the synthesized intruding strand. BLM helicase and FANCM could be involved in unwinding the D-loop. At the end the second strand is synthesized and the repair is completed with annealing of the ends. The DSBR sub-pathway involves formation of a Holliday junction and resolution of the Holliday junction after synthesis of both strands. The process of opening double Holliday junctions is rather complex and can result in cross-overs (e.g. sister chromatid exchange). There are different models for opening of the double Holliday junctions by movement of the double Holliday junction towards each other. The opening of the Holiday junction is performed by Topo3, FANCM helicase, RecQ family motor proteins like BLM, and also endonucleases that can resolve the Holliday junctions like GEN1. The DSBR sub-pathway is favoured in germ cells during meiotic recombination, while SDSA does not

involve crossovers and is preferred in somatic cells. The SDSA (illustrated in Figure 2.3) is the major HR sub-pathway, since in vitro experiments confirms Rad51 capturing the second end and avoiding double Holliday junction formation.

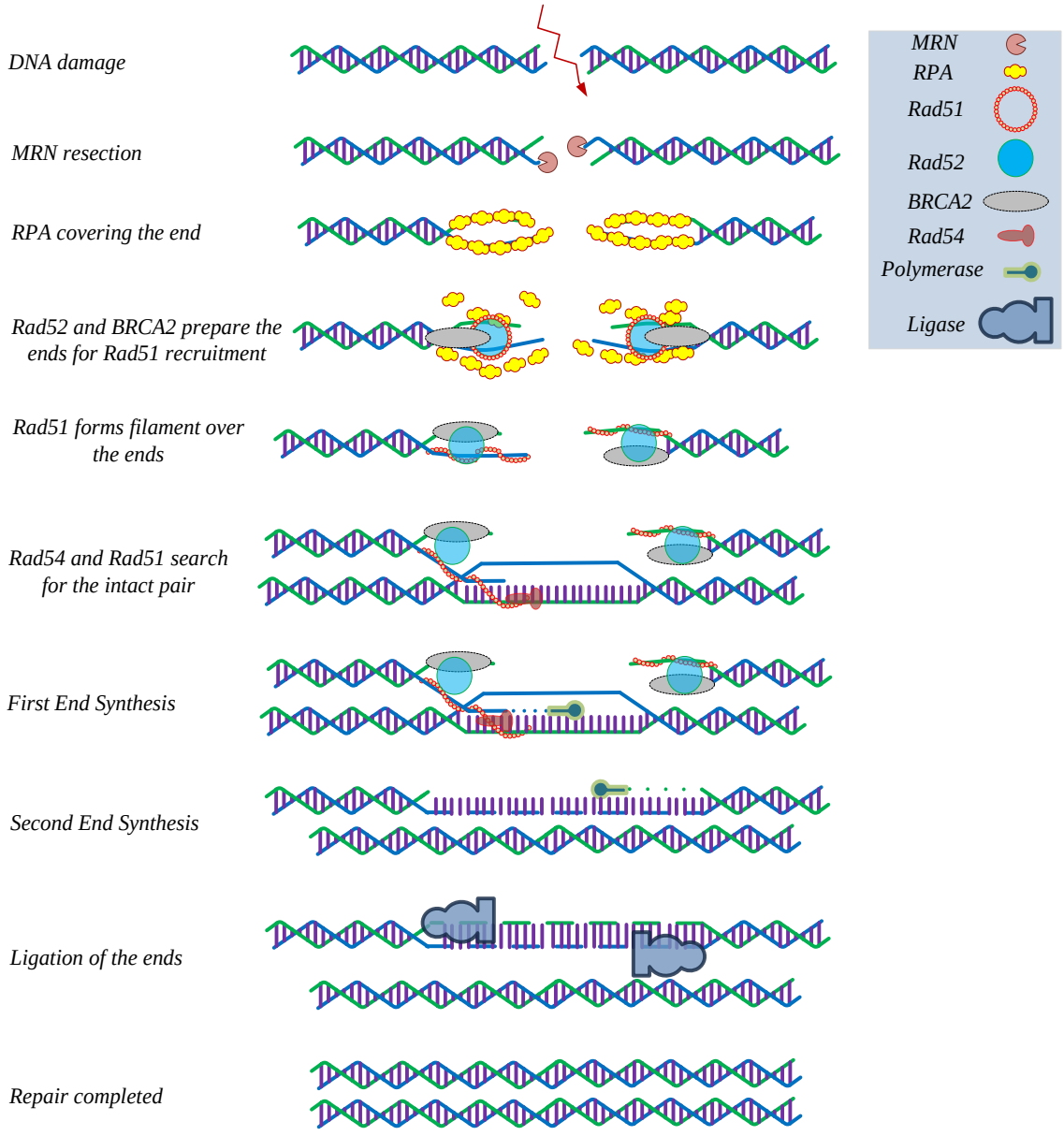

Figure 2.3 HR synthesis-dependent strand annealing (SDSA) sub-pathway. The biochemical end processes before synapsis involves end resection by MRN, covering the ends by RPA and recruitment of Rad51 mediated by Rad52 and BRCA2. Synapsis is produced by invading the intact pair and formation of a D-loop by Rad51 and Rad54. Using the template, the first strand is synthesized. The D-loop is opened and the second strand in synthesized. Finally the repair ends with ligation.

2.2.3 Single Strand Annealing

Figure 2.4 illustrates a schematic description of the SSA repair pathway. The initial steps of SSA are identical to the HR pathway. The MRN complex resects the DSB ends to form ssDNA tails. RPA binds very strongly to ssDNA and removes any secondary structure. The binding affinity of RPA to 5' and 3' ssDNA increases when it binds to Rad52. Phosphorylated RPA and monomeric Rad52 interaction enhances the affinity of Rad52 to bind ssDNA. After Rad52 binds to phosphorylated RPA, it is able to proceed with the repair process by annealing the strand ends. Rad51 plays an important role in mediating the HR pathway and prevents Rad52 from promoting a Rad51-independent SSA repair pathway [124]. As shown in Figure 2.4, the SSA pathway can successfully repair the DSB by a Rad52 annealing process. A direct repeat sequence is necessary for this approach. ERCC1/XPF endonuclease in vertebrates interacts functionally with Rad52 to remove the 3'-overhangs. Finally, ligation by Ligase III ends the SSA repair process.

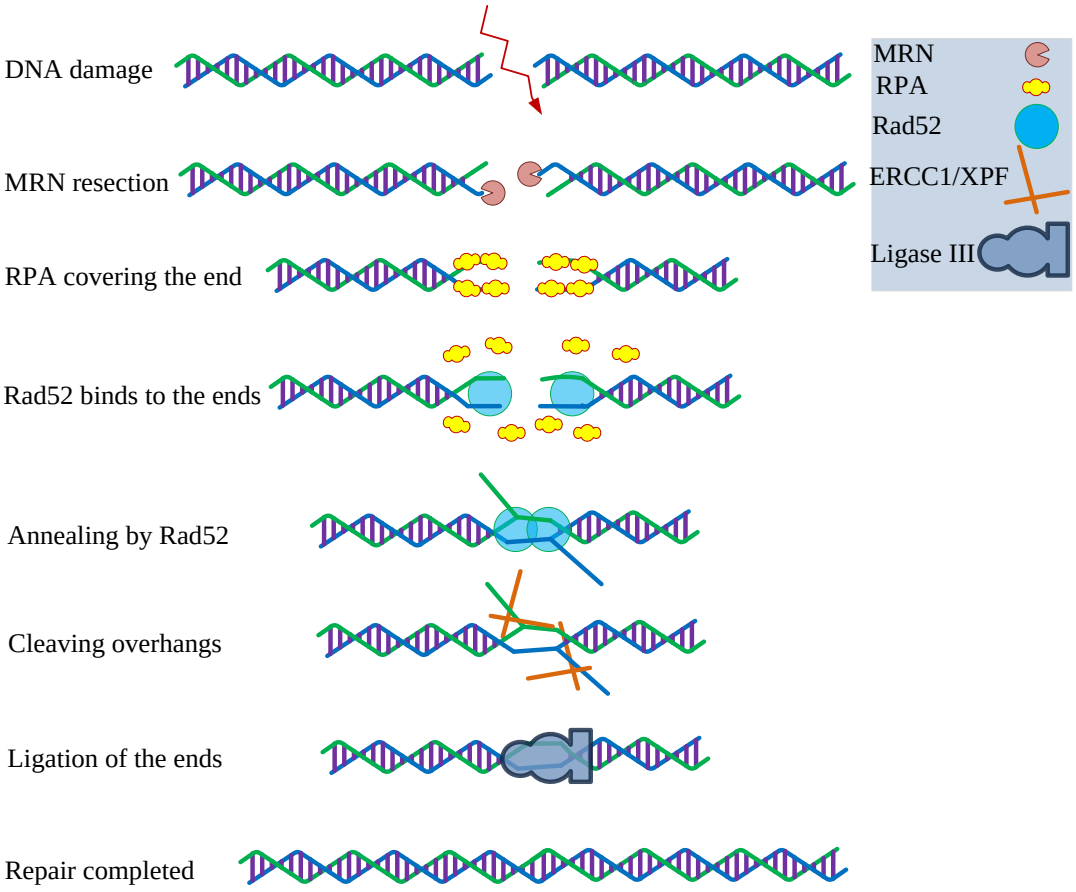

Figure 2.4 Biochemical end processing of SSA. The initial steps are similar to HR repair involving the MRN and RPA proteins. Rad52 in the absence of Rad51 performs annealing activities. The overhangs are cleaved by ERCC1/XPF and finally ligation completes the repair

2.2.4 Microhomology-Mediated End-Joining

A schematic description of the MMEJ repair pathway is shown in Figure 2.5. It is known that radiation can activate microhomology-mediated end-joining (MMEJ) DSB repair in yeast and mammalian cells [22]. MMEJ was considered as a backup or alternative NHEJ repair pathway, since MMEJ repair is enhanced especially when Ku70 is deficient. However it has been recently shown that MMEJ in mammalian cells is a very robust repair mechanism, especially in the case of class switch recombination in B lymphocytes. Therefore the name alternative NHEJ (alt-NHEJ) pathway suits MMEJ.

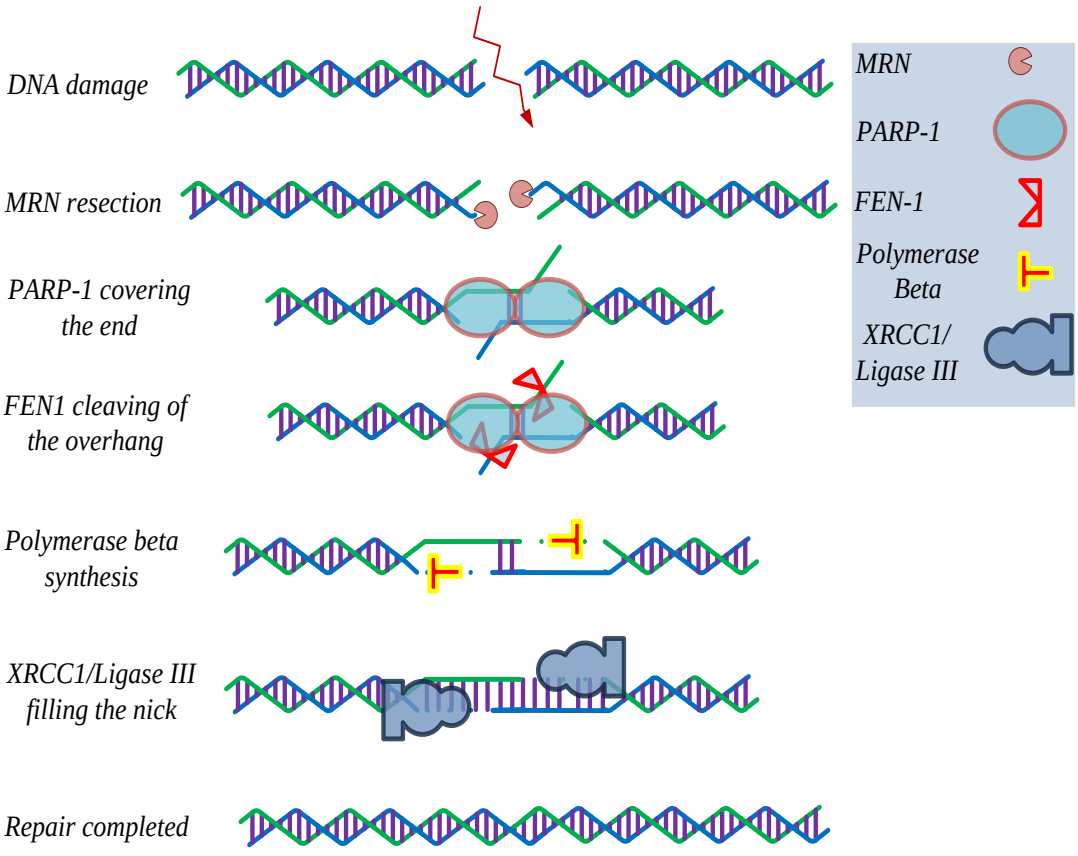

Figure 2.5 Biochemical end processing performed by MMEJ. Resection by MRN is followed by PARP-1 synapsis formation. The repair continues by FEN-1 overhang cleavage, DNA synthesis, and ligation.

The MMEJ repair starts with end resection by MRN, which is mediated by CtIP especially in G_1 [125, 126]. The accurate functions of the proteins which perform the catalysis of the DNA DSB ends remains to be further identified. However it has been seen that MMEJ in fission yeast is dependent on Rad52 protein [127]. The homology length for MMEJ is between 5-25 bp. The repair ends with more than 8 bp homology increasingly require Rad52 for the repair process [23]. The outcome of the repair can include variation in the size of deleted or inserted nucleotides. Most of our knowledge

about MMEJ is derived from experiments on yeast and not mammalian cells. Human ligase I and ligase III but not ligase IV are involved in MMEJ [128]. It has been also speculated that PCNA facilitates formation of the repair complexes including FEN-1 and ligase 1 at the damage site. The other scenario could be that PARP-1 synapsis is followed by XRCC1-ligase III activity [129] . In the model illustrated in Figure 2.5, MRN starts with resection and PARP-1 performs the synapsis. PARP-1 is in direct competition with Ku70 [130]. The DSB ends are coupled by base pairing. FEN-1 endonuclease activity is required to remove the flap. Polymerase β (or possibly polymerase λ) fills any possible gaps and finally the repair finishes with ligation by XRCC1/ligase III.

3 REVIEW OF EXPERIMENTAL DATA USED IN THIS WORK

Recent experiments have expanded our understanding of the biological relevance and function of the repair and signalling protein recruitment. The protein-protein and protein DNA biochemical interactions determine the hierarchy and order of sequential assembly of repair proteins at the site of damage. Post-translational modification of the proteins including phosphorylation, ubiquitylation, SUMOylation, methylation and acetylation plays an important role in both repair and signalling pathways in response to radiation exposure. The biological experiments that have been widely used in this work with their limitation and applications are discussed in this chapter.

3.1 GEL ELECTROPHORESIS

Constant-field gel electrophoresis (CFGE) has been conventionally used to separate DNA fragments. The CFGE takes advantage of DNA negative charge due to the phosphate (PO_4^-) in the sugar-phosphate backbone. DNA charge is linearly proportional to its size (expressed in bp) or molecular weight. Therefore the force (F) applied to DNA fragments in a uniform electrical field is linearly proportional to the charge (q) and electrical field strength (E). Enhanced migration of smaller DNA fragments in the gel allows separation of DNA fragments with the CFGE method. CFGE does not separate fragments larger than 50 kbp with any practical field strength [131]. The limitation of large fragment separation (>50 kbp) limits the application of CFGE for moderate and low doses. Schwartz and Cantor improved the separation of fragments from 50 kbp to 2 Mbp by generating an inhomogeneous field with two sets of electrodes [132]. In pursuit, it was observed that inhomogeneous field is not a necessary condition for separation of large fragments and Pulsed-field gel electrophoresis (PFGE) method was introduced. With the PFGE method, the electric field is periodically alternated with pulses of 120^O reorientation that allows fragment separation from 10 kbp to 10 Mbp. Among the limitations of PFGE method are that a large radiation dose and large number of cells is required to obtain statistically reliable signal for analysis. During cell culture radiolabel ^{14}C is incorporated to the DNA. β-decay of ^{14}C is counted to quantify DSB. 10^5-10^6 cells embedded in each plug gives rise to 10^3-5×10^4 disintegrations per minute that is sufficient for analysis [133]. Doses lower than 10 Gy has been used for PFGE, however doses higher than 20 Gy are statistically more reliable [134]. In order to avoid repair during irradiation, the dishes of the cells are cooled down on ice. The cells can repair DSB when incubated at 37^oC. The naked double helical DNA is extracted from the cell nucleus to run on PFGE. The fraction of activity released (FAR) is determined by the proportion of radioactive labeled DNA in each segment to the total radioactivity of the lane. The number of DSB is nonlinearly related to the FAR. The Blöcher random breakage model is used to calculate the number of DSB from FAR.

$$F_{<k} = 1 - e^{-\frac{rk}{n}}\left(1 + \frac{rk}{n}\left(1 - \frac{k}{n}\right)\right), k \ll n \qquad 3.1$$

Where, $F_{<k}$ is the fraction of DNA smaller than the threshold cut-off k, r is the average number of randomly distributed DSB in chromosome, and n is the size of the chromosome. Numerical methods are used to solve the equations and calculate the number of DSB from FAR. The random breakage model is based on the assumption that the damage is randomly distributed, according to a uniform distribution. However the fragment sizes tend to become smaller with the increase of LET. Therefore the number of DSB is underestimated with the increase of LET. In order to solve this problem careful analysis of the fragment sizes is required. The complexity of high LET irradiation fragment measurement increases with the low resolution of FAR method to smaller fragment sizes [135].

It is possible to optimize PFGE protocols for better fragment separation by changing the parameters such as total electrophoresis duration, pulse duration, electric field pulsing frequency, electric field strength, electrophoresis buffer temperature, and gel agarose concentration presented in several PhD theses [136-138]. In order to increase the sensitivity of the assay it is possible to optimize the protocols for separate ranges of fragment sizes. For the separation of large fragments long pulse durations and stronger electric field could be used and for the separation of smaller fragments higher concentrations of agarose gel could be used.

PFGE experiments are used to measure the repair kinetics of DSB with different dose and radiation qualities. In order to derive the repair kinetic curves each data point presents the amount of unrepaired DSB after certain time of post irradiation incubation. Further assays are available to measure the fidelity of repair by measuring the mis-rejoin fragment yield [139, 140]. The experimental protocols and analysis of the PFGE data could differ from lab to lab that affect the results. Temperature effect is one of the important parameters that has been extensively studied. During the analysis of the lysis process, it has been noticed that the duration of lysis affects the FAR values and it was initially recommended to lysis for 17 hours at 50^{o}C (hot lysis) [141]. Further studies revealed that lysis at 50^{o}C could introduce heat labile sites that convert to DSB [142]. The DSB heat labile sites are repaired fast and independent of some of the core NHEJ proteins [143]. New protocols have proposed cold lysis to avoid induction of heat labile sites [144].

Single gel electrophoresis or comet assay is another electrophoresis assay to assess the repair of SSB and DSB [145]. In this method, single cells are embedded in low density agarose, lysed and exposed to electric field. As explained earlier negatively charged DNA fragments migrate in the electric field inversely proportional to their mass. Fluorescent microscopy of the experiment results in a picture resembling a comet. The comet tail intensity indicates the amount of damage. Neutral lysis is used for DSB assessment, while lysis under alkaline conditions is used for SSB assessment. The method is not an accurate method for DSB measurement. The advantage of the comet assay to PFGE is lower dose (~1 Gy) and low number of cells for the assay. In terms of accuracy for repair kinetic measurements the PFGE experiments are favoured.

The CFGE and PFGE experiments illustrate the kinetics of DSB repair for cells irradiated with photons [146-176] and ions [135, 157, 169, 174, 176-203]. PFGE assays have been used to study the effect of repair protein mutation [146, 147] or radiation quality [179, 187, 199] on repair kinetics. Figure 3.1 illustrates DSB repair kinetics for Chinese Hamster V79 cells irradiated with photon, proton (11 keV/µm and 31 keV/µm), deuteron (13 keV/µm and 62 keV/µm), and helium (53 keV/µm, 81 keV/µm, and 123 keV/µm) ions using CFGE [179]. Figure 3.2 illustrates DSB repair kinetics for Primary Human Dermal Fibroblasts irradiated with photons, helium 7 keV/µm, 70 keV/µm, and 120 keV/µm) and nitrogen (97 keV/µm) ions using PFGE [187]. Figure 3.3 illustrates DSB repair kinetics for Normal Skin Human Fibroblasts irradiated with photons, helium (40 keV/µm) and nitrogen (80 keV/µm,125 keV/µm, 175 keV/µm, and 225 keV/µm) ions using PFGE [199]. As illustrated in Figure 3.1, Figure 3.2, and Figure 3.3 DSB repair kinetics show at least two components. The slow component is enhanced with the increase of LET. These are the few experiments that have measured the DSB repair kinetics of ions with different LET using PFGE and CFGE methods. As explained, neutral elution is used for DSB repair kinetics measurements. Similarly, alkaline elution could be used for the SSB repair kinetic measurements [204, 205].

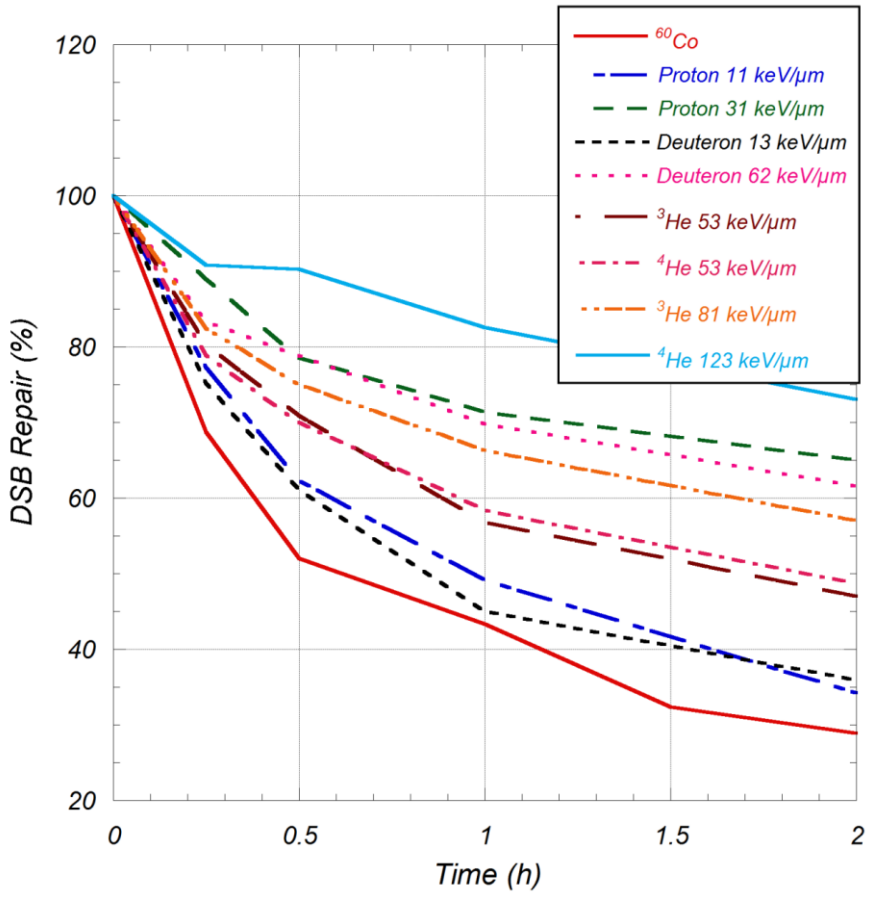

Figure 3.1DSB repair kinetics for Chinese Hamster V79 cells irradiated with photon, proton, deuteron and helium ions [179]. CFGE was used to measure the repair kinetics.

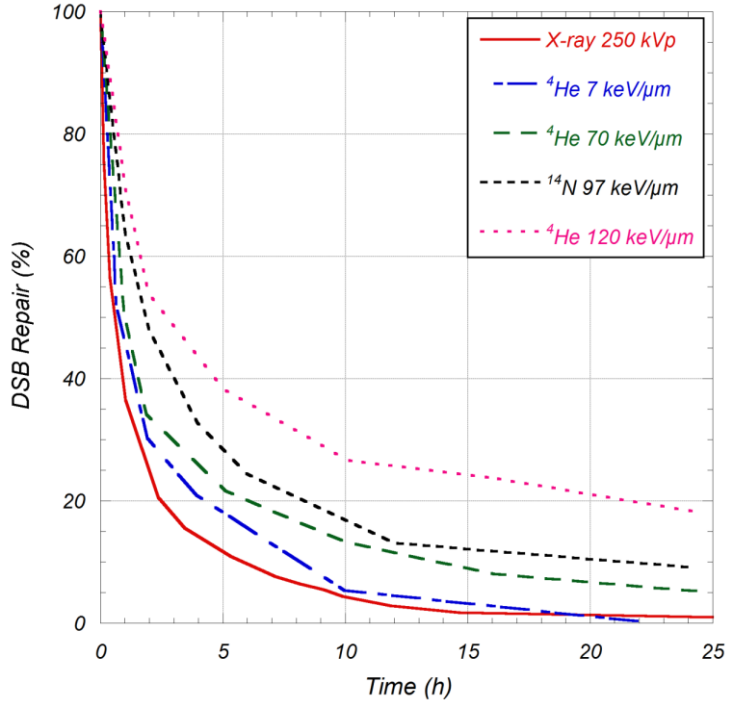

Figure 3.2 DSB repair kinetics for Primary Human Dermal Fibroblasts irradiated with photons, helium and nitrogen ions [187]. PFGE was used to measure the repair kinetics.

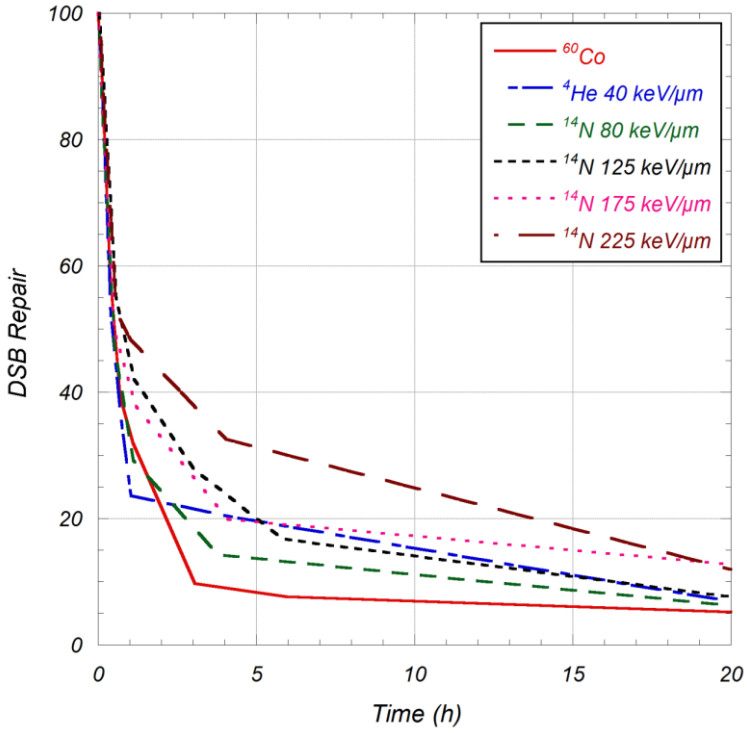

Figure 3.3 DSB repair kinetics for Normal Skin Human Fibroblasts irradiated with photons, helium and nitrogen ions [199]. PFGE was used to measure the repair kinetics.

3.2 RADIATION-INDUCED FOCI

Radiation induced foci are foci that appear in response to DNA DSB damage and repair. The foci can be detected under the microscope by immunostaining or protein tagged to a fluorescent protein such as green fluorescent proteins (GFP). The protein recruitment at the site of damage is an ordered and sequential process, however the damage are dynamic in a confined region (locally dynamic) as observed by various experiments. There is a wealth of information resulting from foci data regarding the kinetics and position of the damage in the cell nucleus, and spatio-temporal modifications. However the method has its own limitations and advantages. Not all repair proteins form foci with ionizing radiation. Histone H2AX phosphorylation (γ-H2AX) produces the most common foci induced by radiation and have been well-studied in the literature [206-211]. HR repair proteins like Mre11 and Rad51, BRCA, and RPA have been studied [25, 212]. NHEJ repair proteins don't tend to form foci since few proteins are sufficient to deal with a DSB. However laser irradiation has been used to intensify the signal from proteins like DNA-PKcs and observe them under the microscope. Other proteins that have been studied are mainly signalling proteins such as 53BP1, ATM, and MDC1 [212-215]. Mediator of DNA check point 1 (MDC1) protein orchestrates the downstream damage signalling protein recruitment. MDC1 binds to γ-H2AX with high affinity through its BRCA1 C terminal (BRCT) and facilitates recruitment of ATM [216]. MDC1 interacts with MRN through NBS1 [217]. The recruitment of MDC1 occurs rapidly within 1-2 minutes [218]. MDC1 mediates the downstream protein recruitment such as 53BP1 (p53-binding protein 1) and BRCA1 with delay [219]. BRCA1 is a HR repair protein and shows low level recruitment during G1 [220]. The radiation-induced foci have been extensively reviewed in the literature [206, 218, 221-226] . In the next section γ-H2AX assay that is relevant to this work is discussed.

3.2.1 γ-H2AX assay

The chromatin structure allows nearly 2 meters of DNA to be compacted in a cell nucleus of 10 μm diameter. The fundamental structure of the 30 nm chromatin fiber is the nucleosome. The nucleosome is composed of about 147 bp DNA wrapped around two members of each core histone family [227]. The core histone families are H2A, H2B, H3, and H4. The nucleosomes are connected to each other with the aid of linker histones (H1) and 20-80 bp DNA. Figure 3.4 illustrates the structure of the nucleosome with histones in the middle of the DNA [228, 229]. Histone 2AX (H2AX) is among the core histone families that contributes to the nucleosome formation. Human diploid cells containing 23 pairs of chromosome with 6.4×10^9 bp wrapped around ~3.2×10^7nucleosomes. Depending on the cell type about 2% (including lymphocytes and HeLa cells) to 25% of the H2A variant is H2AX [230, 231].

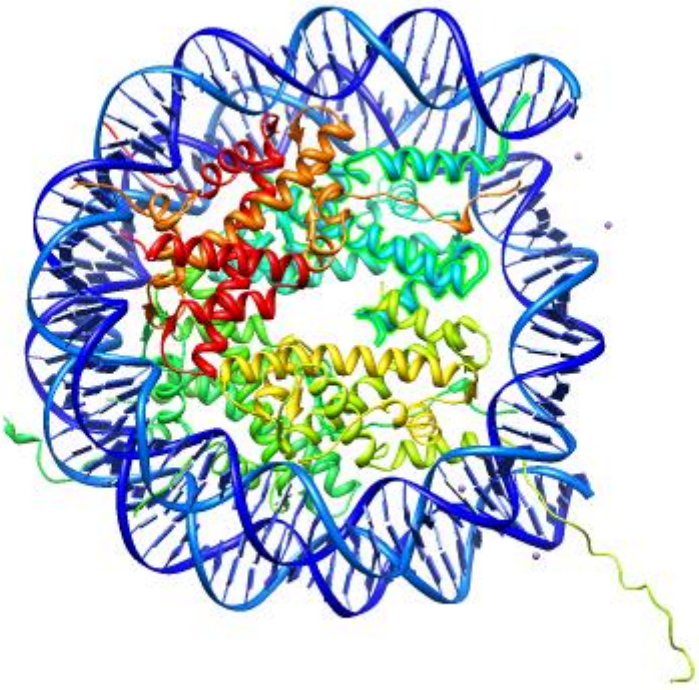

Figure 3.4 The crystallography image of the nucleosome with PDB (Protein Data Bank) entry 1aoi [228, 229]. The nucleosome consists of the octamer histones and double helix DNA. The 147 bp of DNA double helix (in blue) wrapped around core histones shown in the middle of the nucleosome.

In response to radiation induced DSB the H2AX histones are phosphorylated at serine S139 forming γ-H2AX [231]. Several thousands of H2AX proteins surrounding the damage start forming γ-H2AX foci within seconds post irradiation. The maximum phosphorylation is recorded 15-30 min post irradiation [206], and the level of it is shown to increase linearly with the number of DSB for γ irradiated cells [232]. Phosphatidylinositol-3 (PI-3)-like protein kinase family members such as DNA-PK, ATM, and ATR phosphorylate H2AX. ATR is activated by single stranded DNA that is created by stalled replication forks or resection by homologous recombination repair. ATM and DNA-PK are more effective in phosphorylating H2AX [233]. DNA-PK can redundantly and separately to ATM phosphorylate H2AX, however DNA-PK has a limited range of phosphorylation in comparison to ATM [234]. NBS1 (one of the MRN complex proteins) may facilitate phosphorylation by ATM [235].

Apart from γ-H2AX, many other repair and signalling proteins such as 53BP1, BRCA1, Rad51, and NBS1 form foci. Co-localization of DNA repair and signalling foci with γ-H2AX foci has been observed. Most of the NHEJ repair proteins don't form foci unless compact damage is induced (with a laser). Phosphatase 2A facilitates dephosphorylation of γ-H2AX [236]. γ-H2AX can be detected by immunofluorescence using a microscope or flowcytometry. Cells tend to show a background level of γ-H2AX foci. In addition to DSB, replication fork collapse in S phase and, apoptosis could form γ-H2AX foci [237]. It has been shown that for MRC-5 cells γ-H2AX foci

count approximately the same number of DSB, and the number of foci is linearly proportional with dose at its maximum signal (approximately 30 min post irradiation) [232]. It is estimated that approximately 2000 H2AX molecules are phosphorylated per DSB [231]. About 0.03 % of the H2AX molecules are phosphorylated per DSB induced by γ-ray. Respectively about 1 % of the H2AX molecules are phosphorylated for one Gy of γ-ray dose. The size of the foci is around 0. 3 square micrometres that covers about 2 Mbp of chromatin for gamma irradiated cells. The size of the foci increases with LET. The large size of the foci in comparison to the size of the DSB (defined within 2-3 helix of DNA) is attributed to amplification of damage response by γ-H2AX foci. Another probable function for γ-H2AX foci is to mediate synapsis in order to avoid separation of the ends. H2AX facilitates recruitment of MDC1 and consequently 53BP1 [238]. The low dose sensitivity of γ-H2AX foci and the simplicity of the experiments raised hopes to apply this method for biodosimetry (reviewed in [149, 239]). Supporting experiments for this application showed that visible γ-H2AX foci are almost exclusively induced by DSB and not by other types of damage such as SSB [232]. ^{125}IdU labelling of DNA experiments is an accurate method to count the number of DSB that has a 1 to 1 correlation to the number ^{125}I disintegration in cell. The ^{125}IdU labelling of DNA has shown that γ-H2AX foci counts can closely estimate the number of DSB under optimal conditions [240]. The first limitation of γ-H2AX foci is that its kinetics does not accurately express the kinetics of induction and repair of DSB measured by PFGE. This is due to the fact that H2AX phosphorylation is not a direct reaction to the damage and is indirectly phosphorylated by proteins such as ATM, ATR and DNA-PK. Similarly the dephosphorylation is conveyed indirectly therefore the kinetics of foci induction and removal does not accurately mimic DSB repair kinetics measured by PFGE and involves delays. Beside background levels, γ-H2AX foci are not induced exclusively by DSB, other processes such as apoptosis or replication fork collapse may induce γ-H2AX foci. Evidence for DSB repair independent of γ-H2AX is observed by formation of 53BP1, MRN, BRCA1, RPA, Rad51 foci independent of H2AX [241-245]. Co-localization of RIF (radiation induced foci) with γ-H2AX is observed in many studies [246-249]. However, the co-localization is transient and partial [157, 250, 251]. At early stages of repair (< 5 min) less than half of the Nbs1 and Mre11 foci co-localize with γ-H2AX foci, while co-localization increases up to 75 % two hours post-irradiation [250]. Long persistent γ-H2AX foci do not always correspond to remaining DSB and it could be due to other persistent problems such as remaining changes in the chromatin structure [157, 252, 253]. The number of maximum initial foci is reported to be correlated to the number DSB and linearly proportional to radiation dose [232, 240]. However more investigation shows that in some cell types there is no linear correlation between the number of foci and DSB [254, 255], and there is a dose dependence effect in the appearance of the foci [149, 212, 213].

Since the DSB induced in the cell by γ-ray is randomly located in the cell nucleus, a simple analysis could be done to count the foci per dose in Gy. In the analysis it is assumed that foci are induced randomly in the cell nucleus, and there are no endogenous foci. One Gy of γ-ray irradiation is assumed to induce 35 DSB. The foci have a spherical shape with a radius of 0.3 μm, and the cells have a spherical shape with a radius of 10 μm. Figure 3.5 illustrates the number of foci per cell nucleus for

doses from ~0.05 Gy to 50 Gy. From the analysis it can be concluded that for large doses 2 or more foci could overlap. Overlapping of the foci could be experimentally observed with large foci. Therefore linearity of the number of foci with dose is lost for large doses. At doses above 2 Gy the yield of γ-H2AX foci is underscored [256]. γ-H2AX foci enumeration underestimates the number of DSB for high LET (in comparison to γ-ray) exposures. It is also observed from Figure 3.5 that the method is not suitable for doses higher than 5 Gy.

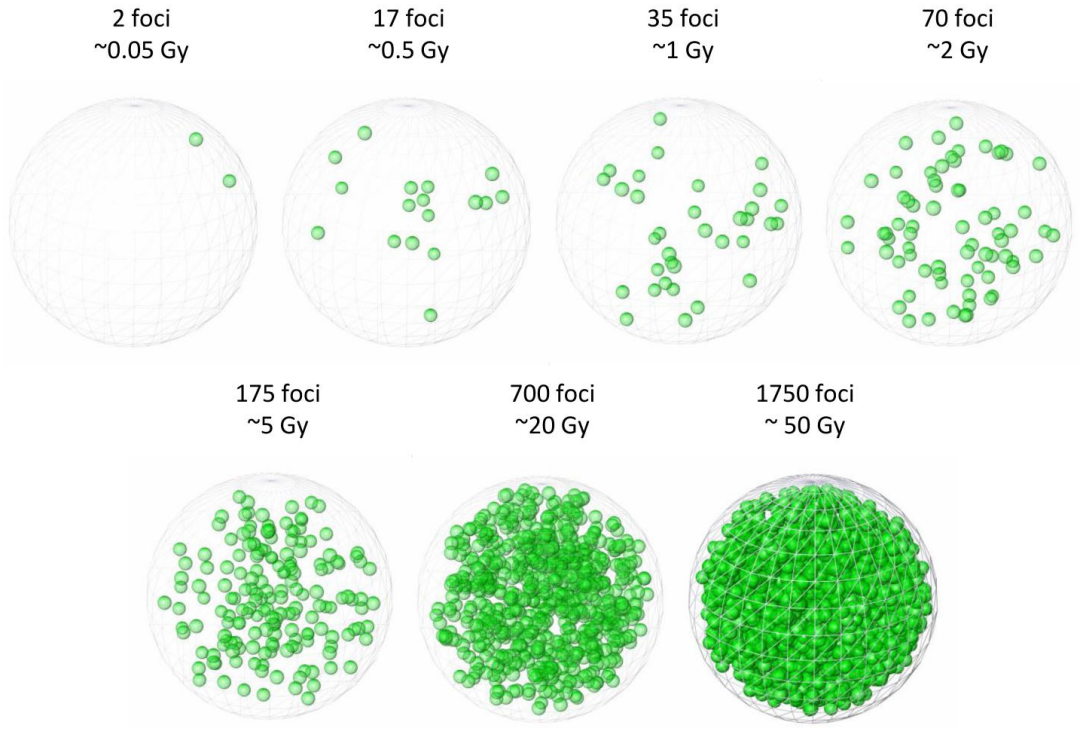

Figure 3.5 Green spheres simulate foci with radius of 0.3 μm in a spherical 10 μm cell nucleus diameter for various doses ranging from 0.05 Gy to 50 Gy. It is assumed that 35 DSB (foci) are produced per Gy of photon irradiation. The number of foci for doses higher than 5 Gy saturates the system.

4 MODEL OF DNA REPAIR

Biological experiments including protein expression measurements and mass spectrometry provide valuable information of the protein levels in the cells. However, identifying the function of the proteins is a difficult task. Computational methods have been employed to bridge the task. For this purpose mechanistic models are of great importance [257]. In order to model biological responses, the cell is considered as a system. By defining a cell as a system, under certain modelling criteria it is possible to analyse and ultimately predict cellular behaviour. In addition, computational modelling allows testing conditions that are not feasible in the lab or have not been experimentally tested. In the system that is analysed in this work radiation is considered as a perturbation to the system that activates certain repair and signalling activities that are required to retain genomic integrity. The repair activities are cascades of protein actions at the site of damage. The proteins react sequentially and are exclusive to the type of damage as explained earlier. One of the methods that is applied to deal with molecular and chemical reactions is biochemical kinetic modelling. A kinetic model translates an enzymatic or molecular reaction into a differential equation. The law of mass action is the basis of the biochemical kinetic model or a mechanistic model. The law of mass action states that the rate of the reaction is proportional to the product of concentrations or activities of the reactants. In order to mathematically express the law of mass action, consider a simple consecutive first order reaction that product C is formed from reactant B and A consecutively with the reaction rates k_2 and k_1 as illustrated in Figure 4.1.

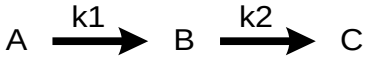

Figure 4.1 Reactant A and B react continuatively to form product C with k_1 and k_2 rate constants.

The rate equations for reactants A and B and product C is expressed in equations 4.1, 4.2 and 4.3. As is illustrated in Figure 4.1 and equations 4.1, 4.2 and 4.3, concentration of reactant A or [A] decreases with rate constant k_1, while concentration of reactant B or [B] increases with rate constant k_1 and decreases with rate constant k_2 and finally concentration of product C or [C] increases with rate constant k_2. In order to solve the first order linear differential equations, rate constants k_1, k_2 and initial values of reactants A and B and product C concentrations are required.

$$\frac{d[A]}{dt} = -k1[A] \quad 4.1$$

$$\frac{d[B]}{dt} = k1[A] - k2[B] \quad 4.2$$

$$\frac{d[C]}{dt} = k2[B] \quad 4.3$$

The same concepts explained for the simple consecutive first order reaction are used to model DNA repair processes by BER, NEHJ in absence of HR, and NEHJ in presence of HR and MMEJ models.

4.1 BER MODEL

Base lesions and single strand breaks are repaired by the BER pathway. BER includes two main subpathways of short and long patch. Both processes start with a glycosylase and AP endonuclease that leads to an abasic site and nick in the phosphodiester backbone. Depending on the type of damage the repair may proceed via separate processes leading to removal of either one nucleotide with short patch BER or 2-13 nucleotides in long patch repair. The short patch repair is proposed for simple type base lesions in a fast process and long patch repair is proposed for clustered base lesions in a slow process. In this section we propose a kinetic model that explains the BER biochemical processes illustrated in Figure 4.2. The repair processes are described mathematically with a formulism based on law of mass action. In the mathematical description of the model, protein concentrations are specified in the brackets, and nomenclatures Y_i, V_i, and K_i represent respectively the repair complex, repair rate, and repair rate constant at stage i of repair. BER starts with a glycosylase [258]. There are many different types of chemically modified bases that require BER, therefore the cells employ many glycosylases that are specific to specific base lesions and act with different kinetics [259-263]. For simplicity of the model, the first step of repair is expressed as removing the damaged base without differentiating the different glycosylases exclusive to every specific base lesion. Equations 4.4 and 4.5 explain the first step of repair that is damaged base removal.

$$\frac{dY_1}{dt} = \alpha \frac{dD}{dt} - V_1 \qquad 4.4$$

$$V_1 = K_1[Glycosylase]Y_1 \qquad 4.5$$

Human apurinic/apyrimidinic endonuclease 1 (APE1) recognizes abasic site and creates a nick in the sugar-phosphate backbone [264]. APE1 makes a nick by hydrolysing the phosphodiester bond 5’ to the abasic site to produce a 5’-deoxyribose phosphate (dRP) and 3’-OH explained by equations 4.6 and 4.7.

$$\frac{dY_2}{dt} = V_1 - V_2 \qquad 4.6$$

$$V_2 = K_2[APE\ 1]Y_2 \qquad 4.7$$

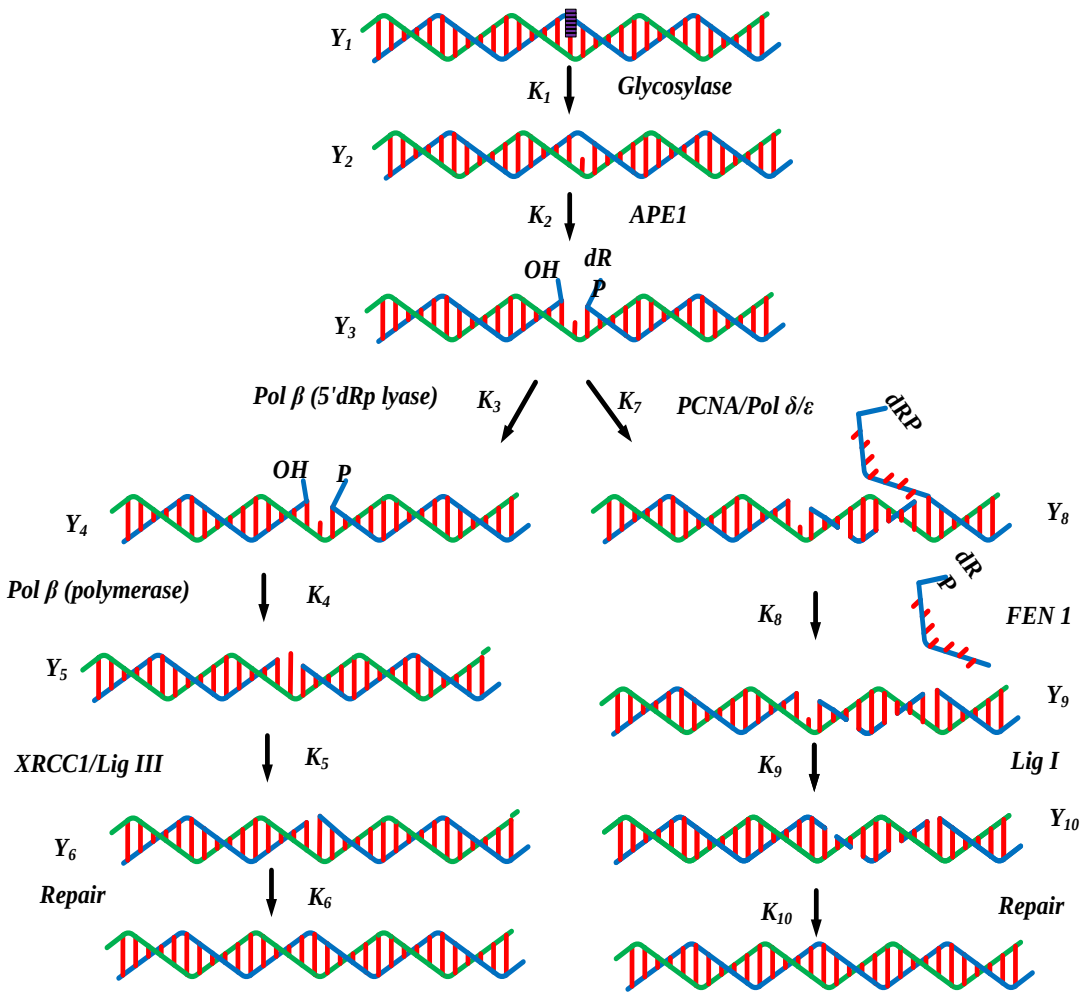

Figure 4.2 The BER model is illustrated. The repair starts with glycosylase and endonuclease. The repair continues with short or long patch pathways. The rate constants of the repair processes are shown with K_1 to K_{10}

The dRP is removed by Polymerase β lyase activity [265]. The repair then proceeds the short patch pathway [266]. The long patch repair continues with the complex of proteins Polymerase δ/ε, proliferating cell nuclear antigen (PCNA), and replication factor C (RFC) proteins [267, 268]. The proteins work together to replace 2-13 nucleotides 3' to the gap [269, 270]. The initiation of short and long patch repair is explained in equations 4.8 to 4.10 .

$$\frac{dY_3}{dt} = V_2 - V_3 - V_7 \qquad 4.8$$

$$V_3 = K_3[Pol\beta, dRplyase]Y_2 \qquad 4.9$$

$$V_7 = K_7[Pol\delta/\varepsilon, PCNA, RFC]Y_3 \qquad 4.10$$

The short patch repair continues by synthesizing the single nucleotide with Polymerase β as explained in equations 4.11 and 4.12.

$$\frac{dY_4}{dt} = V_3 - V_4 \quad 4.11$$

$$V_4 = K_4[Pol\beta]Y_4 \quad 4.12$$

The final step of short patch repair is ligation of the nick by XRCC1 and Ligase III proteins explained by equations 4.13 to 4.16.

$$\frac{dY_5}{dt} = V_4 - V_5 \quad 4.13$$

$$V_5 = K_5[XRCC1, LigIII]Y_5 \quad 4.14$$

$$\frac{dY_6}{dt} = V_5 - V_6 \quad 4.15$$

$$V_6 = K_6Y_6 \quad 4.16$$

The long patch repair continues by removing the single strand flap with flap endonuclease (FEN-1) explained in equations 4.17 and 4.18

$$\frac{dY_8}{dt} = V_7 - V_8 \quad 4.17$$

$$V_8 = K_8[FEN\ 1]Y_8 \quad 4.18$$

The final step of repair is sealing the nick by Ligase I as explained with equations 4.19 to 4.22.

$$\frac{dY_9}{dt} = V_8 - V_9 \quad 4.19$$

$$V_9 = K_9[Lig\ I]Y_9 \quad 4.20$$

$$\frac{dY_{10}}{dt} = V_9 - V_{10} \quad 4.21$$

$$V_{10} = K_{10}Y_{10} \quad 4.22$$

4.1.1 Scaling of BER equations

In order to solve the system of equations the parameters have been scaled with a scaling factor C_i large enough to assure that the sum of total concentration of the repair complexes and proteins remain constant. For this purpose it is assumed that the sum of total concentration of the repair complexes and proteins (Y_i and E_i) is constant and equal to C_i.

$$C_i = [E_i] + \sum_{i=1}^{10} Y_i = cte \quad 4.23$$

$$y_i = \frac{Y_i}{C_i} \quad 4.24$$

$$k_i = C_i K_i \quad 4.25$$

$$c_i = \frac{\sum_{i=1}^{10} y_i}{C_i} \quad 4.26$$

$$c'_i = \frac{\sum_{i=1}^{6} y_i}{C_i} \quad 4.27$$

The following equations are derived considering the scaling factor C_i and substituting the new parameters in the model. The scaled equations are shown with equations 4.28 to 4.36.

$$\frac{dy_1}{dt} = \frac{\alpha}{C_1}\frac{dD}{dt} - v_1 \quad 4.28$$

$$\frac{dy_2}{dt} = v_1 - v_2 \quad 4.29$$

$$\frac{dy_3}{dt} = v_2 - v_3 - v_7 \quad 4.30$$

$$\frac{dy_4}{dt} = v_3 - v_4 \quad 4.31$$

$$\frac{dy_5}{dt} = v_4 - v_5 \quad 4.32$$

$$\frac{dy_6}{dt} = v_5 - v_6 \quad 4.33$$

$$\frac{dy_7}{dt} = v_7 - v_8 \quad 4.34$$

$$\frac{dy_8}{dt} = v_8 - v_9 \quad 4.35$$

$$\frac{dy_9}{dt} = v_9 - v_{10} \quad 4.36$$

v_1 to v_{10} are shown with equations 4.37 to 4.46.

$$v_1 = k_1(1 - c_2)y_1 \quad (4.37)$$

$$v_2 = k_2(1 - c_3)y_2 \quad (4.38)$$

$$v_3 = k_3(1 - c'_4)y_3 \quad (4.39)$$

$$v_4 = k_4(1 - c'_5)y_4 \quad (4.40)$$

$$v_5 = k_5(1 - c'_6)y_5 \quad (4.41)$$

$$v_6 = K_6 y_6 \quad (4.42)$$

$$v_7 = k_7(1 - c_8)y_3 \quad (4.43)$$

$$v_8 = k_8(1 - c_9)y_8 \quad (4.44)$$

$$v_9 = k_9(1 - c_{10})y_9 \quad (4.45)$$

$$v_{10} = K_{10} y_{10} \quad (4.46)$$

4.1.2 Results of BER kinetic model

In order to solve the system of nonlinear equations the initial values and rate constants are required. At time zero, we assume that the repair activity of all proteins is zero and repair starts directly after the damage is induced. The maximum number of SSB damage (100%) is assumed to be induced at time zero. The rate constants for this model is not experimentally measured, therefore the rate constants used to solve the equations should be separately validated with dedicated experiments. Table 4.1 lists the rate constants that are used to solve the BER model.

The solution of the model provides the individual protein activity kinetics and overall base excision repair model kinetics. Figure 4.3 illustrates the comparison of the overall repair kinetics from the model calculations and experimental measurements. The solid line, circle and triangle illustrate the repair kinetics for the BER model, CHO-K1, xrs-7 cell lines [204]. The CHO-K1and xrs-7 cells are irradiated with 5.8 Gy X-rays and alkaline elution technique is used to measure the SSB repair kinetics [204]. The xrs-7 cells are X-ray sensitive mutant form of CHO-K1 cells. The xrs-7 cells show reduced levels of DNA-PKcs expression. The SSB repair kinetics of the xrs-7 and CHO-K1 cells are similar. The SSB repair kinetics show a two component repair and show a good agreement between model calculation and experiments.

Table 4.1 Repair rate constants used in BER model calculations

Rate Constants	BER Model
k_1 (h^{-1})	200
k_2 (h^{-1})	100
k_3 (h^{-1})	85
k_4 (h^{-1})	70
k_5 (h^{-1})	60
K_6 (h^{-1})	40
k_7 (h^{-1})	28
k_8 (h^{-1})	35
k_9 (h^{-1})	50
K_{10} (h^{-1})	1.28

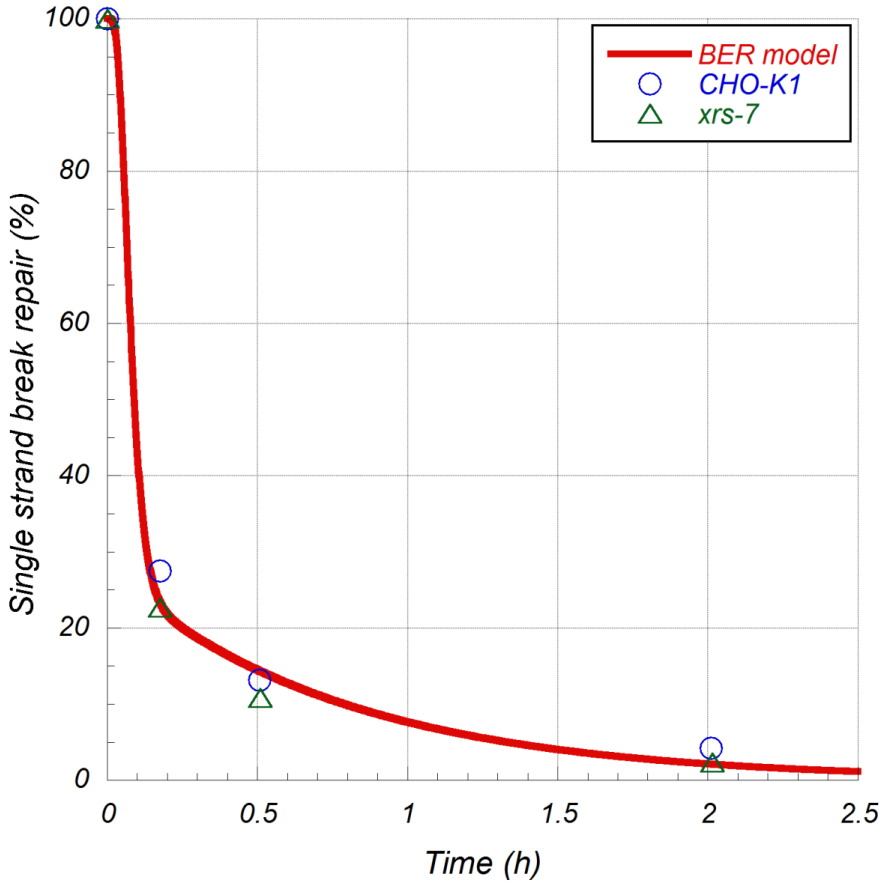

Figure 4.3 Repair kinetics of single strand breaks by BER model (solid line), CHO-K1 cells (circle) [204], and xrs-7 cells (triangle) [204] .

4.2 DSB REPAIR MODELS

We have proposed two models for DSB-repair. The first model considers NHEJ repair in the absence of HR and MMEJ pathways. This model was used in situations where cells were irradiated by electrons or X-ray. In this model the damage in the heterochromatin was not considered. The second model considers NHEJ, HR, and MMEJ pathways for DSB produced in the heterochromatin and the influence of the cell cycle. The model was divided into two parts of the cell cycle. In the G1 and early S phases of the cell cycle NHEJ and MMEJ are considered to be active, while in the G2 and late S phases of the cell cycle NHEJ and HR pathways are active. For both phases of the cell cycle the repair starts with the NHEJ pathway. If the damage is a complex DSB type or in the heterochromatin it is assumed that further end processing is required.

4.2.1 NHEJ repair model

Figure 4.4 presents a model of NHEJ pathway for the repair of DSB in absence of HR. In this model the repair proteins are sequentially recruited to the damage sites. Ku heterodimer and DNA-PKcs are required to form the synapsis. The simple type DSB is easily ligated, while the complex type DSB require further end processing by Artemis. The repair processes are described mathematically with a formulism based on the law of mass action. In the mathematical description of the model, protein concentrations are specified in the brackets, and nomenclatures Y_i, V_i, and K_i represent respectively the repair complex, repair rate, and repair rate constant at stage i of repair.

It is assumed that the total dose to the cell is delivered at time zero (no repair during irradiation) and the initial number of DSB is the initial condition of the equations. The rate of DSB induction is linearly related to the dose rate ($\frac{dD}{dt}$), with the DSB induction-rate per unit dose constant (α). The first repair protein to bind to the DSB is Ku70/Ku80 heterodimer as expressed in equations 4.47 and 4.48. As illustrated in Figure 4.5 The Ku heterodimer binds to 2-4 helical turns of the DNA [271]. Ku heterodimer has a toroidal configuration that makes them capable of inward translocation even when they binds to different damage configurations [101]. Ku also has a higher affinity for double-stranded than single-stranded DNA [272].

$$\frac{dY_1}{dt} = \alpha \frac{dD}{dt} - V_1 \qquad 4.47$$

$$V_1 = K_1[Ku70, Ku80]Y_1 \qquad 4.48$$

In the second step DNA-PKcs binds to the Ku-DNA complex with high affinity [102]. The second complex rate (V_2) increases with the Ku70/Ku80 recruitment and decreases with the DNA-PKcs recruitment that is explained with equations 4.49 and 4.50.

$$\frac{dY_2}{dt} = V_1 - V_2 \qquad 4.49$$

$$V_2 = K_2[DNA - PKcs]Y_2 \qquad 4.50$$

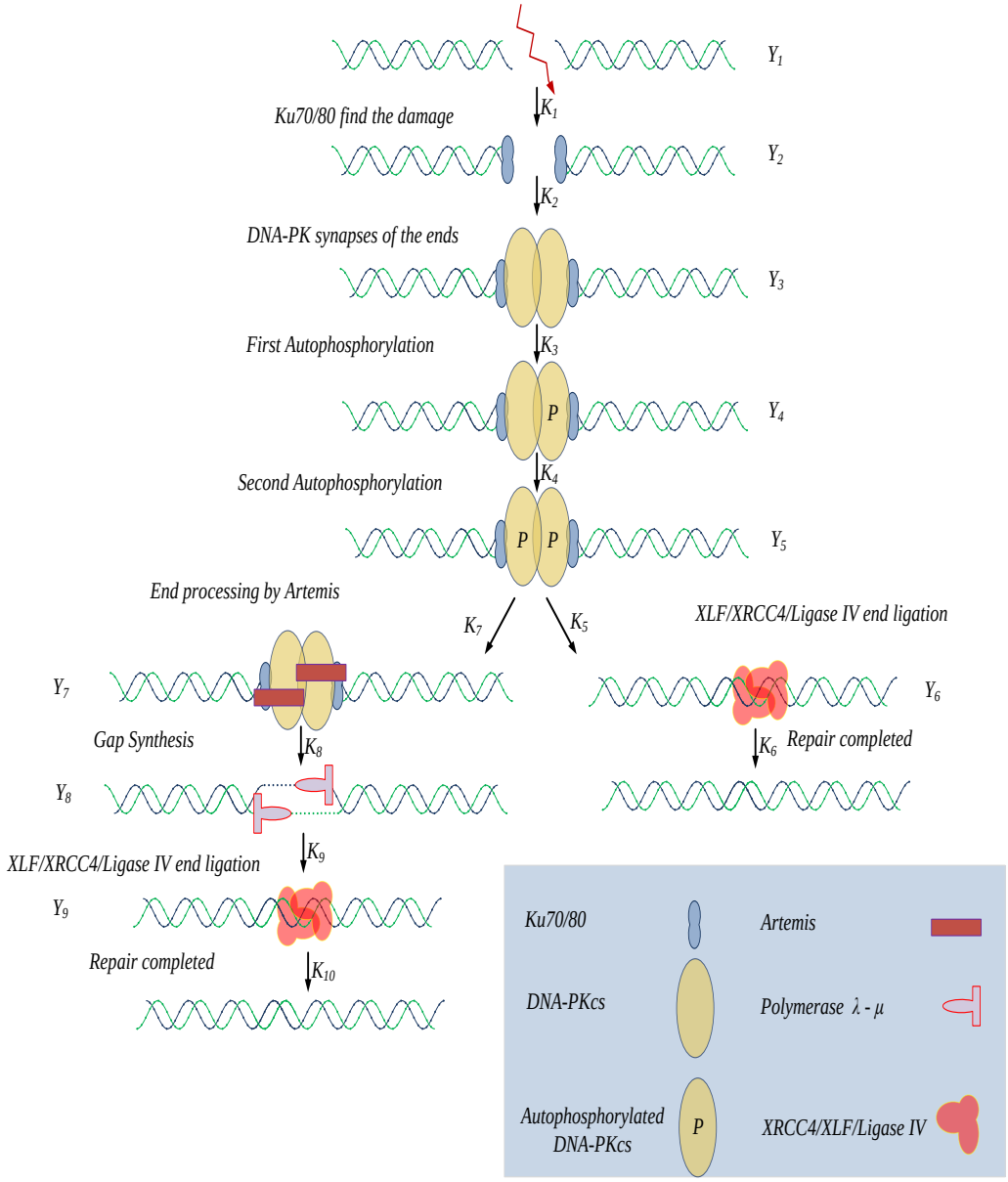

Figure 4.4 NHEJ model is illustrated. The repair starts with Ku70/80 heterodimer recruitment to the damage and forming the synapsis with phosphorylated DNA-PKcs. The repair continues with simple ligation or further end processing for simple and complex type DSB, respectively. The rate constants of the repair processes are shown with K_1 to K_{10}

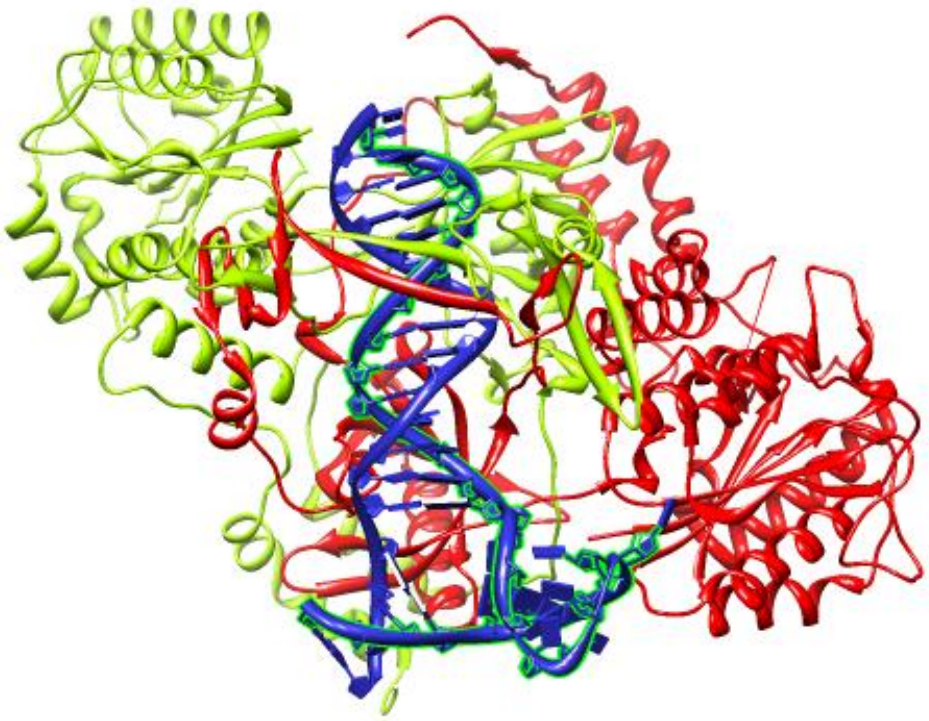

Figure 4.5 Structure of human Ku heterodimer bound to DNA with PDB entry 1JEY [271]. The DNA is shown with blue colour. Ku binds to 2-4 helical turns of the DNA. The DNA double helix is shown in blue and the Ku70/80 heterodimer is in red and green.

In order to form the synapsis and continue the repair, DNA-PKcs autophosphorylates at two sites known as ABCDE and RQR clusters [105]. DNA-PKcs regulates access to the damage ends [103]. The ABCDE autophosphorylation is required for efficient ligation. Inefficient autophosphorylation renders the end termini inaccessible to other proteins [273]. V_3 and V_4 represent the rates of DNA-PKcs autophosphorylation of the two sites that is explained with equations 4.51 to 4.54.

$$\frac{dY_3}{dt} = V_2 - V_3 \tag{4.51}$$

$$V_3 = K_3 Y_3 \tag{4.52}$$

$$\frac{dY_4}{dt} = V_3 - V_4 \tag{4.53}$$

$$V_4 = K_4 Y_4 \tag{4.54}$$

The presynaptic processes of DSB repair is completed by DNA-PKcs autophosphorylation. Depending on the type of damage the repair continues with ligation or end modification before ligation. It is assumed that simple type DSB undergo fast repair by ligation with the XLF/XRCC4/LIG IV complex [274] as explained by equations 4.55 to 4.58.

$$\frac{dY_5}{dt} = V_4 - V_5 - V_7 \quad 4.55$$

$$V_5 = K_5[XLF, XRCC\ 4, Lig\ IV]Y_5 \quad 4.56$$

$$\frac{dY_6}{dt} = V_5 - V_6 \quad 4.57$$

$$V_6 = K_6 Y_6 \quad 4.58$$

Since there is another break in the close proximity of the complex type DSB, end processing is required. The end processing is performed by Artemis that functions as an endonuclease. The XLF/XRCC4/LIG IV complex seals the nick for the complex damages after Artemis end-processing and synthesis activity of Polymerase μ or λ [275] as explained by equations 4.59 to 4.65.

$$\frac{dY_7}{dt} = V_7 - V_8 \quad 4.59$$

$$V_7 = K_7[Artemis]Y_5 \quad 4.60$$

$$V_8 = K_8[Polymerase\ \mu - \lambda]Y_7 \quad 4.61$$

$$\frac{dY_8}{dt} = V_8 - V_9 \quad 4.62$$

$$V_9 = K_9[XLF, XRCC\ 4, Lig\ IV]Y_9 \quad 4.63$$

$$\frac{dY_9}{dt} = V_9 - V_{10} \quad 4.64$$

$$V_{10} = K_{10} Y_{10} \quad 4.65$$

4.2.1.1 Scaling of NHEJ equations

In order to solve the system of equations the parameters have been scaled with a scaling factor C_i large enough to assure that the sum of total concentration of repair the complexes and proteins remain constant. For this purpose it is assumed that the sum of total concentration of the repair complexes and proteins (Y_i and E_i) is constant and equal to C_i. The scaling factor C_i is equal to a value >2800 (this is justified by assuming 35 DSB/Gy induced by 80 Gy radiation dose).

$$C_i = [E_i] + \sum_{i=1}^{9} Y_i = cte \quad 4.66$$

$$y_i = \frac{Y_i}{C_i} \quad 4.67$$

$$k_i = C_i K_i \quad 4.68$$

$$c_i = \frac{\sum_{i=1}^{9} y_i}{C_i} \quad 4.69$$

The following equations are derived considering the scaling factor C_i and substituting the new parameters in the model.

$$\frac{dy_1}{dt} = \frac{\alpha}{C_1}\frac{dD}{dt} - v_1 \quad 4.70$$

$$\frac{dy_2}{dt} = v_1 - v_2 \quad 4.71$$

$$\frac{dy_3}{dt} = v_2 - v_3 \quad 4.72$$

$$\frac{dy_4}{dt} = v_3 - v_4 \quad 4.73$$

$$\frac{dy_5}{dt} = v_4 - v_5 - v_7 \quad 4.74$$

$$\frac{dy_6}{dt} = v_5 - v_6 \quad 4.75$$

$$\frac{dy_7}{dt} = v_7 - v_8 \quad 4.76$$

$$\frac{dy_8}{dt} = v_8 - v_9 \quad 4.77$$

$$\frac{dy_9}{dt} = v_9 - v_{10} \quad 4.78$$

v_1 to v_{10} are shown with equations 4.79 to 4.88.

$$v_1 = k_1(1 - c_2)y_1 \quad 4.79$$

$$v_2 = k_2(1 - c_3)y_2 \quad 4.80$$

$$v_3 = K_3 y_3 \quad 4.81$$

$$v_4 = K_4 y_4 \quad 4.82$$

$$v_5 = k_5(1 - c_6)y_5 \quad 4.83$$

$$v_6 = K_6 y_6 \quad 4.84$$

$$v_7 = k_7(1 - c_7)y_5 \quad 4.85$$

$$v_8 = k_8(1 - c_8)y_7 \quad (4.86)$$

$$v_9 = k_9(1 - c_9)y_8 \quad (4.87)$$

$$v_{10} = K_{10}y_9 \quad (4.88)$$

4.2.1.2 Results of NHEJ kinetic model

Since repair is a biochemical process, it is assumed that the reaction rate constants are applicable to mammalian cells under the same conditions. At time zero, we assume that the repair activity of all proteins is zero and repair starts directly after the damage is induced. The maximum number of DSB (100%) is assumed to be induced at time zero. Table 4.2 lists the rate constants that are used to solve the NHEJ model.

Table 4.2 Repair rate constants used in NHEJ model calculations

Rate Constants	NHEJ Model
k_1 (h^{-1})	350
k_2 (h^{-1})	500
K_3 (h^{-1})	50
K_4 (h^{-1})	20
k_5 (h^{-1})	15
K_6 (h^{-1})	5
k_7 (h^{-1})	3.6
k_8 (h^{-1})	8
k_9 (h^{-1})	0.25
K_{10} (h^{-1})	0.55

The solution of the model provides the individual protein activity kinetics and overall DSB repair kinetics. Figure 4.6 illustrates the comparison of the overall repair kinetics from the model calculations and experimental measurements. The solid line and the symbols illustrate the repair kinetics for the NHEJ model, experimental measurements for DT40 cells mutated in HR repair. DT40 cells are irradiated with 80 Gy. For lower doses down to 20 Gy the model calculations are in a good agreement in comparison to experimental measurements [27]. The measurements of the repair kinetics were done with the PFGE method. The repair kinetics shows at least two components of slow and fast repair.

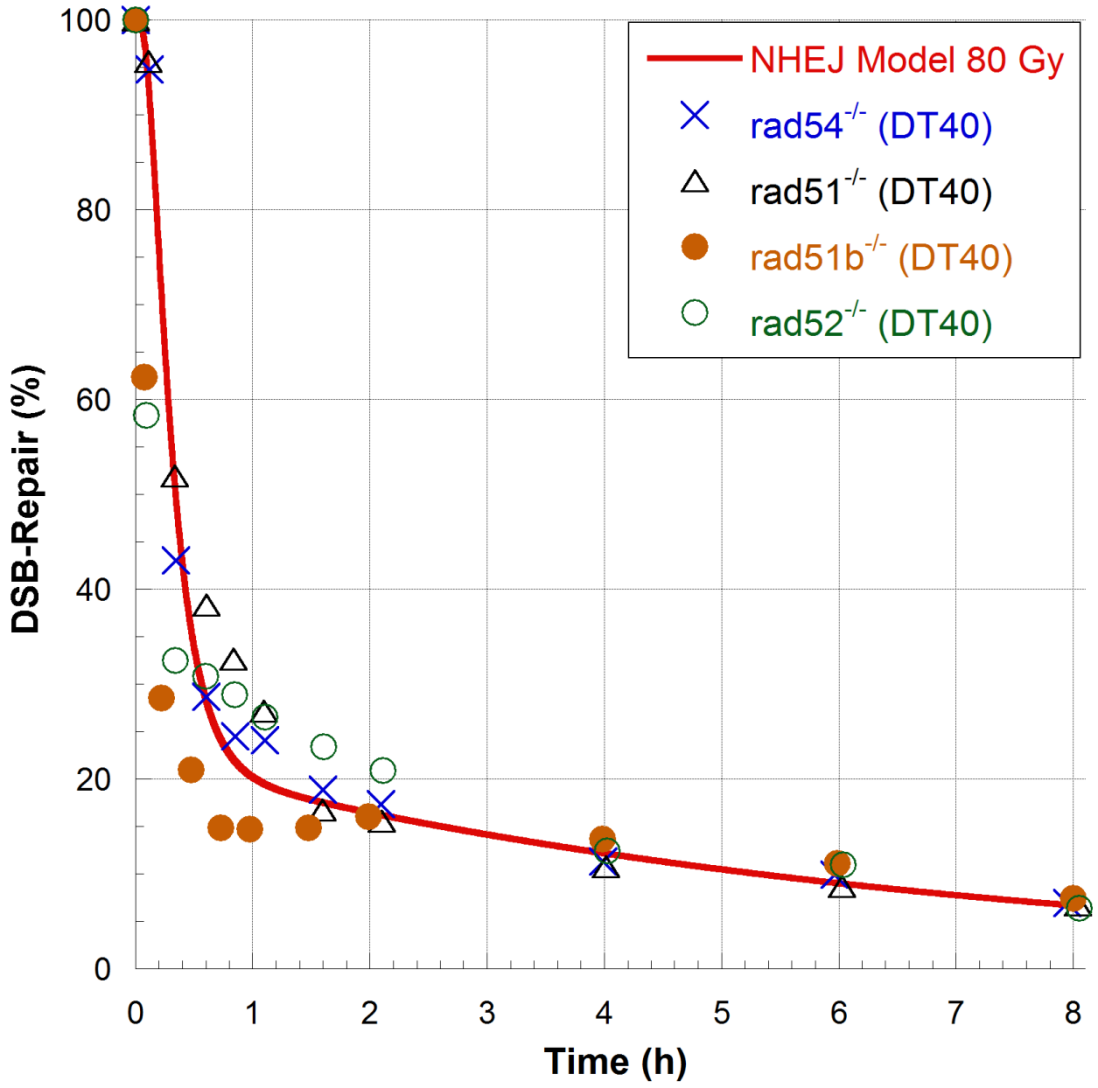

Figure 4.6 Repair kinetics of the double strand breaks by NHEJ model (solid line), and DT40 cells mutated in homologous recombination pathway (symbols) [19]. The DT40 cells are irradiated with 80 Gy X-rays and pulsed-field gel electrophoresis is used to measure the repair kinetics

4.2.2 G1 and Early S phases repair

The NHEJ model was proposed for cells mutated in HR pathway. Therefore NHEJ is suitable to model the DSB-repair of the photon irradiated cells where HR is not a dominant repair pathway. By increasing the LET of radiation exposure, HR becomes increasingly involved in the repair of the complex DSB in late S and G2 phases of the cell cycle. In our model we assume that the complex type DSB (defined as DSB in close proximity (within 10 bp) of a strand break) undergo resection. It is assumed that the complex DSB require further end processing (such as resection) because the actual binding site of NHEJ core repair proteins is about 10 bp [101, 271, 276, 277] and the presence of another SSB impairs repair activity of DSB proteins. In support of this assumption it is observed that increasing the LET results in higher level of resection

[25] that is probably due to higher frequency of complex type DSB. Resection activates repair processes such as HR and MMEJ. The most probable repair pathway for complex type DSB in late S and G2 is HR, because Rad51 foci in G1 cells are not observed indicating that HR is not active during G1 [278-280]. We assume that MMEJ could preserve the repair for the complex DSB in G1 and early S phases of the cell cycle. ATM phosphorylates KAP-1 that facilitates heterochromatin remodelling [25]. CtIP is phosphorylated by ATM and CDK2 that allows resection of the DSB to pursue homologous recombination repair in G2 cells. In G1 cells CtIP foci is not observed and it is shown that NHEJ repairs the DSB that are not resected [25]. It has been observed that CDK2 interacts with Mre11 and BRCA1 to promote HR repair in late S and G2 cells [281]. It has been suggested that DNA-PKcs binds rapidly to all DSB and makes the first attempt to repair by NHEJ in a fast process [25].

Figure 4.7 presents a model of DSB-repair pathway in G1 and early S phases of the cell cycle. In this model the repair proteins are sequentially recruited to the damage sites. Ku heterodimer and DNA-PKcs are required to form the synapsis. The simple type DSB are easily ligated, while the complex type DSB require further end processing that start with MRN resection. For the simple type DSB in the heterochromatin further end processing starts with Artemis/ATM proteins to relax the compact heterochromatin. The repair processes are described mathematically with a formulism based on the law of mass action. In the mathematical description of the model, protein concentrations are specified in the brackets, and nomenclatures Y_i, V_i, and K_i represent respectively the repair complex, repair rate, and repair rate constant at stage i of repair. The number of DSB is linearly proportional to radiation dose with DSB induction-rate per unit dose constant (α). The repair starts with the presynaptic process of NHEJ. Ku70/80 heterodimer is recruited to the DSB and inhibit MRN protein [130, 282]. The law of mass action is employed to derive equations 4.89 and 4.90 that explain Y_1 increases with the initial dose and decreases with Ku70 and Ku80 heterodimer recruitment at the site of damage. As explained in the earlier models, Ku70 and Ku80 heterodimer is the first repair protein to bind to the DSB.

$$\frac{dY_1}{dt} = \alpha \frac{dD}{dt} - V_1 \qquad 4.89$$

$$V_1 = K_1[Ku70, Ku80]Y_1 \qquad 4.90$$

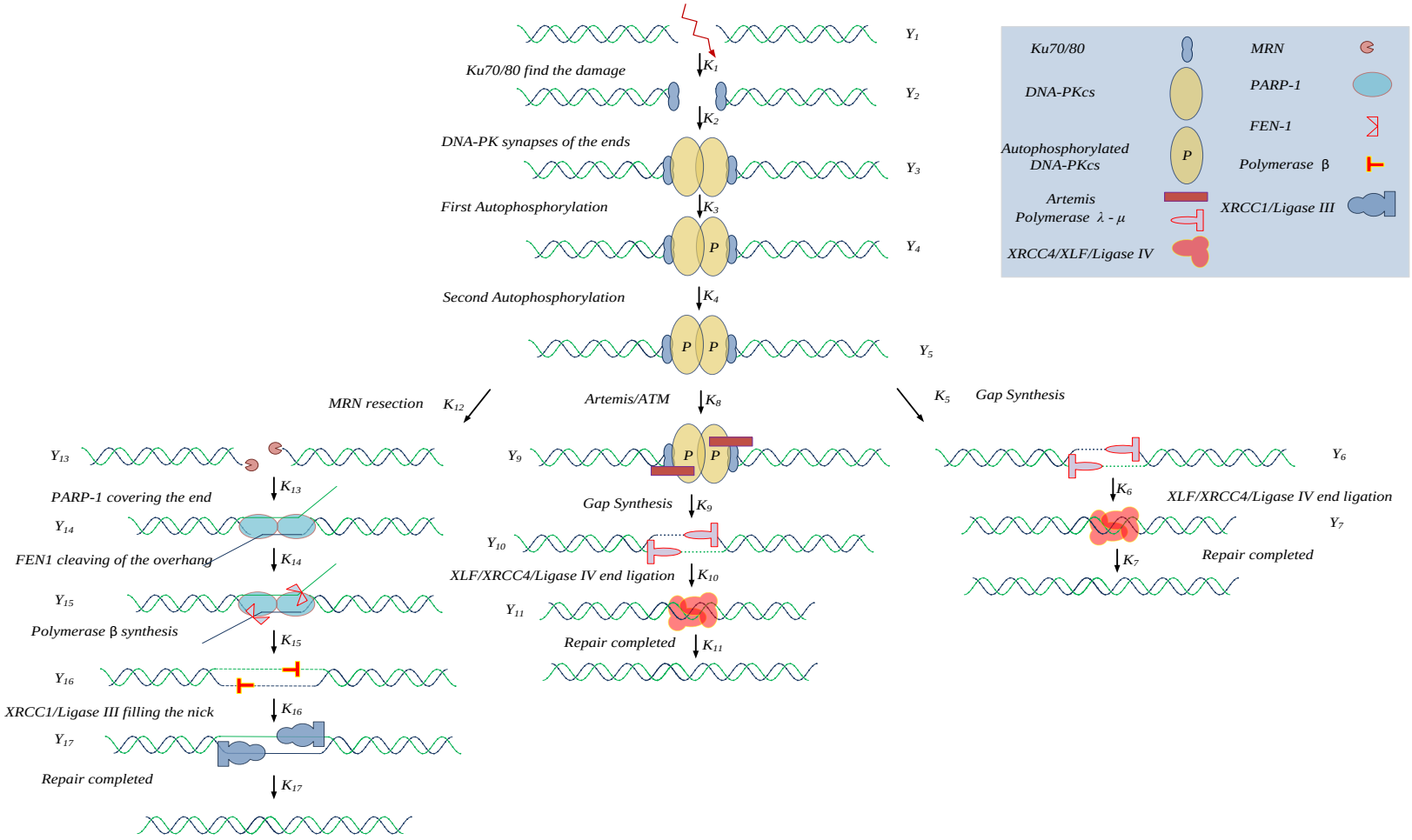

Figure 4.7 DSB-repair model in G1 and early S phases of the cell cycle is illustrated. The repair starts with Ku70/80 heterodimer recruitment to the damage and forming the synapsis with phosphorylated DNA-PKcs. The repair continues with simply ligation for simple type damage in the euchromatin. The simple type damage in the heterochromatin requires end processing starts with Artemis/ATM proteins to relax the compact heterochromatin. Finally the complex type damage undergoes resection with MRN and repair with MMEJ. The rate constants of the repair processes are shown with K_1 to K_{17}

The presynaptic steps are similar to NHEJ model that includes DNA-PKcs recruitment and autophosphorylation at ABCDE and PQR sites. These steps are explained with equations 4.91 to 4.96.

$$\frac{dY_2}{dt} = V_1 - V_2 \quad (4.91)$$

$$V_2 = K_2[DNA - PKcs]Y_2 \quad (4.92)$$

$$\frac{dY_3}{dt} = V_2 - V_3 \quad (4.93)$$

$$V_3 = K_3 Y_3 \quad (4.94)$$

$$\frac{dY_4}{dt} = V_3 - V_4 \quad (4.95)$$

$$V_4 = K_4 Y_4 \quad (4.96)$$

As explained earlier autophosphorylation of DNA-PKcs determines the process of repair. For simple type DSB in euchromatin the repair continues by NHEJ pathway. For simple type damage in the heterochromatin the repair continues by relaxing the compact heterochromatin. Finally, for the complex type DSB in euchromatin or heterochromatin the repair continues with resection that is explained by equations 4.97 to 4.100.

$$\frac{dY_5}{dt} = V_4 - V_5 - V_8 - V_{12} \quad (4.97)$$

$$V_5 = K_5[Polymerase\ \mu - \lambda]Y_5 \quad (4.98)$$

$$V_8 = K_8[Artemis, ATM]Y_5 \quad (4.99)$$

$$V_{12} = K_{12}[MRN]Y_5 \quad (4.100)$$

The simple DSB in euchromatin are ligated by the XLF/XRCC4/LIG IV complex and explained by equations 4.101 to 4.104. XRCC4 binds to both DNA and DNA ligase IV. XRCC4 and XLF play a key role in the recruitment DNA ligase IV and regulate its activity.

$$\frac{dY_6}{dt} = V_5 - V_6 \quad (4.101)$$

$$V_6 = K_6[XLF, XRCC\ 4, Lig\ IV]Y_6 \quad (4.102)$$

$$\frac{dY_7}{dt} = V_6 - V_7 \quad (4.103)$$

$$V_7 = K_7 Y_7 \quad 4.104$$

Artemis is involved with the fraction of DSB that are repaired slowly [107]. The DNA-PKcs phosphorylation of Artemis is essential for the endonuclease activity for the DSB in the HC series of actions including Artemis end processing, and ATM phosphorylation of KAP-1 is required for chromatin remodelling. ATM phosphorylates KAP-1 that facilitates heterochromatin remodelling [11-13, 25]. The repair is ensued by gap filling and ligation explained with equations 4.105 to 4.110. The second option for simple DSB in the heterochromatin is to undergo resection. We have not considered the second option in this model.

$$\frac{dY_9}{dt} = V_8 - V_9 \quad 4.105$$

$$V_9 = K_9[Polymerase\ \mu - \lambda]Y_9 \quad 4.106$$

$$\frac{dY_{10}}{dt} = V_9 - V_{10} \quad 4.107$$

$$V_{10} = K_{10}[XLF, XRCC\ 4, Lig\ IV]Y_{10} \quad 4.108$$

$$\frac{dY_{11}}{dt} = V_{10} - V_{11} \quad 4.109$$

$$V_{11} = K_{11}Y_{11} \quad 4.110$$

The complex DSB in G1 and early S phases of the cell cycle are assumed to undergo resection and repair by MMEJ. As MMEJ is masked by NHEJ, the proteins involved in DSB repair and their molecular mechanisms are not fully known yet [283]. Inhibition of the MRN complex components suggests that the MRN complex is involved in the resection of DSB that are consequently repaired by MMEJ [282, 284, 285]. PARP-1 is one of the proteins that is inhibited by the Ku heterodimer [130, 282] and is involved in MMEJ repair [286, 287]. PARP-1 is also involved in the initial steps of MMEJ repair after resection. It is proposed that PARP-1 may control the subsequent repair steps of MMEJ [130]. Equations 4.100 and 4.112 represent the MRN and PARP-1 initial processes leading to MMEJ repair.

$$\frac{dY_{13}}{dt} = V_{12} - V_{13} \quad 4.111$$

$$V_{13} = K_{13}[PARP - 1]Y_{13} \quad 4.112$$

The flap endonuclease 1 (FEN-1) removes the mismatched nucleotides as explained by equations 4.113 and 4.114 [288].

$$\frac{dY_{14}}{dt} = V_{13} - V_{14} \quad 4.113$$

$$V_{14} = K_{14}[FEN - 1]Y_{14} \quad 4.114$$

The final step of MMEJ repair is gap synthesis by Polymerase β [289] and ligation by the XRCC1/Ligase III complex [164, 290, 291] as described mathematically with equations 4.119 to 4.120.

$$\frac{dY_{15}}{dt} = V_{14} - V_{15} \quad 4.115$$

$$V_{15} = K_{15}[Polymerase\ \beta]Y_{15} \quad 4.116$$

$$\frac{dY_{16}}{dt} = V_{15} - V_{16} \quad 4.117$$

$$V_{16} = K_{16}[XRCC\ 1, Lig\ III]Y_{16} \quad 4.118$$

$$\frac{dY_{17}}{dt} = V_{16} - V_{17} \quad 4.119$$

$$V_{17} = K_{17}Y_{17} \quad 4.120$$

4.2.2.1 Scaling of DSB repair (G1 and early S) equations

In order to solve the system of equations the parameters have been scaled with a scaling factor C_i large enough to assure that the sum of total concentration of repair the complexes and proteins remain constant. For this purpose it is assumed that the sum of total concentration of the repair complexes and proteins (Y_i and E_i) is constant and equal to C_i. The scaling factor C_i is equal to a value >2800 (this is justified by assuming 35 DSB/Gy induced by 80 Gy radiation dose).

$$C_i = [E_i] + \sum_{i=1}^{17} Y_i = cte \quad 4.121$$

$$y_i = \frac{Y_i}{C_i} \quad 4.122$$

$$k_i = C_i K_i \quad 4.123$$

$$c_i = \frac{\sum_{i=1}^{17} y_i}{C_i} \quad 4.124$$

$$c'_i = \frac{\sum_{i=1}^{7} y_i}{C_i} \quad 4.125$$

$$c''_i = \frac{\sum_{i=1}^{11} y_i}{C_i} \quad 4.126$$

The following equations are derived considering the scaling factor C_i and substituting the new parameters in the model.

$$\frac{dy_1}{dt} = \frac{\alpha}{C_1}\frac{dD}{dt} - v_1 \quad 4.127$$

$$\frac{dy_2}{dt} = v_1 - v_2 \quad 4.128$$

$$\frac{dy_3}{dt} = v_2 - v_3 \quad 4.129$$

$$\frac{dy_4}{dt} = v_3 - v_4 \quad 4.130$$

$$\frac{dy_5}{dt} = v_4 - v_5 - v_8 - v_{12} \quad 4.131$$

$$\frac{dy_6}{dt} = v_5 - v_6 \quad 4.132$$

$$\frac{dy_7}{dt} = v_6 - v_7 \quad 4.133$$

$$\frac{dy_9}{dt} = v_8 - v_9 \quad 4.134$$

$$\frac{dy_{10}}{dt} = v_9 - v_{10} \quad 4.135$$

$$\frac{dy_{11}}{dt} = v_{10} - v_{11} \quad 4.136$$

$$\frac{dy_{13}}{dt} = v_{12} - v_{13} \quad 4.137$$

$$\frac{dy_{14}}{dt} = v_{13} - v_{14} \quad 4.138$$

$$\frac{dy_{15}}{dt} = v_{14} - v_{15} \quad 4.139$$

$$\frac{dy_{16}}{dt} = v_{15} - v_{16} \quad 4.140$$

$$\frac{dy_{17}}{dt} = v_{16} - v_{17} \quad 4.141$$

v_1 to v_{17} are shown with equations 4.142 to 4.158.

$$v_1 = k_1(1 - c_2)y_1 \quad 4.142$$

$$v_2 = k_2(1 - c_3)y_2 \quad 4.143$$

$$v_3 = K_3 y_3 \quad 4.144$$

$$v_4 = K_4 y_4 \quad 4.145$$

$$v_5 = k_5(1 - c'_6)y_5 \quad 4.146$$

$$v_6 = k_6(1 - c'_7)y_6 \quad 4.147$$

$$v_7 = K_7 y_5 \quad 4.148$$

$$v_8 = k_8(1 - c''_9)y_5 \quad 4.149$$

$$v_9 = k_9(1 - c''_9)y_9 \quad 4.150$$

$$v_{10} = k_{10}(1 - c''_{11})y_{10} \quad 4.151$$

$$v_{11} = K_{11} y_{11} \quad 4.152$$

$$v_{12} = k_{12}(1 - c_{13})y_5 \quad 4.153$$

$$v_{13} = k_{13}(1 - c_{14})y_{13} \quad 4.154$$

$$v_{14} = k_{14}(1 - c_{15})y_{14} \quad 4.155$$

$$v_{15} = k_{15}(1 - c_{16})y_{15} \quad 4.156$$

$$v_{16} = k_{16}(1 - c_{17})y_{16} \quad 4.157$$

$$v_{17} = K_{17} y_{17} \quad 4.158$$

4.2.2.2 Results of DSB repair (G1 and early S) kinetic model

In order to solve the system of equations the initial values and rate constants are required. The repair starts at time zero therefore the activity of all proteins is zero before radiation exposure. The maximum number of DSB damage (100%) is assumed to be induced at time zero. Table 4.3 lists the rate constants that are used to solve the repair model.

Table 4.3 Repair rate constants used in model calculations

Rate Constants	G1 and early S Model
k_1 (h^{-1})	350
k_2 (h^{-1})	500
K_3 (h^{-1})	50
K_4 (h^{-1})	20
k_5 (h^{-1})	25
k_6 (h^{-1})	18
K_7 (h^{-1})	3
k_8 (h^{-1})	9
k_9 (h^{-1})	2
k_{10} (h^{-1})	0.8
K_{11} (h^{-1})	0.5
k_{12} (h^{-1})	3
k_{13} (h^{-1})	1
k_{14} (h^{-1})	0.7
k_{15} (h^{-1})	0.75
k_{16} (h^{-1})	0.5
K_{17} (h^{-1})	0.15

The solution of the model provides the individual protein activity kinetics and overall DSB repair kinetics. Figure 4.6 illustrates the comparison of the overall repair kinetics from the model calculations and experimental measurements. The solid line and the symbols illustrate the repair kinetics for the repair model in G1 and early S, and experimental measurements [179, 187]. The experimental measurements are performed for V79 cells and primary human dermal fibroblasts. The V79 cells were irradiated with 45 Gy of ^{60}Co γ-rays and constant-field gel electrophoresis was used to measure the repair kinetics up to 2 hours. The primary human dermal fibroblasts were irradiated with 250 kV_P X-rays and pulsed-field gel electrophoresis was used to measure the repair kinetics up to about 30 hours.

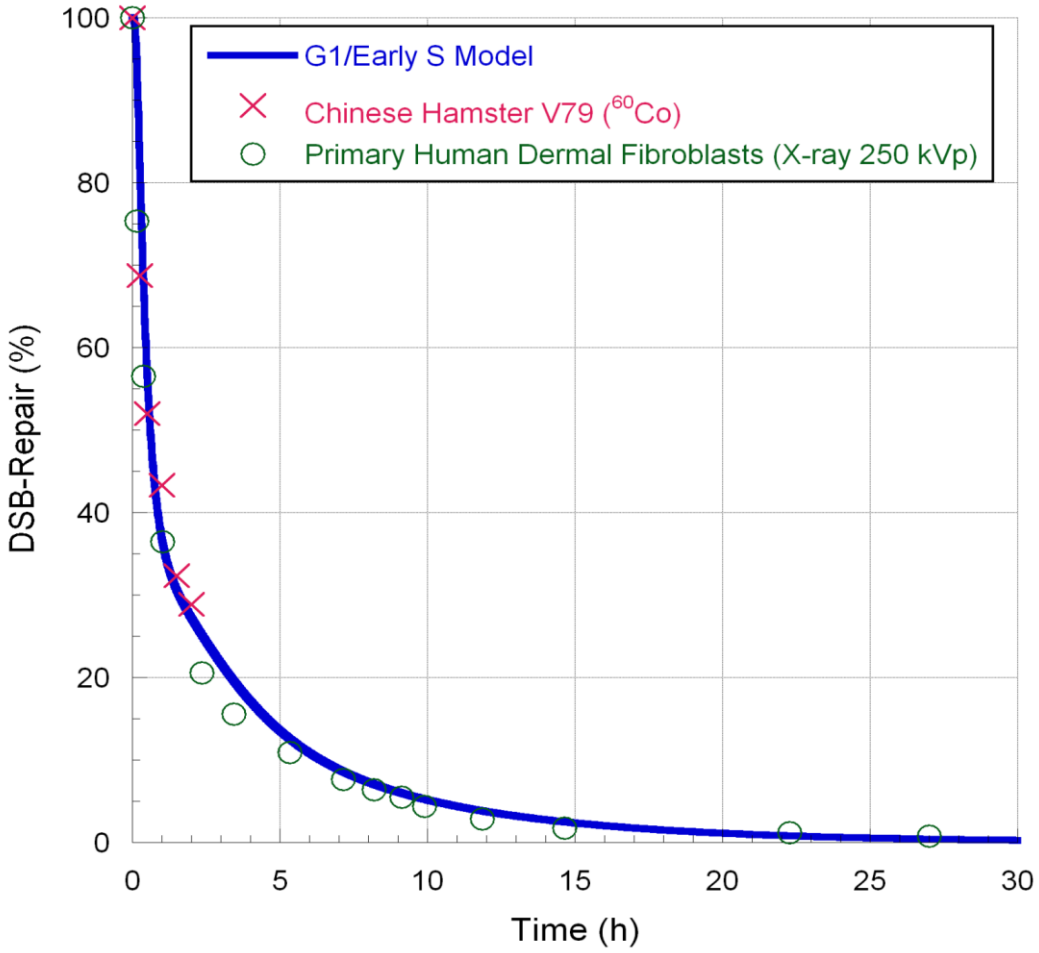

Figure 4.8 Repair kinetics of the double strand breaks by DSB-repair model in G1 and early S phases of the cell cycle (solid line) and V79 cells (X symbols) [179] and primary human dermal fibroblasts (Circles) [187]. The V79 cells were irradiated with 45 Gy of ^{60}Co γ-rays and constant-field gel electrophoresis is used to measure the repair kinetics. The primary human dermal fibroblasts were irradiated with 250 kV_P X-rays and pulsed-field gel electrophoresis is used to measure the repair kinetics.

4.2.3 Late S and G2 phases repair

In late S and G2 phases NHEJ and HR repair are actively involved in the repair of DSB. In late S and G2 phases, there might be competition between NHEJ and HR repair pathways or between Ku70 and the MRN complex [124]. Ku 70 inhibits MRN from resection. In the model all DSB are first recognized by the Ku70/80 heterodimer. Similar to NHEJ and early S and G1 models DNA-PKcs is recruited to the DSB. If the damage is simple, NHEJ repairs the DSB in a fast process. If the simple damage is in the heterochromatin similar to the model in early S and G1, the Artemis and ATM proteins start the process of relaxing the HC that delays the repair. Finally if the damage is complex, MRN starts resection and the DSB is repaired by the HR pathway. Figure 4.9 presents a model of DSB-repair pathway in late S and G2 phases of the cell cycle. The proteins are sequentially recruited at the site of DSB for different types and topology of DSB.

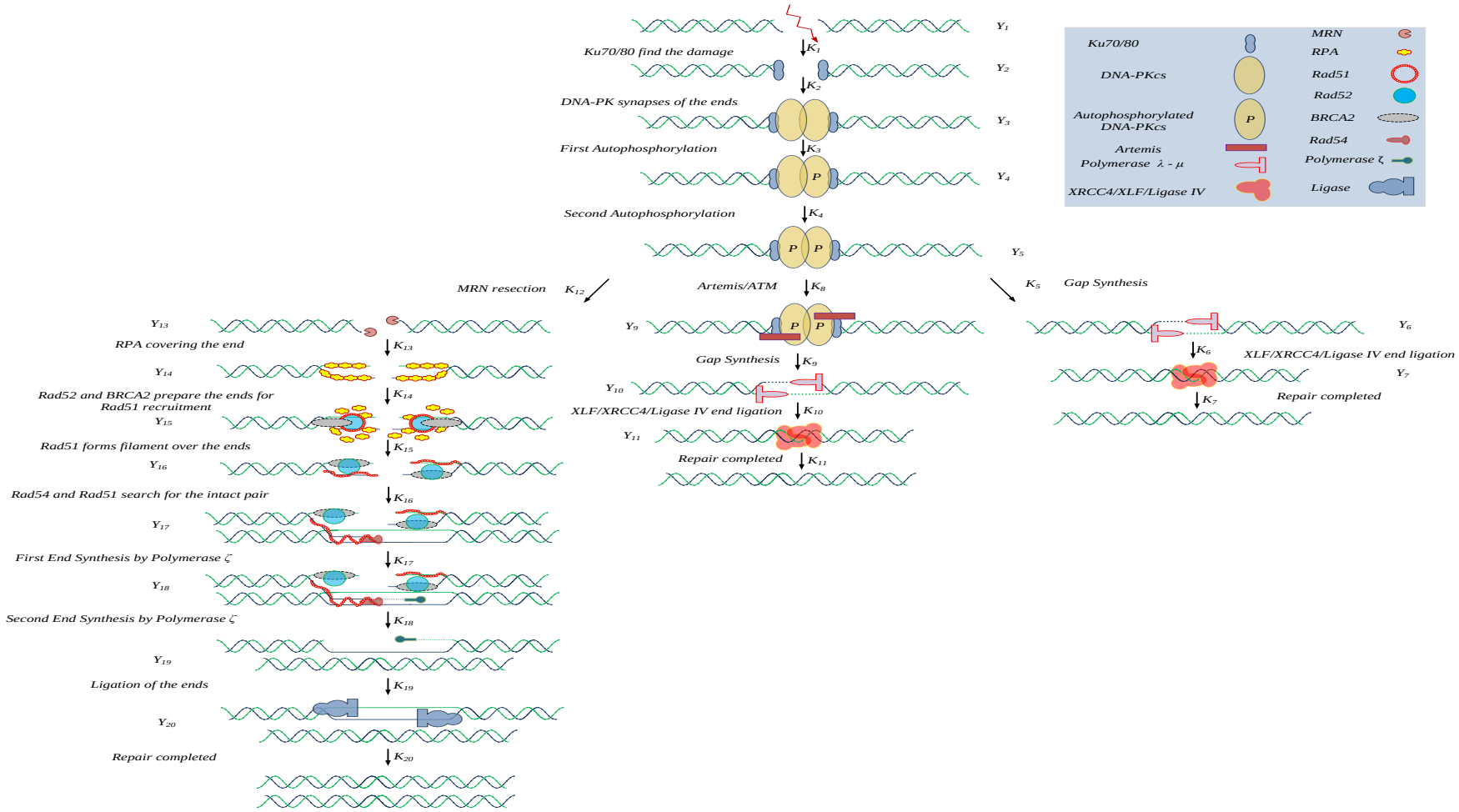

Figure 4.9 DSB-repair model in late S and G2 phases of the cell cycle is illustrated. The repair starts with Ku70/80 heterodimer recruitment to the damage and performing the synapsis with phosphorylated DNA-PKcs. The repair continues with simply ligation for simple type damage in the euchromatin. The simple type damage in the heterochromatin requires end processing starts with Artemis/ATM proteins to relax the compact heterochromatin. Finally the complex type damage undergoes resection by MRN and repair by HR. The rate constants of the repair processes are shown with K_1 to K_{20}

The repair processes are described mathematically with a formulism based on the law of mass action. In the mathematical description of the model, protein concentrations are specified in the brackets, and nomenclatures Y_i, V_i, and K_i represent respectively the repair complex, repair rate, and repair rate constant at step i of repair. The number of DSB is linearly proportional to radiation dose with DSB induction-rate per unit dose constant (α). The repair starts with the presynaptic process of NHEJ. Ku70/80 heterodimer is recruited to the DSB and inhibit MRN protein [130, 282]. The law of mass action is employed to derive equations 4.159 and 4.160 that explain Y_1 increases with the initial dose and decreases with Ku70/80 heterodimer recruitment at the site of damage.

$$\frac{dY_1}{dt} = \alpha \frac{dD}{dt} - V_1 \qquad 4.159$$

$$V_1 = K_1[Ku70, Ku80]Y_1 \qquad 4.160$$

The presynaptic steps are similar to the NHEJ model that includes DNA-PKcs recruitment and autophosphorylation at ABCDE and PQR sites. These steps are explained with equations 4.161 to 4.166.

$$\frac{dY_2}{dt} = V_1 - V_2 \qquad 4.161$$

$$V_2 = K_2[DNA - PKcs]Y_2 \qquad 4.162$$

$$\frac{dY_3}{dt} = V_2 - V_3 \qquad 4.163$$

$$V_3 = K_3Y_3 \qquad 4.164$$

$$\frac{dY_4}{dt} = V_3 - V_4 \qquad 4.165$$

$$V_4 = K_4Y_4 \qquad 4.166$$

Similar to the model in G1 and early S phases of the cell cycle, depending on the type of DSB the repair process ensues with fast ligation of simple DSB, further end-processing and relaxation of the HC as illustrated in Figure 4.9. Since the model for simple type DSB, and DSB in the HC is identical to G1 and early S phases of the cell cycle, the explanations for equations 4.167 to 4.180 are as explained in section 4.2.2.

$$\frac{dY_5}{dt} = V_4 - V_5 - V_8 - V_{12} \qquad 4.167$$

$$V_5 = K_5[Polymerase\ \mu - \lambda]Y_5 \qquad 4.168$$

$$V_8 = K_8[Artemis, ATM]Y_5 \quad 4.169$$

$$V_{12} = K_{12}[MRN]Y_5 \quad 4.170$$

$$\frac{dY_6}{dt} = V_5 - V_6 \quad 4.171$$

$$V_6 = K_6[XLF, XRCC\ 4, Lig\ IV]Y_6 \quad 4.172$$

$$\frac{dY_7}{dt} = V_6 - V_7 \quad 4.173$$

$$V_7 = K_7Y_7 \quad 4.174$$

$$\frac{dY_9}{dt} = V_8 - V_9 \quad 4.175$$

$$V_9 = K_9[Polymerase\ \mu - \lambda]Y_9 \quad 4.176$$

$$\frac{dY_{10}}{dt} = V_9 - V_{10} \quad 4.177$$

$$V_{10} = K_{10}[XLF, XRCC\ 4, Lig\ IV]Y_{10} \quad 4.178$$

$$\frac{dY_{11}}{dt} = V_{10} - V_{11} \quad 4.179$$

$$V_{11} = K_{11}Y_{11} \quad 4.180$$

The initial step for homologous recombination repair is 5'-3' resection that is nucleolytic degradation of 5' end to 3' [292]. The single stranded DNA can be aligned to the homology strand prior to ligation. After resection by MRN, RPA binds strongly to the single stranded DNA and removes all secondary structures [293] explained by equations 4.181 and 4.182.

$$\frac{dY_{13}}{dt} = V_{12} - V_{13} \quad 4.181$$

$$V_{13} = K_{13}[RPA]Y_{13} \quad 4.182$$

Phosphorylation of RPA allows Rad52 and BRCA2 recruitment at the site of damage [262, 294]. Rad52 and BRCA2 mediate recruitment of Rad51 in mammalian cells [259, 260] , explained by equations 4.183 and 4.184.

Rad52

$$\frac{dY_{14}}{dt} = V_{13} - V_{14} \quad 4.183$$

$$V_{14} = K_{14}[Rad52, BRCA\ 2]Y_{14} \quad 4.184$$

Rad51 is the central protein in HR pathway. Rad51 forms a filament over the single stranded DNA, explained by equations 4.185 and 4.186

$$\frac{dY_{15}}{dt} = V_{14} - V_{15} \quad 4.185$$

$$V_{15} = K_{15}[Rad51]Y_{15} \quad 4.186$$

Rad 54 mediates Rad51 in finding the intact DNA and forming the displacement loop (D-loop) that is explained by equations 4.187 and 4.188

$$\frac{dY_{16}}{dt} = V_{15} - V_{16} \quad 4.187$$

$$V_{16} = K_{16}[Rad51, Rad54]Y_{16} \quad 4.188$$

It has been shown that the polymerase ζ is most probably involved the DNA synthesis [295, 296]. Equations 4.189 and 4.190, and equations 4.191 and 4.192 show the first and second strand synthesis.

$$\frac{dY_{17}}{dt} = V_{16} - V_{17} \quad 4.189$$

$$V_{17} = K_{17}[Pol\zeta(1)]Y_{17} \quad 4.190$$

$$\frac{dY_{18}}{dt} = V_{17} - V_{18} \quad 4.191$$

$$V_{18} = K_{18}[Pol\zeta(2)]Y_{18} \quad 4.192$$

The final step of homologous recombination repair is sealing the nick by DNA ligase that is explained with equations 4.193 to 4.196

$$\frac{dY_{19}}{dt} = V_{18} - V_{19} \quad 4.193$$

$$V_{19} = K_{19}[Ligase]Y_{19} \quad 4.194$$

$$\frac{dY_{20}}{dt} = V_{19} - V_{20} \quad 4.195$$

$$V_{20} = K_{20}Y_{20} \quad 4.196$$

4.2.3.1 Scaling of DSB repair (G2 and late S) equations

In order to solve the system of equations the parameters have been scaled with a scaling factor C_i large enough to assure that the sum of total concentration of the repair complexes and proteins remain constant. For this purpose it is assumed that the sum of total concentration of the repair complexes and proteins (Y_i and E_i) is constant and equal to C_i. The scaling factor C_i is equal to a value >2800 (this is justified by assuming 35 DSB/Gy induced by 80 Gy radiation dose).

$$C_i = [E_i] + \sum_{i=1}^{20} Y_i = cte \quad 4.197$$

$$y_i = \frac{Y_i}{C_i} \quad 4.198$$

$$k_i = C_i K_i \quad 4.199$$

$$c_i = \frac{\sum_{i=1}^{20} y_i}{C_i} \quad 4.200$$

$$c'_i = \frac{\sum_{i=1}^{7} y_i}{C_i} \quad 4.201$$

$$c''_i = \frac{\sum_{i=1}^{11} y_i}{C_i} \quad 4.202$$

Equations 4.203 to 4.240 are derived considering the scaling factor C_i and substituting the new parameters in the model.

$$\frac{dy_1}{dt} = \frac{\alpha}{C_1}\frac{dD}{dt} - v_1 \quad 4.203$$

$$\frac{dy_2}{dt} = v_1 - v_2 \quad 4.204$$

$$\frac{dy_3}{dt} = v_2 - v_3 \quad 4.205$$

$$\frac{dy_4}{dt} = v_3 - v_4 \quad 4.206$$

$$\frac{dy_5}{dt} = v_4 - v_5 - v_8 - v_{12} \quad 4.207$$

$$\frac{dy_6}{dt} = v_5 - v_6 \quad 4.208$$

$$\frac{dy_7}{dt} = v_6 - v_7 \quad 4.209$$

$$\frac{dy_9}{dt} = v_8 - v_9 \quad 4.210$$

$$\frac{dy_{10}}{dt} = v_9 - v_{10} \quad 4.211$$

$$\frac{dy_{11}}{dt} = v_{10} - v_{11} \quad 4.212$$

$$\frac{dy_{13}}{dt} = v_{12} - v_{13} \quad 4.213$$

$$\frac{dy_{14}}{dt} = v_{13} - v_{14} \quad 4.214$$

$$\frac{dy_{15}}{dt} = v_{14} - v_{15} \quad 4.215$$

$$\frac{dy_{16}}{dt} = v_{15} - v_{16} \quad 4.216$$

$$\frac{dy_{17}}{dt} = v_{16} - v_{17} \quad 4.217$$

$$\frac{dy_{18}}{dt} = v_{17} - v_{18} \quad 4.218$$

$$\frac{dy_{19}}{dt} = v_{18} - v_{19} \quad 4.219$$

$$\frac{dy_{20}}{dt} = v_{19} - v_{20} \quad 4.220$$

v_1 to v_{20} are shown with equations 4.221 to 4.240.

$$v_1 = k_1(1 - c_2)y_1 \quad 4.221$$

$$v_2 = k_2(1 - c_3)y_2 \quad 4.222$$

$$v_3 = K_3 y_3 \quad 4.223$$

$$v_4 = K_4 y_4 \quad 4.224$$

$$v_5 = k_5(1 - c'_6) y_5 \quad 4.225$$

$$v_6 = k_6(1 - c'_7) y_6 \quad 4.226$$

$$v_7 = K_7 y_5 \quad 4.227$$

$$v_8 = k_8(1 - c''_9) y_5 \quad 4.228$$

$$v_9 = k_9(1 - c''_9) y_9 \quad 4.229$$

$$v_{10} = k_{10}(1 - c''_{11}) y_{10} \quad 4.230$$

$$v_{11} = K_{11} y_{11} \quad 4.231$$

$$v_{12} = k_{12}(1 - c_{13}) y_5 \quad 4.232$$

$$v_{13} = k_{13}(1 - c_{14}) y_{13} \quad 4.233$$

$$v_{14} = k_{14}(1 - c_{15}) y_{14} \quad 4.234$$

$$v_{15} = k_{15}(1 - c_{16}) y_{15} \quad 4.235$$

$$v_{16} = k_{16}(1 - c_{17}) y_{16} \quad 4.236$$

$$v_{17} = k_{17}(1 - c_{18}) y_{17} \quad 4.237$$

$$v_{18} = k_{18}(1 - c_{19}) y_{18} \quad 4.238$$

$$v_{19} = k_{19}(1 - c_{20}) y_{19} \quad 4.239$$

$$v_{20} = K_{20} y_{20} \quad 4.240$$

4.2.3.2 Results of DSB repair (G2 and late S) kinetic model

In order to solve the system of equations the initial values and rate constants are required. The repair starts at time zero therefore the activity of all proteins is zero before radiation exposure. The maximum number of DSB damage (100%) is assumed to be induced at time zero. Table 4.4 lists the rate constants that are used to solve the repair model.

Table 4.4 Repair rate constants used in model calculations

Rate Constants	Late S and G2 Model
k_1 (h^{-1})	350
k_2 (h^{-1})	500
K_3 (h^{-1})	50
K_4 (h^{-1})	20
k_5 (h^{-1})	25
k_6 (h^{-1})	18
K_7 (h^{-1})	3
k_8 (h^{-1})	9
k_9 (h^{-1})	2
k_{10} (h^{-1})	0.8
K_{11} (h^{-1})	0.5
k_{12} (h^{-1})	3
k_{13} (h^{-1})	1
k_{14} (h^{-1})	0.7
k_{15} (h^{-1})	0.75
k_{16} (h^{-1})	0.5
k_{17} (h^{-1})	0.5
k_{18} (h^{-1})	0.5
k_{19} (h^{-1})	0.5
K_{20} (h^{-1})	0.15

The solution of the model provides the individual protein activity kinetics and overall DSB repair kinetics. Figure 4.10 illustrates the comparison of the overall repair kinetics from the model calculations and experimental measurements. The solid line and the symbols illustrate the repair kinetics for the repair model in G2 and late S phases of the cell cycle, and experimental measurements [179, 187]. The experimental measurements

are performed for V79 cells and primary human dermal fibroblasts. The V79 cells were irradiated with 45 Gy of ^{60}Co γ-rays and constant-field gel electrophoresis was used to measure the repair kinetics up to 2 hours. The primary human dermal fibroblasts were irradiated with 250 kV_P X-rays and pulsed-field gel electrophoresis was used to measure the repair kinetics up to about 30 hours. The same experimental data sets are used to compare with the models in late S and G2 phases, and in G1 and early S phases. It is preferred to use repair kinetics of synchronized cells in different phases of the cell cycle. Unfortunately these data were not available. However, PFGE kinetic experiments do not show different DSB repair kinetics for G1 and G2 cell cycle phases [26].

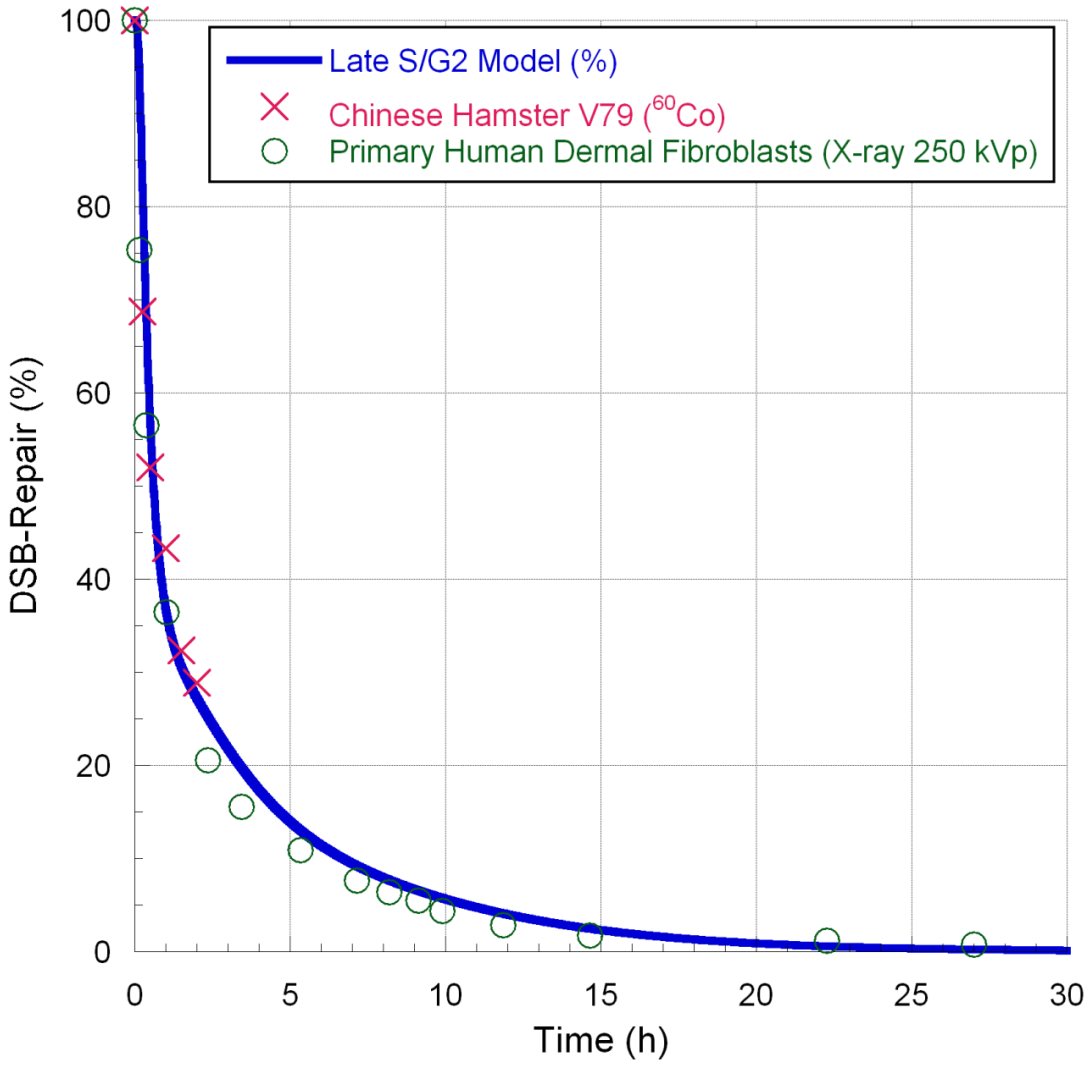

Figure 4.10 Repair kinetics of the double strand breaks by DSB-repair model in late S and G2 phases of the cell cycle (solid line) and V79 cells (X symbols) [179] and primary human dermal fibroblasts (Circles) [187]. The V79 cells were irradiated with 45 Gy of ^{60}Co γ-rays and constant-field gel electrophoresis was used to measure the repair kinetics. The primary human dermal fibroblasts were irradiated with 250 kV_P X-rays and pulsed-field gel electrophoresis was used to measure the repair kinetics.

5 APPLICATION OF DSB-REPAIR MODEL

The solution of repair models could not be directly integrated to the damage simulation. Therefore, first the damage (including induction of DSB) was simulated using Monte Carlo track structure methods, and subsequently those DSBs either in simple or complex form were subjected to the repair model. The repair model uses the law of mass action to derive kinetic rate equations. The equation for every stage explains the biochemical repair action by a specific protein at that stage. The complete sequential repair process composes a system of nonlinear differential equations. The solution of the system of nonlinear differential equations yields the overall repair kinetics and kinetics of every stage of repair. The overall repair kinetics are compared with experimental repair kinetics measured with PFGE for a total dose of 20 to 100 Gy. By assuming 35 DSB per Gy, a total dose of 20 to 100 Gy results in 700 to 3500 DSB. Therefore the overall repair kinetics is calculated for 700 to 3500 DSB. In order to apply the repair models for the repair of damage induced by radiation and calculated by track-structure models, the inverse transform sampling method is used. In this method the repair kinetics for a single DSB are calculated by sampling from the repair kinetics of 700 to 3500 DSB. For this purpose it is required to assume that the repair kinetics do not saturate at high doses up to 100 Gy. For normal cells (not repair deficient), the repair in terms of kinetic response for different doses of radiation is the same. For doses from 10 to 80 Gy, the PFGE experiment shows similar repair kinetics [232, 297, 298]. Using γ-H2AX foci kinetics time course of repair from 0.02 to 2 Gy [232, 299], (although this is not an accurate method for repair kinetics analysis) the unrepaired DSB fraction (residual foci) is 10% after 24 hours [298]. Therefore both PFGE experiments from 10 to 80 Gy and γ-H2AX experiment from 0.02 to 2 Gy show DSB repair kinetics do not saturate with increasing dose up to 80 Gy. In other words it is assumed that a single track effect is the dominant process to induce the damage. Lindborg and colleagues (14) calculated the integral proximity function for ^{60}Co γ-rays and the mean energy imparted for doses of 2, 22, and 60 Gy for different target sizes [300]. From their calculation it is shown that for doses less than 60 Gy, the maximum target size that single track effect dominates is radii of about 70 nm. In other words, since the definition of DSB in the DNA is bi-stranded damage within 2-3 helical turns for doses as high as 60 Gy, the probability of multiple track effects or interaction of pairwise DSB is negligible prior to repair.

In order to perform inverse transform sampling it is assumed that the probability density function (PDF) at every stage of repair is equal to repair activity kinetics normalized to the area under the curve. The PDF is converted to cumulative distribution function (CDF) by cumulative integration over time. By inverse transform sampling of the CDF, it is possible to calculate the time required for each protein to perform its repair action at each stage of repair for a DSB induced by a single track of radiation. The DSB were divided into two main categories of simple and complex types according to our original definition [7]. The final models of repair consider separate pathways for DSB in the heterochromatin region. In those models it is assumed that about 15 % of simple DSB fall into the heterochromatin regions. Therefore, it is possible to investigate the repair time required for every separate protein to perform DSB end modifications and repair, in

addition the average repair kinetics for the simple, and complex DSB is separately calculated.

5.1 LOW ENERGY ELECTRON AND ULTRASOFT X-RAY DAMAGE AND REPAIR

Low energy electrons are of great importance, because a high fraction of energy depositions by ions and photons is through low energy electrons. Experiments using Auger electron emitters and Ultrasoft X-rays with low energy electrons are frequently performed to study DNA damage. The advantage of Auger electron experiments is the very short range of the electrons that is in the order of the size of the cell nucleus.

5.1.1 Damage Simulation

Low energy X-rays (ultrasoft X-rays) such as C_K, Al_K and Ti_K X-rays were used in various radiobiological investigations [301, 302]. Electron tracks with energies from 100 eV to 4.55 keV and ultrasoft X-rays were simulated with the KURBUC-liq code [15, 303-307]. For Ti_K X-rays it is assumed that the electrons are monoenergetic with the energy of 4.55 keV. The electron spectrum for ultrasoft X-rays was generated with X-ray interactions in soft-tissue [308]. The electron spectrum following the absorption of C_K, and Al_K X-rays takes into account all possible Auger and photoelectron emissions from the K, L, M and N shells. Table 5.1 and Table 5.2 summarize the electrons spectrum for C_K, and Al_K X-rays, respectively. The first column lists the frequency of occurrence per 1000. The damage could occur in the DNA or rest of the cell noted by type 1 and type 2 respectively. The atom is left ionized after emission of Auger electrons with the energy known as residual potential energy (RPE). The final columns list the electron energies.

The Monte Carlo track structure simulations are done at three stages, Physical, Prechemical, and Chemical. The electron energy spectrum is sampled to derive the energy of electrons for each run. KURBUC-liq follows primary and secondary electron interactions including excitation, ionization, and elastic scattering in liquid water event by event. In KURBUC-liq the elastic scattering cross sections remain the same as the KURBUC vapour cross sections [309], while new cross sections for inelastic scattering based on dielectric response model [310] is used. For each inelastic collision the location, amount of deposited energy and type of interaction is recorded. The physical tracks are run for monoenergetic electrons with energies of 100, 200, 300, 400, 500, 1000, 1500, and 4550 eV and C_K, and Al_K X-rays. The physical electron tracks for a single track of electrons with energies 100, 200, 300, 400, 500, 1000, 1500, and 4550 eV are shown in Figure 5.1. In the prechemical stage (10^{-15} s to 10^{-12} s) ionization and excitation of water molecules develop into free radical species. The water species are listed in Table 5.3 per radiation track.

Table 5.1 Electron spectrum for C_K X-ray [308]

Frequency per 1000	Type [a]	RPE (eV) [b]	Electron spectrum (eV)			
519	2	29	249	0	0	0
374.2	2	13	265	0	0	0
50.6	2	21	257	0	0	0
22.4	2	33	137	108	0	0
13.6	2	35	171	72	0	0
4.1	2	38	240	0	0	0
3.8	1	33	137	108	0	0
2.3	1	29	249	0	0	0
1.5	1	12	266	0	0	0
1.1	2	53	210	15	0	0
1.1	2	64	108	84	22	0
1.1	1	20	258	0	0	0
1	2	30	204	44	0	0
1	2	64	139	44	31	0
0.8	2	78	171	29	0	0
0.7	2	33	161	84	0	0
0.4	2	24	217	37	0	0
0.4	1	64	108	84	22	0
0.3	2	13	221	44	0	0
0.3	1	33	161	84	0	0
0.2	1	17	261	0	0	0
0.1	2	17	247	14	0	0
0	0	0	0	0	0	0

[a] Interaction in the DNA type 1, interaction in the remainder of the cell type 2

[b] After the emission of Auger electrons the original atom is left ionized, carrying a potential energy due to its charge known as residual potential energy (RPE).

Table 5.2 Electron spectrum for Al_K X-ray [311]

Frequency per 1000	Type [a]	RPE (eV) [b]	Electron spectrum (eV)				
849.9	2	32	950	505	0	0	0
58.2	2	42	1198	247	0	0	0
46.5	2	29	1458	0	0	0	0
25.7	2	42	1083	362	0	0	0
2.9	2	19	1468	0	0	0	0
2.7	1	32	950	505	0	0	0
2	2	69	1105	261	33	19	0
1.9	2	92	937	410	28	20	0
1.3	2	42	1198	247	0	0	0
1.1	2	113	1105	217	30	22	0
0.9	2	61	972	410	44	0	0
0.8	1	42	1083	362	0	0	0
0.7	2	36	1281	170	0	0	0
0.7	2	12	1475	0	0	0	0
0.6	2	30	1273	184	0	0	0
0.5	2	74	1253	131	29	0	0
0.49	2	67	1293	104	23	0	0
0.4	2	80	1212	170	25	0	0
0.4	2	123	766	518	47	33	0
0.3	2	138	1098	177	49	25	0
0.2	2	30	1317	140	0	0	0
0.2	2	60	1105	289	33	0	0
0.2	2	116	766	518	87	0	0
0.2	1	29	1458	0	0	0	0
0.1	2	20	1419	28	20	0	0
0.1	2	36	1451	0	0	0	0
0.1	2	37	1346	104	0	0	0
0.1	2	36	1212	239	0	0	0
0.1	2	56	1186	218	27	0	0
0.1	2	143	1044	250	37	13	0
0.1	2	214	636	518	48	39	32
0.1	2	20	1387	47	33	0	0
0.1	1	19	1468	0	0	0	0
0.1	1	12	1475	0	0	0	0
0.1	1	68	1293	103	23	0	0
0.1	1	30	1293	164	0	0	0
0.1	1	37	1346	104	0	0	0
0	0	0	0	0	0	0	0

[a] Interaction in the DNA type 1, Interaction in the remainder of the cell type 2

[b] After the emission of Auger electrons the original atom is left ionized, carrying a potential energy due to its charge known as residual potential energy (RPE).

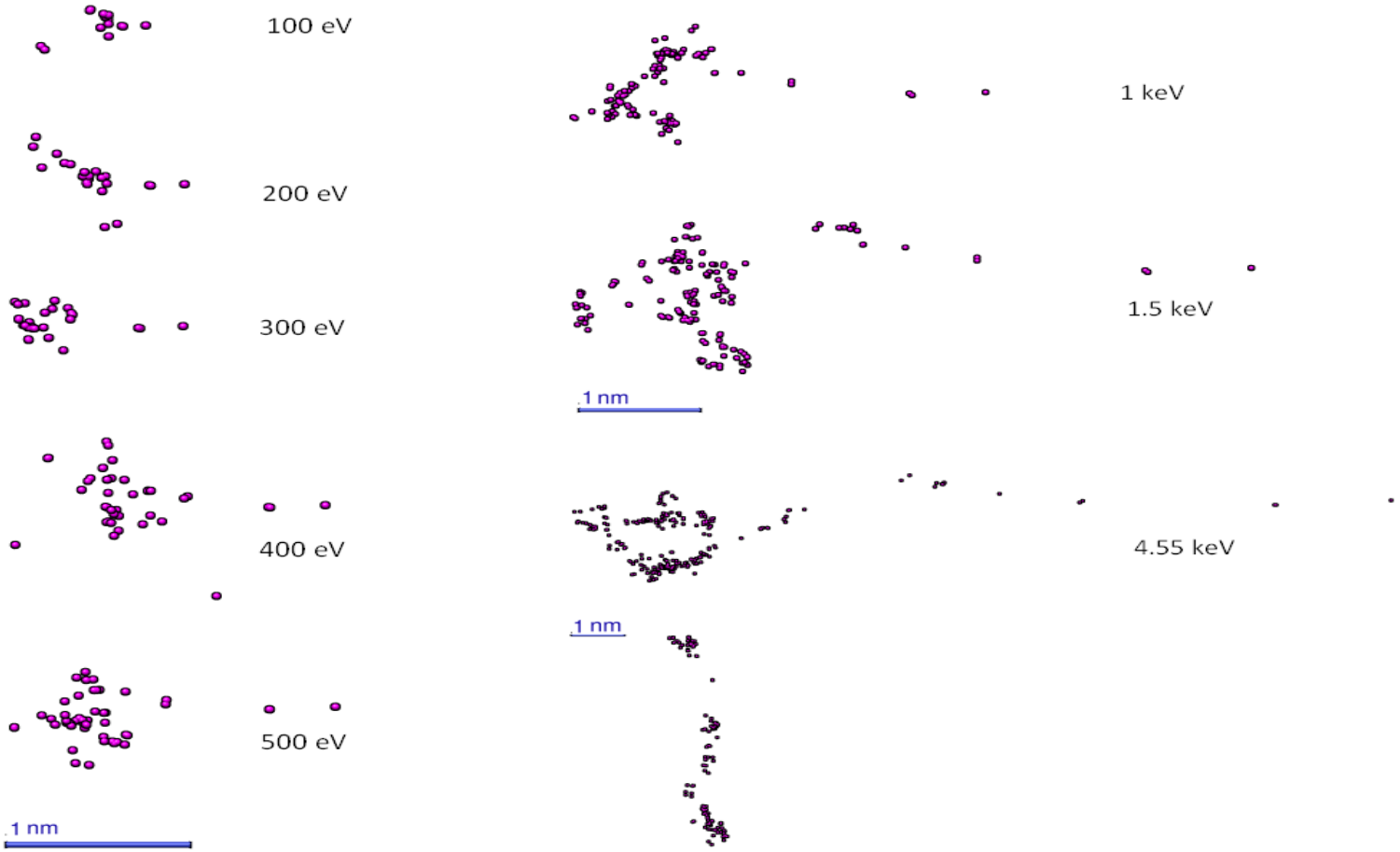

Figure 5.1 Electron tracks for single track of electrons with energies 100 eV to 4.55 keV. The electron tracks were simulated with the electron track structure code KURBUC-liq [303, 304, 306, 307]

Table 5.3 Yield of water species per radiation track at 10^{-12}s.

Energy (eV)	100	200	300	400	500	1000	1500	4550	C_K X-ray	Al_K X-ray
Total species	177	348	517	688	858	1702	2531	7627	488	2537
OH	57	116	173	232	290	580	861	2608	161	859
e_{aq}^-	51	95	140	183	228	448	663	1988	137	674
H	16	32	43	60	72	142	209	633	44	215
H_3O^+	41	85	130	173	218	438	652	1975	117	644
H_2	6	10	16	20	25	47	73	211	15	73
H_2O_2	6	10	16	20	25	47	73	211	15	73
HO_2	-	-	-	-	-	-	-	-	-	-
O_2	-	-	-	-	-	-	-	-	-	-
OH^-	-	-	-	-	-	-	-	-	-	-
O_2^-	-	-	-	-	-	-	-	-	-	-
HO_2^-	-	-	-	-	-	-	-	-	-	-

In the chemical stages the water radicals are diffused (10^{-12} s to 10^{-9} s) and followed with their reactions. The radical diffusion is followed up to 10^{-9} s that is relevant to ~4 nm diffusion [312, 313]. The model of damage considers direct energy deposition in the DNA and indirect damage contribution by water radicals. A molecular B-DNA model is considered as target. The diameter of the DNA molecule is 2.3 nm and the length is 54 bp. The direct energy deposition to the sugar-phosphate backbone exceeding 15 eV leads to single strand break. The value of 17.5 $\pm$2.5 eV was calculated [314] by comparing to experimental damage induced by ^{125}I decay [315]. 20% of the OH radicals that reach the DNA interact with the sugar-phosphate backbone and 80 % of the OH radicals interact with nucleobases. 65 % of sugar-phosphate radicals lead to SSB. Therefore 0.13 is the activation probability of OH radical interaction with sugar-phosphate backbone that lead to SSB [316]. All the OH radicals that react with nucleobases are assumed to lead to base damage. Table 5.4 lists the number of damages with the threshold energy of 15 eV and 17.5 eV for direct damage induction in comparison to experimental results.

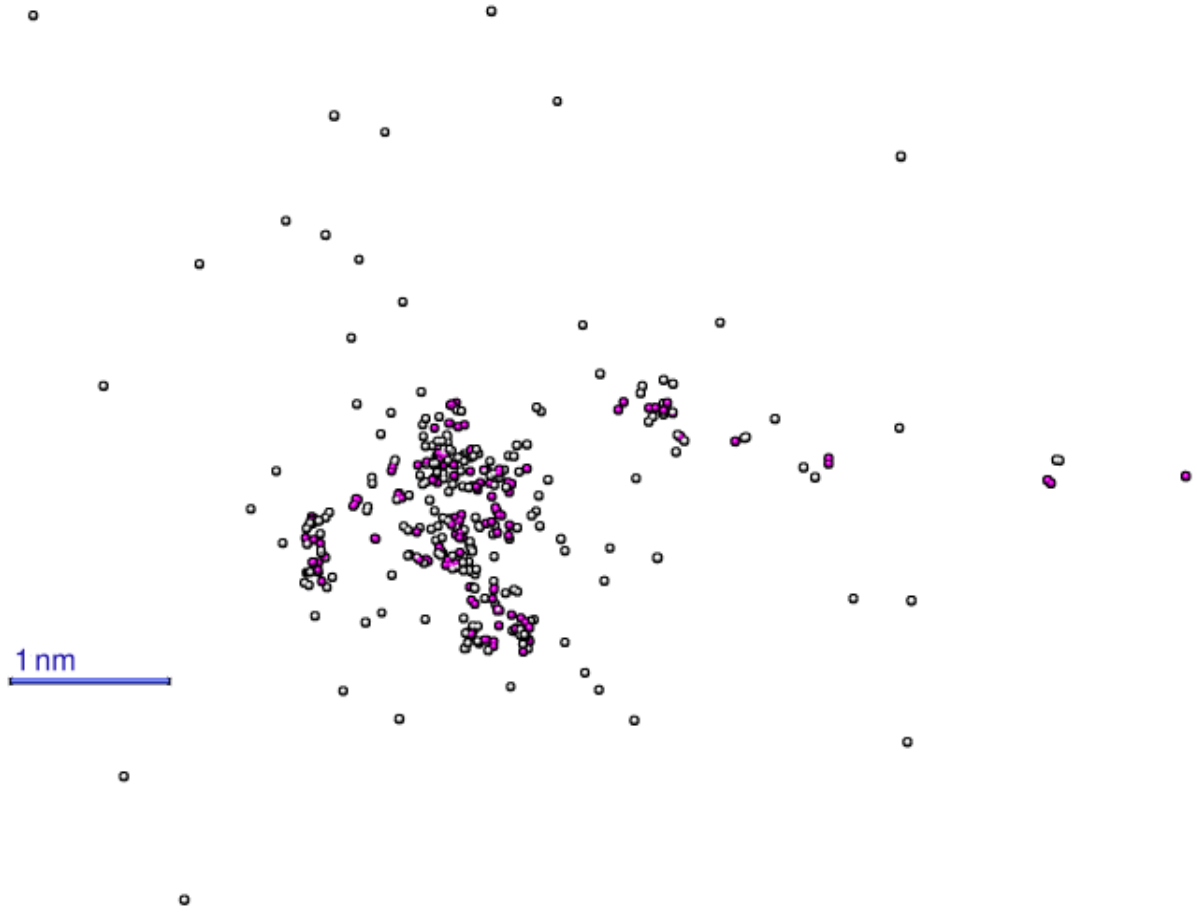

Figure 5.2 Electron track with the energy of 1.5 keV including the physical track and OH radicals (grey spheres). The electron tracks were simulated with the electron track structure code KURBUC-liq [303, 304, 306, 307]

The number of SSB and DSB in DNA segments per track was used to calculate the number of SSB and DSB in the cell nucleus per Gy. For this purpose, the mean molecular weight of a chromosome was calculated by considering an average number of 245 Mbp per chromosome, and 22 chromosomes with a relative mass of 650 g/mol.bp [317]. The comparison of the number of damages induced per cell per Gy with the experimental results is shown in Table 5.4. The number of SSB remains almost constant with the change of energy (~700). The number of DSB increases with energy from 100 eV to 300 eV and decreases for energies higher than 300 eV. The ^{60}Co source induces around 30 DSB/Gy/cell [301], that is about 3 times less than that for low energy electrons and ultrasoft X-rays, and 1000 SSB/Gy/cell [301] which is around the same number for low energy electrons and ultrasoft X-rays. For ultrasoft X-rays, the number of DSB per cell per Gy increases with the decrease in energy as expected. As is shown in Table 5.4 the 15 eV threshold energy shows a better agreement with the experimental measurements. Table 5.5 lists the number of DSB and SSB for 500 tracks of monoenergetic electrons and ultrasoft X-rays. The ratio of direct, indirect and mixed interaction SSB and DSB are listed in Table 5.5.

Table 5.4 Yield of DSB and SSB per cell per Gy and comparison with experimental measurements [301, 302].

Energy (eV)	100	200	300	400	500	1000	1500	4550	Al_K X-ray	C_K X-ray
SSB (#/Gycell)*	650	717	739	786	698	781	774	776	746	746
SSB (#/Gycell)$^+$	440	533	545	598	524	582	558	564	541	543
Measurements SSB (#/Gycell)									935	
DSB (#/Gycell)*	33	81	99	94	79	86	65	81	91	101
DSB (#/Gycell)$^+$	20	38	47	53	42	50	41	42	56	45
Measurements DSB (#/Gycell)								56	77	112

* The minimum energy for the induction of a single strand break was set to 15 eV

$^+$ The minimum energy for the induction of a single strand break was set to 17.5 eV

Table 5.5 Number of SSB and DSB induced by 500 tracks of radiation and fraction of DSB and SSB that are induced by direct, indirect or mixed interaction.

Energy (eV)	100	200	300	400	500	1000	1500	4550	Al_K X-ray	C_K X-ray
Ratio of SSB to DSB	28.38	16.43	16.97	14.83	14.83	17.42	17.53	22.72	15.63	15.42
Total number of SSB	1731	3204	4751	6184	7758	15765	23835	73495	4236	22932
Total number of DSB	61	195	280	417	523	905	1360	3235	271	1487
Fraction of SSB induced by indirect interaction	0.78	0.75	0.77	0.76	0.78	0.78	0.78	0.79	0.77	0.78
Fraction of SSB induced by direct action	0.21	0.22	0.19	0.2	0.19	0.18	0.19	0.18	0.19	0.18
Fraction of SSB induced by mixed interactions	0.02	0.04	0.03	0.04	0.04	0.04	0.04	0.03	0.04	0.04
Fraction DSB by direct interaction	0.25	0.26	0.25	0.24	0.23	0.22	0.22	0.2	0.23	0.23
Fraction of DSB by indirect interaction	0.39	0.4	0.38	0.41	0.4	0.4	0.4	0.43	0.4	0.43
Fraction of DSB by mixed interactions	0.36	0.34	0.38	0.35	0.37	0.38	0.38	0.37	0.37	0.34

5.1.2 Damage by Type (Complex and Simple Damage)

DNA damage arises either from direct interaction of electron or ion with the DNA, or by reaction of water radicals generated in the bulk water surrounding the DNA. As the DNA also contains a hydration shell, interaction of electrons with this layer was considered to be via direct pathway. We considered an energy deposition of 17.5 eV in the volume of the sugar-phosphate as a measure for the induction of a SSB, or similarly in a base moiety for the induction of a base damage [318]. A probability of 0.13 was considered for the reaction of OH radicals to produce a single strand break, and a probability of 0.8 for the production of a base damage.

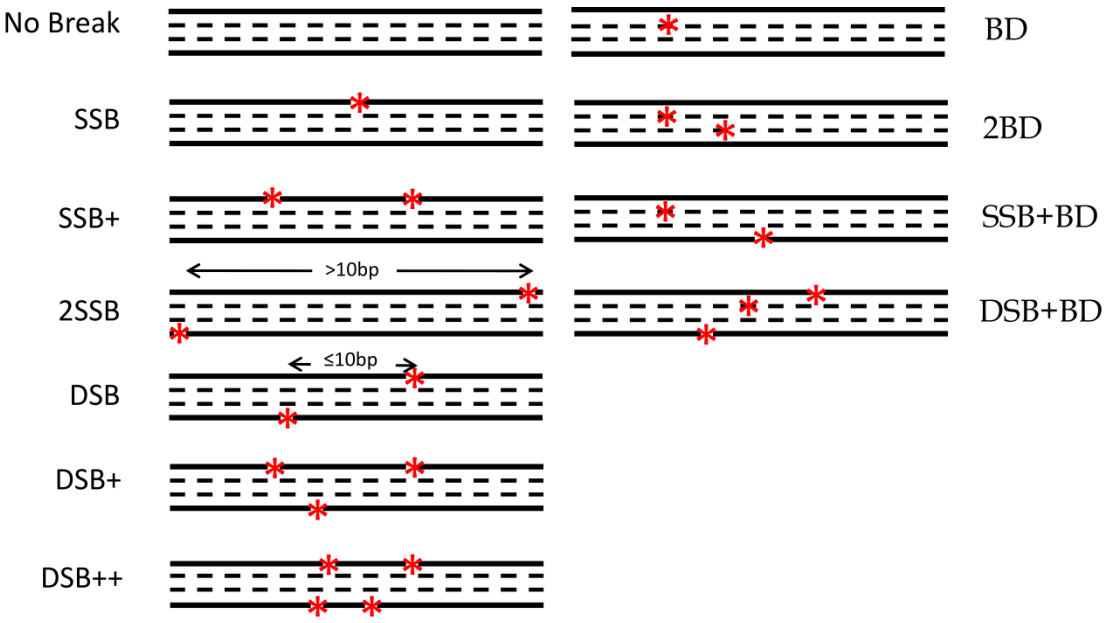

Figure 5.3 The damage classification according to the complexity [319]. The double helix DNA is shown with four lines. The solid lines present the sugar-phosphate (S-P) backbones and the dashed lines present the bases of the DNA. The left column classifies the damages on the S-P backbone. Damage on the (S-P) backbones compose a 'SSB' and two tandem SSB in close proximity (<10 bp) is defined as 'SSB^{+}'. Two bi-stranded SSB in close proximity is defined as 'DSB' and separated with more than 10 bp is defined as '2SSB'. A DSB in close proximity of a SSB and a DSB is defined as 'DSB^{+}' and 'DSB^{++}', respectively. The complex DSB are defined as 'DSB_C'= 'DSB^{+}' and 'DSB^{++}'. The right column illustrates the damage on the base. The first damage is a simple base damage ('BD'). Two base damages are defined as '2BD' and base damage in close proximity of SSB and DSB. A single strand break (SSB) or base damage (BD) may arise either from the direct hits or the reaction of an OH radical.

In this work 54 bp long DNA is used. The atomic model of the DNA is according to the linear B-DNA decamer including the hydration shell [320]. In the naked DNA model, a virtual sphere big enough to contain the entire tracks and the water radicals is considered to score the damage. Cylindrical chords are randomly positioned in the sphere. The random chords contain the DNA segments with 54 bp length and 2.3 nm diameters. The damage to the DNA is classified into simple and complex illustrated in Figure 5.3. The simple damage contains DSB, SSB, and base lesions, and the complex damages include SSB^{+}, DSB^{+}, and DSB^{++}. SSB^{+} is a SSB in a close proximity (~ 10

bp) to another SSB. DSB^{+} is a DSB in close proximity to SSB, and DSB^{++} is a DSB in close proximity to another DSB.

5.1.3 Repair Simulation (Inverse Transform Sampling Method)

The biochemical repair kinetic model solution provides the repair kinetics of each stage of repair for a total number of 600 to 2400 DSB for 20-80 Gy doses (assuming 30 DSB per Gy). In order to calculate the repair time for every DSB separately the inverse transform sampling (ITS) method is used. The probability density function (PDF) in the ITS model is defined as equal to repair activity kinetics normalized to the area under the curve. The cumulative distribution function CDF of the repair process at each stage of repair ($Y_i(t)$) is calculated by cumulative integration over time of the PDF at every stage of repair. $Y_i(t)$ is a monotone increasing function with a maximum value of 1: where t is time and $Y_i(t)$ represents the cumulative distribution function at stage i of the repair process. In order to calculate time t for a single DSB at every stage of repair a random number U between 0-1 is generated. Time t is calculated by the expression $Y_i(t)=U$. The repair activity kinetics at stage i, $y_i(t)$ illustrated in Figure 5.4, is the solution of the linear differential equation system for the NHEJ model.

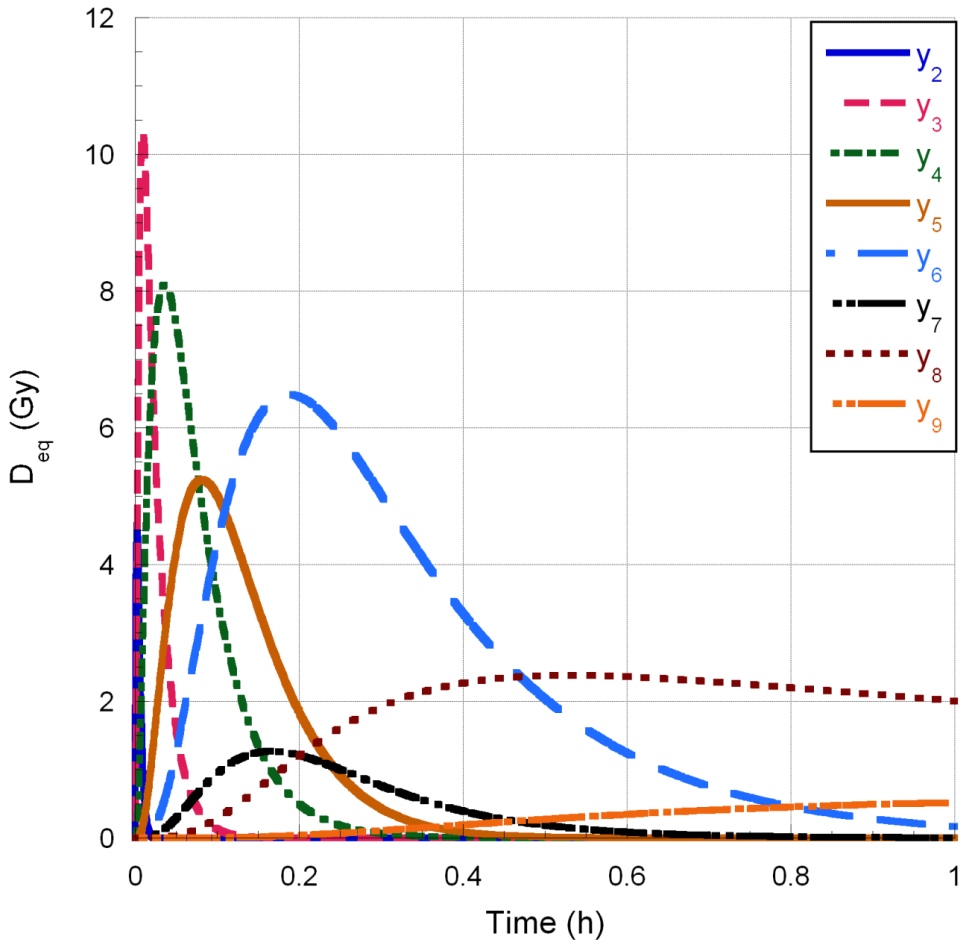

Figure 5.4 Kinetics of protein repair Y_2 to Y_9. The protein repair kinetics are assumed to be the probability density function (PDF) of the protein activity

In order to calculate CDF from PDF, $y_i(t)$ is normalized to the area under the curve and cumulativly integrated over time that results in $Y_i(t)$ illustrated in Figure 5.5.

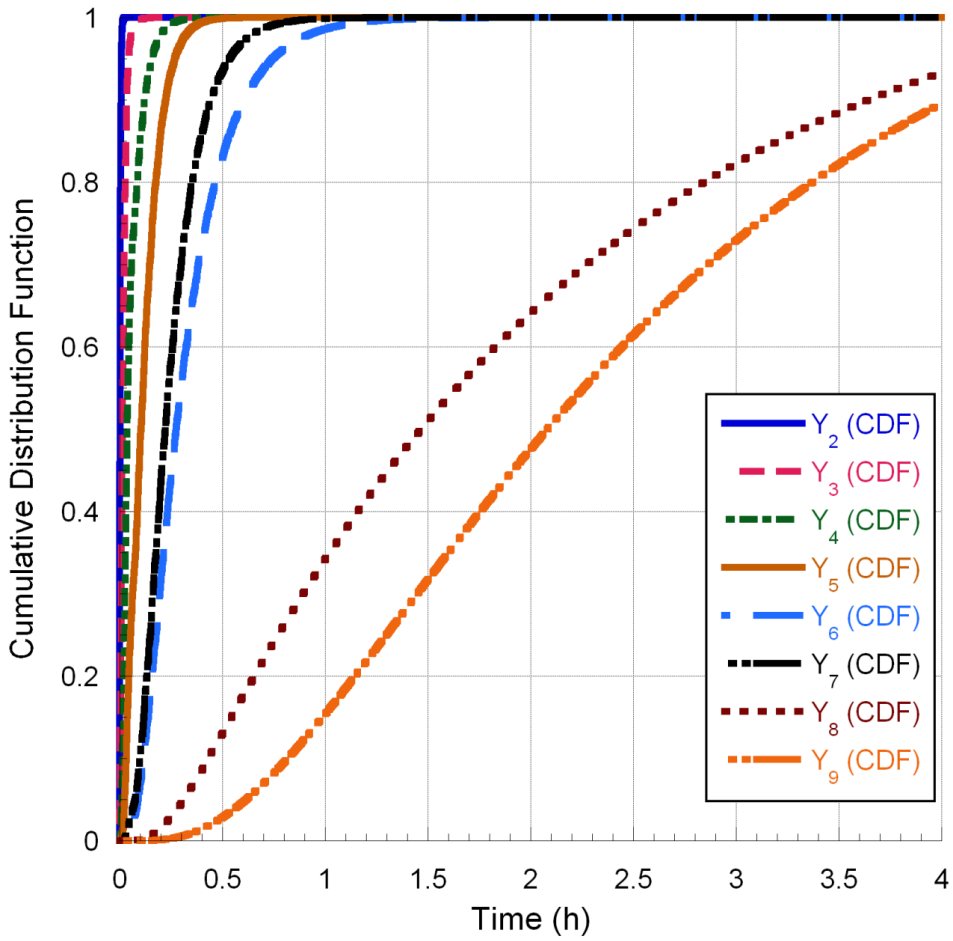

Figure 5.5 Cumulative distribution function (CDF) function of Y_2-Y_9

The DSB spectrum computed by track structure simulations are subject to the repair model to calculate the time of repair for every individual DSB and the overall DSB repair kinetics. Inverse sampling of CDF function of Y_2 to Y_9 for every single DSB provides the repair time at every step and total repair time. With the NHEJ model the DSB are divided to two groups of simple and complex. For simple type DSB Y_2 to Y_5 present the presynaptic repair kinetics and Y_6 presents the ligation kinetic or total repair time. For the complex type DSB Y_2 to Y_5 present the presynaptic repair kinetics and Y_7 to Y_9 present the end processing and ligation kinetics.

Figure 5.6 presents unrejoined DSB kinetics. The symbols and the lines represent the experimental measurements, and calculations, of repair kinetics for the DSB induced by C_K, Ti_K and Al_K X-rays, respectively. The repair kinetics were normalised to the total (initial) number of DSB for 500 tracks of low energy electrons or ultrasoft X-rays.

Table 5.6 summarizes the number of DSB induced by 500 tracks of monoenergetic electrons and ultrasoft X-rays. The DSB are categorized as complex and simple and the

average time for the repair of the simple and complex damage are listed. The average time for the repair of simple DSB is around 20 minutes, while the average time for the complex DSB is around 340 minutes.

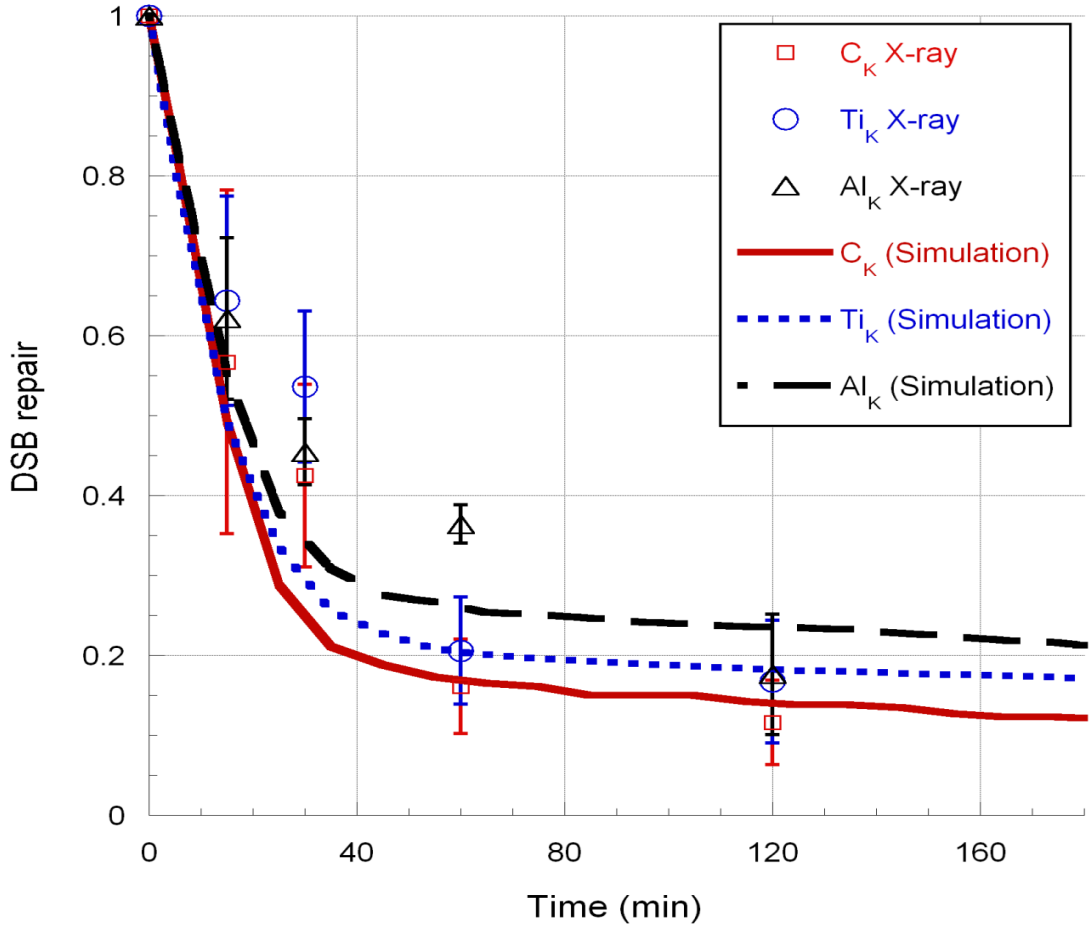

Figure 5.6 Unrejoined DSB kinetics calculated for 500 tracks of C_K, Al_K X-rays and 4.55 keV electrons and compared to the pulsed-field gel electrophoresis experiment measurements with C_K [302] , Al_K [301], and Ti_K [302] X-rays inducing damage in V79-4 cells. The solid line presents the modelling results. Inverse transform sampling of the protein repair kinetics is used to calculate the repair kinetics of DSB.

Table 5.6 Yield and repair time of DSB ultrasoft X-rays and monoenergetic electrons

Energy (eV)	100	200	300	400	500	1000	1500	C_K	Al_K	Ti_K (4550)
Total number of DSB	61	195	280	417	523	905	1360	271	1487	3235
Number of DSB_s	52	146	211	294	397	709	1044	217	1099	2568
Number of DSB_c	9	49	69	123	126	196	316	54	388	667
Average time for DSB_s repair (min)	20	20	20	20	20	20	20	20	20	19
Average time for DSB_c repair (min)	348	349	341	340	328	344	348	338	341	349

Simple DSB: DSB_S

Complex DSB: DSB_C

6 DISCUSSION AND CONCLUSIONS

Since the discovery of X-ray [321] in 1895 by Röntgen, IR has been employed as a powerful tool for imaging and radiotherapy. In the early days after the discovery of radiation, scientists were interested in understanding the physics of different types of IR as well as their applications. It did not take long to discover the hazards of radiation. Skin erythema due to high doses of radiation was among the first symptoms observed. Eventually it was noticed that radiation is a potential risk for cancer induction by observing the cancer incidence of exposure to radiation, among them Marie Curie and her daughter. IR is known as a double edged sword that could cause or be used to eradicate cancer. IR has been studied mainly by its effects, however its mechanism of action is still not fully understood. In response to IR cells activate DNA repair and cell signalling processes to protect the cell either by repair or by causing cell death in order to avoid adverse effects such as mutation [322], chromosome aberration [323] and cancer [324]. DNA repair plays the central role in the cell response to radiation. Intensive laboratory research is evolving in DNA repair and cell signalling processes, however the link from DNA damage to mutation, cancer and cell death is not easily formed. On the other hand, the advances in understanding the mechanisms of DNA repair and cell signalling pathways and human genome research have opened up unprecedented opportunities to develop 'bottom-up' modelling approaches. These approaches are aimed at linking induced DNA damage through cellular DNA repair processes with deletions, duplications or other rearrangements (that arise as a result of such processing) and with the potential adverse health consequences (cancer and hereditary effects) that may ensue. The applications of the damage and repair modelling is to develop new protein targets for cancer treatment [325], improve radiation therapy protocols [34, 40, 326] and propose novel methods to enhance therapeutic ratios [34], develop targeted cancer therapy [327], and estimate genetic and carcinogenic risk to human populations exposed to ionizing radiation [45]. The current work is focused simulating initial induced DNA damage and the repair processes, for which we have constructed a comprehensive mechanistic computational model of DNA repair. Enhancing therapeutic ratio by combining DNA repair targeting and radiotherapy is an active field of research [328-330]. Cancer cells show a number of defects for repair and signalling pathways such as frequent BRCA mutation in breast and ovarian cancers [331] and p53 mutation in different types of human cancer [332, 333]. Targeting mutated pathways in cancer cells seems to be a promising method to cure cancer.

The present work describes a theoretical framework for modelling repair processes for different types of damage induced by ionizing radiation. We have selected the biochemical kinetic modelling approach, since it is simple and explains the biochemical repair processes step by step, with minimum simplifying assumptions. In paper II the most prevalent DSB repair pathway is explained. The NHEJ model was developed by taking into consideration the biological DSB end processing in the absence of homologous recombination. The model considers separate treatment for the simple and complex types of DSB. However the initial steps of the end modifications before synapsis is common for slow and fast repair. The model explains the presynaptic processes in detail, since there exits more experimental information regarding the core

NHEJ protein involvement in the presynaptic repair processes. The end biochemical modifications were translated to sets of equations. In the absence of experimental data for rate constants we determined the rate constants for a sample dose of 20 Gy. The same rate constants proved to be predictive for higher doses up to 80 Gy and several different mammalian cell lines. The initial recruitment kinetics of DNA-PKcs and Ku heterodimer were compared with experimental data measured by green fluorescent protein tagged DNA-PKcs and Ku. Additional experiments are needed to reduce uncertainties in the estimated NHEJ rate constants.

The NHEJ repair model kinetic results were compared with experiments on cells mutated in the HR repair pathway. The NHEJ model is suitable for low LET radiation in which the frequency of the complex DSB is low. It has been observed that upon increase of LET the damage complexity increases and the repair of the complex DSB are delayed [25, 334]. Recently it is shown that increasing the LET results in more resection by MRN [25]. Our interpretation from these observations is that core NHEJ proteins have difficulty in repairing the DSB in close proximity to another strand break, and open the ends for resection by MRN [25]. In order to use the repair model for high LET irradiated cells we have proposed two separate models dependent on the availability of the HR pathway. In G1 and early S phases of the cell cycle homologous recombination is not active, therefore the only option for repair of the DSB that have undergone resection is MMEJ as explained in paper V. Besides the complex type DSB, it is proposed that DSB in the heterochromatin prolong the repair process. Biochemical repair handling of both types of DSB are considered in G1 and early S phases of the cell cycle and in late S and G2 phases of the cell cycle. The repair model is based on the law of mass action and calculates the overall and step-by-step repair kinetics. For all DSB the repair starts with NHEJ presynaptic steps and continues the end processing and ligation depending on the type of DSB. The difference between G1 and early S phases of the cell cycle and in late S and G2 phases of the cell cycle is that the complex damage is repaired by MMEJ and HR, respectively. The solution of the model in terms of overall DSB repair kinetics is in good agreement with experimental measurements for low LET irradiated cells. The model provides valuable step-by-step repair kinetics that could add to the detailed understanding of the DSB repair processes.

With the assumption that cells under test show two-component DSB repair kinetics, the two exponential method explains the characteristics of the curves. The repair fractions and repair half-life show different mammalian cells are similar within the accepted uncertainty of the experiments. The differences could arise from experimental uncertainties and differences in cell size, nucleus size, and amount of heterochromatin. The two-exponential method like other phenomenological models does not inform about the detail of the mechanism and explains the graphical features of the response.

We employed the new version of track structure code KURBUC-liq for simulation of electron track and ultrasoft X-rays (100 eV to 1.5 keV monoenergetic electrons, and C_K, Al_K and Ti_K ultrasoft X-rays) [15, 335] to model DNA damage spectra. The present biophysical computer simulation method is the only way to precisely identify and quantify the forms and frequencies of the simple and complex DSB. To access the reparability of the induced DSB, a mechanistic mathematical model of the NHEJ kinetic repair was applied to simulated DNA DSB induced by low energy electrons and

ultrasoft X-rays. The set of nonlinear equations describing the NHEJ biophysical repair activities on the DSB ends was solved to derive the protein activity kinetics for a total dose of 15 Gy of C_K X-rays. The protein activities were sampled to estimate the repair time required for DSB induced by 1 track of radiation at a time. In order to employ the repair model, the inverse transform sampling method was used to calculate the repair time from the CDF of the protein repair kinetics. The method is capable of calculating the repair time for every single DSB. The overall DSB repair kinetics for DSB induced by 500 tracks of radiation for C_K, Ti_K and Al_K X-rays were compared with experimental measurements. The total DSB repair kinetics for C_K, Al_K, and Ti_K showed good agreement with experimental measurements and model calculation. This approach provides details of repair timing that are not easily measured for protein activities on the DSB ends. The results show that the NHEJ model based on the complexity hypothesis is capable of predicting the DSB-repair kinetics of cells irradiated with electrons.

For future work the models proposed for early S and G1 phases of the cell cycle and late S and G2 phases of the cell cycle can be used to calculate the repair kinetics of DSB damage spectrum simulated track structure models. The overall repair kinetics of DSB induced by radiation of different quality can be compared with the experimental results [135, 179, 184, 187, 197, 199, 336]. We are currently running track structure simulations which require high CPU usage and very high memory requirement (such calculations are done on supercomputers).

In short the advantages of a mechanistic model is that under certain assumptions the model could be used for predicting the overall repair kinetics of high LET irradiated cells. Track structure simulations have shown that both low LET and high LET radiations induce simple and complex DSB. As explained in our publications, the sampling method was used to calculate the step-by-step repair time of DSB induced by electrons and X-rays. In future work, the DSB induced by radiation of different quality will be simulated and subjected to the repair model. The overall repair kinetics predicted by track structure simulation will be compared with experimental data to test the model. The comparison of the DSB-repair kinetics with different LET irradiated cells could test the hypothesis of our model that the repair is delayed because of the local complexity of the DSB or distribution of the damage in the heterochromatin.

7 ACKNOWLEDGEMENTS

I would like to express my gratitude to all those who helped me to complete this thesis.

Foremost it is with immense gratitude to acknowledge the support of my supervisor Prof. Hooshang Nikjoo. He guided me throughout my PhD research with patience, motivation, and immense knowledge. Besides your support during my PhD project, I appreciate your care and your efforts to build a friendly scientific environment for the benefit of all the PhD students in the department with the endless time and energy you spent for us.

It gives me a great pleasure in acknowledging the support and help of my co-supervisors Professor Mats Harms-Ringdahl and Professor Michael Weinfeld. I would like to thank you for your encouragement, insightful comments and questions. I would like to thank Professor Micheal Weinfeld for his kind support and comments on the manuscripts. I would like to thank Professor Mats Harms-Ringdahl for his support and comments on the repair models.

I would like to thank the support, and comments of our MSF supervisors Professors Anders Brahme, Pedro Andreo, Lennart Lindberg, Karen Belkic, and Dzevad Belkic, and Associate Professors Bo Nilsson, Irena Gudowska, Iuliana Dasu and Albert Siegbahn.

I would like to acknowledge the scientific comments and discussions during international meetings and seminars by Professor Anders Brahme, Professor Penny Jeggo, Professor Dzevad Belkic, Professor George Iliakis, Professor Bo Stenerlöw, Professor Linda Yasui, Professor Eduard Azzam, Dr Werner Friedland, Professor Susan Wallace, Professor David Chen, Dr Giesela Taucher-Scholz, Dr Siamak Haghdoost, and Dr Sylvian Costes.

I would like to thank my supportive friends and colleagues in the Radiation Biophysics Group: Peter Girard, Thiansin Liamsuwan, Tommy Sundström, Shirin Rahmanian and Alfredo Metere.

I am indebted to my colleagues at MSF and CCK who supported me during my PhD studies. Martha Hultqvist, Björn Andreason, Marta Lazzeroni, Bahram Andisheh, Kristin Wiklund, Patrick Vreede, Johanna Kempe, Johan Staaf, Lucilio Matias, Eleftheria Alevronta, Minna Wedenberg, Tobias Böhlen, Sara Strååt, Alireza Azimi, Pedram Kharaziha, Mahdi Mojallal, Salah Mahmoudi, Lisa Viberg, Ma Ran, Kaveh Moazemi, Sophia Ceder, Anna Maria Marino and Claire Sanchez Many thanks for your friendship and support.

I would like to thank the kind support and help in the administrative work of Lil Engström and Marianne Edgren, Henriette Cederlöf.

I would like to share the credit of my work to my friends in Stockholm for their great support. It is a long list of friends that I am grateful for their support and friendship.

Finally, I cannot find words to thank my parents, brothers, family for their endless love.

8 REFERENCES

1. Little, J.B., *Radiation carcinogenesis.* Carcinogenesis, 2000. **21**(3): 397-404.
2. Thompson, L.H., *Recognition, signaling, and repair of DNA double-strand breaks produced by ionizing radiation in mammalian cells: The molecular choreography.* Mutation Research-Reviews in Mutation Research, 2012. **751**(2): 158-246.
3. Ward, J., *Nature of lesions formed by ionizing radiation.* DNA damage and repair, 1998. **2**: 65-84.
4. Nikjoo, H., P. O'Neill, M. Terrissol and D.T. Goodhead, *Quantitative modelling of DNA damage using Monte Carlo track structure method.* Radiation and Environmental Biophysics, 1999. **38**(1): 31-38.
5. Friedland, W., P. Jacob, H.G. Paretzke, A. Ottolenghi, F. Ballarini, et al., *Simulation of light ion induced DNA damage patterns.* Radiation Protection Dosimetry, 2006. **122**(1-4): 116-120.
6. Nikjoo, H., P. O'Neill, W.E. Wilson and D.T. Goodhead, *Computational approach for determining the spectrum of DNA damage induced by ionizing radiation.* Radiation Research, 2001. **156**(5): 577-583.
7. Charlton, D.E., H. Nikjoo and J.L. Humm, *Calculation of initial yields of single- and double-strand breaks in cell nuclei from electrons, protons and alpha particles.* Int J Radiat Biol, 1989. **56**(1): 1-19.
8. Ballarini, F., D. Alloni, A. Facoetti and A. Ottolenghi, *Heavy-ion effects: from track structure to DNA and chromosome damage.* New Journal of Physics, 2008. **10**.
9. Nikjoo, H. and L. Lindborg, *RBE of low energy electrons and photons.* Physics in Medicine and Biology, 2010. **55**(10): R65-R109.
10. Lindborg, L., M. Hultqvist, A. Carlsson Tedgren and H. Nikjoo, *Lineal energy and radiation quality in radiation therapy: model calculations and comparison with experiment.* Phys Med Biol, 2013. **58**(10): 3089-3105.
11. Goodarzi, A.A., P. Jeggo and M. Löbrich, *The influence of heterochromatin on DNA double strand break repair: Getting the strong, silent type to relax.* DNA Repair (Amst), 2010. **9**(12): 1273-1282.
12. Goodarzi, A.A., A.T. Noon and P.A. Jeggo, *The impact of heterochromatin on DSB repair.* Biochem Soc Trans, 2009. **37**(3): 569-576.
13. Goodarzi, A.A., A.T. Noon, D. Deckbar, Y. Ziv, Y. Shiloh, et al., *ATM signaling facilitates repair of DNA double-strand breaks associated with heterochromatin.* Mol Cell, 2008. **31**(2): 167-177.
14. Goodarzi, A.A. and P.A. Jeggo, *The heterochromatic barrier to DNA double strand break repair: how to get the entry visa.* Int J Mol Sci, 2012. **13**(9): 11844-11860.
15. Taleei, R. and H. Nikjoo, *Repair of the double-strand breaks induced by low energy electrons: a modelling approach.* Int J Radiat Biol, 2012. **88**(12): 948-953.
16. Fromme, J.C. and G.L. Verdine, *Base excision repair*. DNA Repair and Replication, 2004. **69**: 1-41.
17. Frankenberg-Schwager, M., A. Gebauer, C. Koppe, H. Wolf, E. Pralle, et al., *Single-strand annealing, conservative homologous recombination, nonhomologous DNA end joining, and the cell cycle-dependent repair of DNA*

double-strand breaks induced by sparsely or densely ionizing radiation. Radiat Res, 2009. **171**(3): 265-273.

18. Saleh-Gohari, N. and T. Helleday, *Conservative homologous recombination preferentially repairs DNA double-strand breaks in the S phase of the cell cycle in human cells.* Nucleic Acids Res, 2004. **32**(12): 3683-3688.

19. Iliakis, G., H. Wang, A.R. Perrault, W. Boecker, B. Rosidi, et al., *Mechanisms of DNA double strand break repair and chromosome aberration formation.* Cytogenet Genome Res, 2004. **104**(1-4): 14-20.

20. Lieber, M.R., *The mechanism of double-strand DNA break repair by the nonhomologous DNA end-joining pathway.* Annu Rev Biochem, 2010. **79**: 181-211.

21. Tutt, A., D. Bertwistle, J. Valentine, A. Gabriel, S. Swift, et al., *Mutation in Brca2 stimulates error-prone homology-directed repair of DNA double-strand breaks occurring between repeated sequences.* EMBO J, 2001. **20**(17): 4704-4716.

22. Scuric, Z., C.Y. Chan, K. Hafer and R.H. Schiestl, *Ionizing Radiation Induces Microhomology-Mediated End Joining in trans in Yeast and Mammalian Cells.* Radiation Research, 2009. **171**(4): 454-463.

23. McVey, M. and S.E. Lee, *MMEJ repair of double-strand breaks (director's cut): deleted sequences and alternative endings.* Trends in Genetics, 2008. **24**(11): 529-538.

24. Woodbine, L., H. Brunton, A.A. Goodarzi, A. Shibata and P.A. Jeggo, *Endogenously induced DNA double strand breaks arise in heterochromatic DNA regions and require ataxia telangiectasia mutated and Artemis for their repair.* Nucleic Acids Research, 2011. **39**(16): 6986-6997.

25. Shibata, A., S. Conrad, J. Birraux, V. Geuting, O. Barton, et al., *Factors determining DNA double-strand break repair pathway choice in G2 phase.* EMBO Journal, 2011. **30**(6): 1079-1092.

26. Beucher, A., J. Birraux, L. Tchouandong, O. Barton, A. Shibata, et al., *ATM and Artemis promote homologous recombination of radiation-induced DNA double-strand breaks in G2.* EMBO Journal, 2009. **28**(21): 3413-3427.

27. Taleei, R. and H. Nikjoo, *The Nonhomologous End-Joining (NHEJ) Pathway for the Repair of DNA Double-Strand Breaks: I- A Mathematical Model.* Radiation Research, 2013. **179**: 530-539.

28. Taleei, R., P.M. Girard, K. Sankaranarayanan and H. Nikjoo, *The Nonhomologous End-Joining (NHEJ) mathematical model for the repair of double-strand breaks: II- Application to damage induced by ultrasoft X-rays and low energy electrons.* Radiation Research, 2013. **179**: 540-548.

29. Weinfeld, M., A. Rasouli-Nia, M.A. Chaudhry and R.A. Britten, *Response of base excision repair enzymes to complex DNA lesions.* Radiat Res, 2001. **156**(5): 584-589.

30. Kroemer, G., L. Galluzzi, P. Vandenabeele, J. Abrams, E.S. Alnemri, et al., *Classification of cell death: recommendations of the Nomenclature Committee on Cell Death 2009.* Cell Death and Differentiation, 2009. **16**(1): 3-11.

31. Lea, D.E., *Actions of radiations on living cells.* Actions of radiations on living cells., 1946.

32. Thames, H.D. and J.H. Hendry, *Fractionation in radiotherapy*. 1987: Taylor & Francis London.

33. Fowler, J.F., *The linear-quadratic formula and progress in fractionated radiotherapy.* Br J Radiol, 1989. **62**(740): 679-694.

34. Brahme, A. and B.K. Lind, *A systems biology approach to radiation therapy optimization.* Radiat Environ Biophys, 2010. **49**(2): 111-124.

35. Kappos, A. and W. Pohlit, *A cybernetic model for radiation reactions in living cells. I. Sparsely-ionizing radiations; stationary cells.* Int J Radiat Biol Relat Stud Phys Chem Med, 1972. **22**(1): 51-65.

36. Tobias, C.A., *The repair-misrepair model in radiobiology: comparison to other models.* Radiat Res Suppl, 1985. **8**: S77-95.

37. Curtis, S.B., *Lethal and potentially lethal lesions induced by radiation--a unified repair model.* Radiat Res, 1986. **106**(2): 252-270.

38. Goodhead, D.T., *Saturable repair models of radiation action in mammalian cells.* Radiat Res Suppl, 1985. **8**: S58-67.

39. Guerrero, M. and X.A. Li, *Extending the linear–quadratic model for large fraction doses pertinent to stereotactic radiotherapy.* Physics in Medicine and Biology, 2004. **49**(20): 4825.

40. Lind, B.K., L.M. Persson, M.R. Edgren, I. Hedlof and A. Brahme, *Repairable-conditionally repairable damage model based on dual Poisson processes.* Radiat Res, 2003. **160**(3): 366-375.

41. Millar, W. and P. Canney, *Derivation and application of equations describing the effects of fractionated protracted irradiation, based on multiple and incomplete repair processes. Part I. Derivation of equations.* International journal of radiation biology, 1993. **64**(3): 275-291.

42. Stewart, R.D., *Two-lesion kinetic model of double-strand break rejoining and cell killing.* Radiation Research, 2001. **156**(4): 365-378.

43. Nevaldine, B., J.A. Longo, M. Vilenchik, G.A. King and P.J. Hahn, *Induction and repair of DNA double-strand breaks in the same dose range as the shoulder of the survival curve.* Radiat Res, 1994. **140**(2): 161-165.

44. Sankaranarayanan, K., R. Taleei, S. Rahmanian and H. Nikjoo, *Ionizing radiation and genetic risks. XVII. Bridging the gap between radiation-induced DNA double-strand breaks and the origin of DNA deletions.* Mutation Research-Reviews, 2013. In press.

45. Sankaranarayanan, K. and H. Nikjoo, *Ionising radiation and genetic risks. XVI. A genome-based framework for risk estimation in the light of recent advances in genome research.* International journal of radiation biology, 2011. **87**(2): 161-178.

46. Novak, B. and J.J. Tyson, *A model for restriction point control of the mammalian cell cycle.* J Theor Biol, 2004. **230**(4): 563-579.

47. Tyson, J.J. and B. Novak, *Temporal organization of the cell cycle.* Curr Biol, 2008. **18**(17): R759-R768.

48. Csikasz-Nagy, A., *Computational systems biology of the cell cycle.* Brief Bioinform, 2009. **10**(4): 424-434.

49. Singhania, R., R.M. Sramkoski, J.W. Jacobberger and J.J. Tyson, *A Hybrid Model of Mammalian Cell Cycle Regulation.* Plos Computational Biology, 2011. **7**(2).

50. Tyson, J.J., *In their own words: Interviews with Cell Cycle.* Cell Cycle, 2009. **8**(20): 3261-3261.

51. Sokhansanj, B.A. and D.M. Wilson, *Oxidative DNA damage background estimated by a system model of base excision repair.* Free Radical Biology and Medicine, 2004. **37**(3): 422-427.

52. Sokhansanj, B.A. and D.M. Wilson, *Mathematical modeling of human DNA base excision repair.* Biophysical Journal, 2003. **84**(2): 360a-360a.

53. Sokhansanj, B.A., G.R. Rodrigue, J.P. Fitch and D.M. Wilson, 3rd, *A quantitative model of human DNA base excision repair. I. Mechanistic insights.* Nucleic Acids Res, 2002. **30**(8): 1817-1825.

54. Sokhansanj, B.A. and D.M. Wilson, 3rd, *Estimating the effect of human base excision repair protein variants on the repair of oxidative DNA base damage.* Cancer Epidemiol Biomarkers Prev, 2006. **15**(5): 1000-1008.

55. Cucinotta, F.A., J.F. Dicello, H. Nikjoo and R. Cherubini, *Computational model of the modulation of gene expression following DNA damage.* Radiation Protection Dosimetry, 2002. **99**(1-4): 85-90.

56. Cucinotta, F.A., J.M. Pluth, J.A. Anderson, J.V. Harper and P. O'Neill, *Biochemical kinetics model of DSB repair and induction of gamma-H2AX foci by non-homologous end joining.* Radiat Res, 2008. **169**(2): 214-222.

57. Dolan, D., G. Nelson, A. Zupanic, G. Smith and D. Shanley, *Systems Modelling of NHEJ Reveals the Importance of Redox Regulation of Ku70/80 in the Dynamics of DNA Damage Foci.* Plos One, 2013. **8**(2).

58. Friedland, W., P. Kundrat and P. Jacob, *Stochastic modelling of DSB repair after photon and ion irradiation.* International journal of radiation biology, 2012. **88**(1-2): 129-136.

59. Friedland, W., P. Jacob and P. Kundrat, *Mechanistic Simulation of Radiation Damage to DNA and Its Repair: On the Track Towards Systems Radiation Biology Modelling.* Radiation Protection Dosimetry, 2011. **143**(2-4): 542-548.

60. Friedland, W., M. Dingfelder, P. Kundrat and P. Jacob, *Track structures, DNA targets and radiation effects in the biophysical Monte Carlo simulation code PARTRAC.* Mutation Research-Fundamental and Molecular Mechanisms of Mutagenesis, 2011. **711**(1-2): 28-40.

61. Friedland, W., P. Jacob and P. Kundrat, *Stochastic Simulation of DNA Double-Strand Break Repair by Non-homologous End Joining Based on Track Structure Calculations.* Radiation Research, 2010. **173**(5): 677-688.

62. Dianov, G.L. and J.L. Parsons, *Co-ordination of DNA single strand break repair.* DNA Repair (Amst), 2007. **6**(4): 454-460.

63. Sossou, M., C. Flohr-Beckhaus, I. Schulz, F. Daboussi, B. Epe, et al., *APE1 overexpression in XRCC1-deficient cells complements the defective repair of oxidative single strand breaks but increases genomic instability.* Nucleic Acids Res, 2005. **33**(1): 298-306.

64. Nakamura, J., S. Asakura, S.D. Hester, G. de Murcia, K.W. Caldecott, et al., *Quantitation of intracellular NAD(P)H can monitor an imbalance of DNA single strand break repair in base excision repair deficient cells in real time.* Nucleic Acids Res, 2003. **31**(17): e104.

65. Wallace, S.S., *Enzymatic processing of radiation-induced free radical damage in DNA.* Radiat Res, 1998. **150**(5 Suppl): S60-79.

66. Lindahl, T. and R.D. Wood, *Quality control by DNA repair.* Science, 1999. **286**(5446): 1897-1905.

67. Almeida, K.H. and R.W. Sobol, *A unified view of base excision repair: Lesion-dependent protein complexes regulated by post-translational modification.* DNA Repair, 2007. **6**(6): 695-711.

68. Stivers, J.T. and Y.L. Jiang, *A mechanistic perspective on the chemistry of DNA repair glycosylases.* Chem Rev, 2003. **103**(7): 2729-2759.

69. O'Brien, P.J., *Catalytic promiscuity and the divergent evolution of DNA repair enzymes.* Chem Rev, 2006. **106**(2): 720-752.

70. Memisoglu, A. and L. Samson, *Base excision repair in yeast and mammals.* Mutation Research-Fundamental and Molecular Mechanisms of Mutagenesis, 2000. **451**(1-2): 39-51.

71. Svilar, D., E.M. Goellner, K.H. Almeida and R.W. Sobol, *Base Excision Repair and Lesion-Dependent Subpathways for Repair of Oxidative DNA Damage.* Antioxidants & Redox Signaling, 2011. **14**(12): 2491-2507.

72. Stucki, M., B. Pascucci, E. Parlanti, P. Fortini, S.H. Wilson, et al., *Mammalian base excision repair by DNA polymerases delta and epsilon.* Oncogene, 1998. **17**(7): 835-843.

73. Weinfeld, M., R.S. Mani, I. Abdou, R.D. Aceytuno and J.N.M. Glover, *Tidying up loose ends: the role of polynucleotide kinase/phosphatase in DNA strand break repair.* Trends in Biochemical Sciences, 2011. **36**(5): 262-271.

74. Ballarini, F. and A. Ottolenghi, *Chromosome aberrations as biomarkers of radiation exposure: Modelling basic mechanisms.* Space Life Sciences: Biodosimetry, Biomarkers and Late Stochastic Effects of Space Radiation, 2003. **31**(6): 1557-1568.

75. Ballarini, F., M. Biaggi, A. Ferrari, A. Ottolenghi, M. Pelliccioni, et al., *Modelling the influence of shielding on physical and biological organ doses.* Journal of Radiation Research, 2002. **43**: S99-S102.

76. Moroni, A., U. Abbondanno, C. Agodi, R. Alba, E. Ballarini, et al., *Nuclear detecting systems at LNL and LNS: foreseen experiments to provide basic data for heavy-ion risk assessment.* Physica Medica, 2001. **17**: 124-127.

77. Ottolenghi, A., F. Ballarini and M. Biaggi, *Mechanistic and phenomenological models for the estimate of radiation-induced biological damage.* Physica Medica-European Journal of Medical Physics, 2001. **17**: 3-12.

78. Fiocchi, A., R. Qualizza, J. Onorato, C. Agostoni, R. Altobelli, et al., *Primary prevention of hypersensitivity to food in newborns (Experiments in Milan and surrounding areas).* Rivista Italiana Di Pediatria-Italian Journal of Pediatrics, 1998. **24**(6): 1085-1092.

79. Ballarini, F., M. Merzagora, F. Monforti, M. Durante, G. Gialanella, et al., *Chromosome aberrations induced by light ions: Monte Carlo simulations based on a mechanistic model.* International journal of radiation biology, 1999. **75**(1): 35-46.

80. Hess, C., A. Ottolenghi, J.P. Pouget, C. Schlenker, J.L. Hodeau, et al., *Electronic instabilities in the quasi two-dimensional monophosphate tungsten bronze (PO2)(4)(WO3)(2m) (m=13).* Synthetic Metals, 1997. **86**(1-3): 2169-2170.

81. Gagliardi, G., I. Lax, A. Ottolenghi and L.E. Rutqvist, *Long-term cardiac mortality after radiotherapy of breast cancer - Application of the relative seriality model.* British Journal of Radiology, 1996. **69**(825): 839-846.

82. Ottolenghi, A., M. Merzagora and H.G. Paretzke, *DNA complex lesions induced by protons and alpha-particles: Track structure characteristics determining linear energy transfer and particle type dependence.* Radiation and Environmental Biophysics, 1997. **36**(2): 97-103.

83. Blaisdell, J.O., L. Harrison and S.S. Wallace, *Base excision repair processing of radiation-induced clustered DNA lesions.* Radiat Prot Dosimetry, 2001. **97**(1): 25-31.

84. Blaisdell, J.O. and S.S. Wallace, *Abortive base-excision repair of radiation-induced clustered DNA lesions in Escherichia coli.* Proc Natl Acad Sci U S A, 2001. **98**(13): 7426-7430.

85. Harrison, L., Z. Hatahet and S.S. Wallace, *In vitro repair of synthetic ionizing radiation-induced multiply damaged DNA sites.* J Mol Biol, 1999. **290**(3): 667-684.

86. Inoue, M., G.P. Shen, M.A. Chaudhry, H. Galick, J.O. Blaisdell, et al., *Expression of the oxidative base excision repair enzymes is not induced in TK6 human lymphoblastoid cells after low doses of ionizing radiation.* Radiat Res, 2004. **161**(4): 409-417.

87. Wallace, S.S., *DNA damages processed by base excision repair: biological consequences.* Int J Radiat Biol, 1994. **66**(5): 579-589.

88. Yang, N., M.A. Chaudhry and S.S. Wallace, *Base excision repair by hNTH1 and hOGG1: a two edged sword in the processing of DNA damage in gamma-irradiated human cells.* DNA Repair (Amst), 2006. **5**(1): 43-51.

89. Yang, N., H. Galick and S.S. Wallace, *Attempted base excision repair of ionizing radiation damage in human lymphoblastoid cells produces lethal and mutagenic double strand breaks.* DNA Repair (Amst), 2004. **3**(10): 1323-1334.

90. Bellon, S., N. Shikazono, S. Cunniffe, M. Lomax and P. O'Neill, *Processing of thymine glycol in a clustered DNA damage site: mutagenic or cytotoxic.* Nucleic Acids Res, 2009. **37**(13): 4430-4440.

91. David-Cordonnier, M.H., S. Boiteux and P. O'Neill, *Excision of 8-oxoguanine within clustered damage by the yeast OGG1 protein.* Nucleic Acids Res, 2001. **29**(5): 1107-1113.

92. David-Cordonnier, M.H., J. Laval and P. O'Neill, *Clustered DNA damage, influence on damage excision by XRS5 nuclear extracts and Escherichia coli Nth and Fpg proteins.* J Biol Chem, 2000. **275**(16): 11865-11873.

93. Dianov, G.L., P. O'Neill and D.T. Goodhead, *Securing genome stability by orchestrating DNA repair: removal of radiation-induced clustered lesions in DNA.* Bioessays, 2001. **23**(8): 745-749.

94. Lomax, M.E., S. Cunniffe and P. O'Neill, *Efficiency of repair of an abasic site within DNA clustered damage sites by mammalian cell nuclear extracts.* Biochemistry, 2004. **43**(34): 11017-11026.

95. Lomax, M.E., S. Cunniffe and P. O'Neill, *8-OxoG retards the activity of the ligase III/XRCC1 complex during the repair of a single-strand break, when present within a clustered DNA damage site.* DNA Repair (Amst), 2004. **3**(3): 289-299.

96. Mourgues, S., M.E. Lomax and P. O'Neill, *Base excision repair processing of abasic site/single-strand break lesions within clustered damage sites associated with XRCC1 deficiency.* Nucleic Acids Res, 2007. **35**(22): 7676-7687.

97. Yokoya, A., S.M. Cunniffe and P. O'Neill, *Effect of hydration on the induction of strand breaks and base lesions in plasmid DNA films by gamma-radiation.* J Am Chem Soc, 2002. **124**(30): 8859-8866.

98. Chaudhry, M.A. and M. Weinfeld, *The action of Escherichia coli endonuclease III on multiply damaged sites in DNA.* J Mol Biol, 1995. **249**(5): 914-922.

99. Lomax, M.E., H. Salje, S. Cunniffe and P. O'Neill, *8-OxoA inhibits the incision of an AP site by the DNA glycosylases Fpg, Nth and the AP endonuclease HAP1.* Radiat Res, 2005. **163**(1): 79-84.

100. Cunniffe, S.M., M.E. Lomax and P. O'Neill, *An AP site can protect against the mutagenic potential of 8-oxoG when present within a tandem clustered site in E. coli.* DNA Repair (Amst), 2007. **6**(12): 1839-1849.

101. Yoo, S. and W.S. Dynan, *Geometry of a complex formed by double strand break repair proteins at a single DNA end: recruitment of DNA-PKcs induces inward translocation of Ku protein.* Nucleic Acids Research, 1999. **27**(24): 4679-4686.

102. West, R.B., M. Yaneva and M.R. Lieber, *Productive and nonproductive complexes of Ku and DNA-dependent protein kinase at DNA termini.* Mol Cell Biol, 1998. **18**(10): 5908-5920.

103. Uematsu, N., E. Weterings, K. Yano, K. Morotomi-Yano, B. Jakob, et al., *Autophosphorylation of DNA-PKCS regulates its dynamics at DNA double-strand breaks.* J Cell Biol, 2007. **177**(2): 219-229.

104. Reddy, Y.V., Q. Ding, S.P. Lees-Miller, K. Meek and D.A. Ramsden, *Non-homologous end joining requires that the DNA-PK complex undergo an autophosphorylation-dependent rearrangement at DNA ends.* J Biol Chem, 2004. **279**(38): 39408-39413.

105. Cui, X., Y. Yu, S. Gupta, Y.M. Cho, S.P. Lees-Miller, et al., *Autophosphorylation of DNA-dependent protein kinase regulates DNA end processing and may also alter double-strand break repair pathway choice.* Mol Cell Biol, 2005. **25**(24): 10842-10852.

106. Burgio, G.R., G.L. Marseglia, F. Severi, F. Debenedetti, M. Masarone, et al., *Immunoactivation by Pidotimod in Children with Recurrent Respiratory-Infections.* Arzneimittel-Forschung/Drug Research, 1994. **44-2**(12A): 1525-1529.

107. Jeggo, P. and M. Löbrich, *Radiation-induced DNA damage responses.* Radiat Prot Dosimetry, 2006. **122**(1-4): 124-127.

108. Goodarzi, A.A., Y.P. Yu, E. Riballo, P. Douglas, S.A. Walker, et al., *DNA-PK autophosphorylation facilitates Artemis endonuclease activity.* EMBO Journal, 2006. **25**(16): 3880-3889.

109. Jeggo, P.A. and M. Löbrich, *Artemis links ATM to double strand break rejoining.* Cell Cycle, 2005. **4**(3): 359-362.

110. Dahm, K., *Functions and regulation of human artemis in double strand break repair.* J Cell Biochem, 2007. **100**(6): 1346-1351.

111. Drouet, J., P. Frit, C. Delteil, J.P. de Villartay, B. Salles, et al., *Interplay between Ku, Artemis, and the DNA-dependent protein kinase catalytic subunit at DNA ends.* J Biol Chem, 2006. **281**(38): 27784-27793.

112. Riballo, E., M. Kuhne, N. Rief, A. Doherty, G.C. Smith, et al., *A pathway of double-strand break rejoining dependent upon ATM, Artemis, and proteins locating to gamma-H2AX foci.* Mol Cell, 2004. **16**(5): 715-724.

113. Karimi-Busheri, F., A. Rasouli-Nia, J. Allalunis-Turner and M. Weinfeld, *Human polynucleotide kinase participates in repair of DNA double-strand breaks by nonhomologous end joining but not homologous recombination.* Cancer Res, 2007. **67**(14): 6619-6625.

114. Ahnesorg, P., P. Smith and S.P. Jackson, *XLF interacts with the XRCC4-DNA ligase IV complex to promote DNA nonhomologous end-joining.* Cell, 2006. **124**(2): 301-313.

115. Filippo, J.S., P. Sung and H. Klein, *Mechanism of eukaryotic homologous recombination.* Annual Review of Biochemistry, 2008. **77**: 229-257.

116. Heyer, W.D., K.T. Ehmsen and J. Liu, *Regulation of Homologous Recombination in Eukaryotes.* Annual Review of Genetics, Vol 44, 2010. **44**: 113-139.

117. Yun, M.H. and K. Hiom, *CtIP-BRCA1 modulates the choice of DNA double-strand-break repair pathway throughout the cell cycle.* Nature, 2009. **459**(7245): 460-463.

118. Zakharyevich, K., Y.M. Ma, S.M. Tang, P.Y.H. Hwang, S. Boiteux, et al., *Temporally and Biochemically Distinct Activities of Exo1 during Meiosis: Double-Strand Break Resection and Resolution of Double Holliday Junctions.* Molecular Cell, 2010. **40**(6): 1001-1015.

119. Chung, W.H., Z. Zhu, A. Papusha, A. Malkova and G. Ira, *Defective Resection at DNA Double-Strand Breaks Leads to De Novo Telomere Formation and Enhances Gene Targeting.* Plos Genetics, 2010. **6**(5).

120. Clerici, M., D. Mantiero, I. Guerini, G. Lucchini and M.P. Longhese, *The Yku70-Yku80 complex contributes to regulate double-strand break processing and checkpoint activation during the cell cycle.* Embo Reports, 2008. **9**(8): 810-818.

121. Symington, L.S. and J. Gautier, *Double-Strand Break End Resection and Repair Pathway Choice.* Annual Review Genetics, 2011. **45**: 247-271.

122. Chernikova, S.B., J.C. Game and J.M. Brown, *Inhibiting homologous recombination for cancer therapy.* Cancer Biology & Therapy, 2012. **13**(2): 61-68.

123. Amitani, I., R.J. Baskin and S.C. Kowalczykowski, *Visualization of Rad54, a chromatin remodeling protein, translocating on single DNA molecules.* Molecular Cell, 2006. **23**(1): 143-148.

124. Mansour, W.Y., S. Schumacher, R. Rosskopf, T. Rhein, F. Schmidt-Petersen, et al., *Hierarchy of nonhomologous end-joining, single-strand annealing and gene conversion at site-directed DNA double-strand breaks.* Nucleic Acids Res, 2008. **36**(12): 4088-4098.

125. Hiom, K., *Coping with DNA double strand breaks.* DNA Repair, 2010. **9**(12): 1256-1263.

126. Lee-Theilen, M., A.J. Matthews, D. Kelly, S. Zheng and J. Chaudhuri, *CtIP promotes microhomology-mediated alternative end joining during class-switch recombination.* Nature Structural & Molecular Biology, 2011. **18**(1): 75-79.

127. Decottignies, A., *Microhomology-mediated end joining in fission yeast is repressed by pku70 and relies on genes involved in homologous recombination.* Genetics, 2007. **176**(3): 1403-1415.

128. Liang, L., L. Deng, S.C. Nguyen, X. Zhao, C.D. Maulion, et al., *Human DNA ligases I and III, but not ligase IV, are required for microhomology-mediated end joining of DNA double-strand breaks.* Nucleic Acids Research, 2008. **36**(10): 3297-3310.

129. Audebert, M., B. Salles and P. Calsou, *Involvement of poly(ADP-ribose) polymerase-1 and XRCC1/DNA ligase III in an alternative route for DNA double-strand breaks rejoining.* Journal of Biological Chemistry, 2004. **279**(53): 55117-55126.

130. Wang, M., W. Wu, W. Wu, B. Rosidi, L. Zhang, et al., *PARP-1 and Ku compete for repair of DNA double strand breaks by distinct NHEJ pathways.* Nucleic Acids Res, 2006. **34**(21): 6170-6182.

131. Levene, S.D., *Theories of pulsed-field gel electrophoresis.* Methods Mol Biol, 1992. **12**: 347-365.

132. Schwartz, D.C. and C.R. Cantor, *Separation of yeast chromosome-sized DNAs by pulsed field gradient gel electrophoresis.* Cell, 1984. **37**(1): 67-75.

133. Pinto, M. and U.o. London, *Induction and Rejoining of DNA Double-strand Breaks in Human Cells After Exposure to Ionising Radiation: An Experimental and Theoretical Approach*. 2002: University of London.

134. Gradzka, I. and T. Iwanenko, *A non-radioactive, PFGE-based assay for low levels of DNA double-strand breaks in mammalian cells.* DNA Repair, 2005. **4**(10): 1129-1139.

135. Stenerlöw, B. and E. Höglund, *Rejoining of double-stranded DNA-fragments studied in different size-intervals*. International journal of radiation biology, 2002. **78**(1): 1-7.

136. Karlsson, K., *Role of Non-homologous End-joining in Repair of Radiation-induced DNA Double-strand Breaks*. 2006: Acta Universitatis Upsaliensis.

137. Warner, J.E. and A.B. Onderdonk, *Method for optimizing pulsed-field gel electrophoresis banding pattern data.* Journal of Molecular Diagnostics, 2003. **5**(1): 21-27.

138. Höglund, E., *DNA Fragmentation in Cultured Cells Exposed to High Linear Energy Transfer Radiation*. 2000: Acta Universitatis Upsaliensis.

139. Löbrich, M., M. Kuhne, J. Wetzel and K. Rothkamm, *Joining of correct and incorrect DNA double-strand break ends in normal human and ataxia telangiectasia fibroblasts.* Genes Chromosomes & Cancer, 2000. **27**(1): 59-68.

140. Löbrich, M., B. Rydberg and P.K. Cooper, *An Assay for Determining Double-Strand Break Distributions and Rejoining Quality in Specific Genome Locations.* Journal of Cellular Biochemistry, 1995: 330-330.

141. Blocher, D. and M. Kunhi, *DNA Double-Strand Break Analysis by Chef Electrophoresis.* International journal of radiation biology, 1990. **58**(1): 23-34.

142. Rydberg, B., *Radiation-induced heat-labile sites that convert into DNA double-strand breaks.* Radiation Research, 2000. **153**(6): 805-812.

143. Karlsson, K.H., I. Radulescu, B. Rydberg and B. Stenerlöw, *Repair of radiation-induced heat-labile sites is independent of DNA-PKcs, XRCC1 and PARP*. Radiation Research, 2008. **169**(5): 506-512.

144. Stenerlöw, B., K.H. Karlsson, B. Cooper and B. Rydberg, *Measurement of prompt DNA double-strand breaks in mammalian cells without including heat-labile sites: Results for cells deficient in nonhomologous end joining.* Radiation Research, 2003. **159**(4): 502-510.

145. Ostling, O. and K.J. Johanson, *Microelectrophoretic study of radiation-induced DNA damages in individual mammalian cells.* Biochemical and Biophysical Research Communications, 1984. **123**(1): 291-298.

146. Singh, S.K., W. Wu, L. Zhang, H. Klammer, M. Wang, et al., *Widespread dependence of backup NHEJ on growth state: ramifications for the use of DNA-PK inhibitors.* International journal of radiation oncology, biology, physics, 2011. **79**: 540-548.

147. Singh, S.K., W. Wu, W. Wu, M. Wang and G. Iliakis, *Extensive repair of DNA double-strand breaks in cells deficient in the DNA-PK-dependent pathway of NHEJ after exclusion of heat-labile sites.* Radiation Research, 2009. **172**: 152-164.

148. Wu, W., M. Wang, W. Wu, S.K. Singh, T. Mussfeldt, et al., *Repair of radiation induced DNA double strand breaks by backup NHEJ is enhanced in G2.* DNA Repair, 2008. **7**(2): 329-338.

149. Kinner, A., W. Wu, C. Staudt and G. Iliakis, *Gamma-H2AX in recognition and signaling of DNA double-strand breaks in the context of chromatin.* Nucleic Acids Res, 2008. **36**(17): 5678-5694.

150. Jensen, A., J. Debus and K.-J. Weber, *S-phase cell-specific modification by gemcitabine of PFGE-analyzed radiation-induced DNA fragmentation and rejoining.* International journal of radiation biology, 2008. **84**: 770-777.

151. Terzoudi, G.I., S.K. Singh, G.E. Pantelias and G. Iliakis, *Premature chromosome condensation reveals DNA-PK independent pathways of chromosome break repair.* Int J Oncol, 2008. **33**(4): 871-879.

152. Karlsson, K.H., I. Radulescu and P.R. Res, *Repair of Radiation-Induced Heat-Labile Sites is Independent of.* 2008. **512**: 506-512.

153. Martín, M., A. Genescà, L. Latre, I. Jaco, G.E. Taccioli, et al., *Postreplicative joining of DNA double-strand breaks causes genomic instability in DNA-PKcs-deficient mouse embryonic fibroblasts.* Cancer research, 2005. **65**: 10223-10232.

154. Antonelli, F., M. Belli, G. Cuttone, V. Dini, G. Esposito, et al., *Induction and repair of DNA double-strand breaks in human cells: dephosphorylation of histone H2AX and its inhibition by calyculin A.* Radiation Research, 2005. **164**: 514-517.

155. Alsbeih, G., M. Torres, N. Al-Harbi and M. Alsubael, *Loss of wild-type Trp53 protein in mouse fibroblasts leads to increased radioresistance with consequent decrease in repair of potentially lethal damage.* Radiation Research, 2004. **161**: 185-192.

156. Reitsema, T.J., J.P. Banáth, S.H. MacPhail and P.L. Olive, *Hypertonic saline enhances expression of phosphorylated histone H2AX after irradiation.* Radiation Research, 2004. **161**: 402-408.

157. Karlsson, K.H. and B. Stenerlöw, *Focus formation of DNA repair proteins in normal and repair-deficient cells irradiated with high-LET ions.* Radiation Research, 2004. **161**(5): 517-527.

158. Rothkamm, K., I. Kru, L.H. Thompson and M. Lo, *Pathways of DNA Double-Strand Break Repair during the Mammalian Cell Cycle.* 2003. **23**: 5706-5715.

159. Sun, J., J. Sui, P. Zhou, Y. Geng, Y. Hu, et al., *Decreased efficiency of gamma-ray-induced DNA double-strand break rejoining in malignant transformants of human bronchial epithelial cells generated by alpha-particle exposure.* Int J Radiat Biol, 2002. **78**(9): 730-780.

160. Banáth, J.P., a. Kim and P.L. Olive, *Overnight lysis improves the efficiency of detection of DNA damage in the alkaline comet assay.* Radiation Research, 2001. **155**: 564-571.

161. Perrault, R., N. Cheong, H. Wang, H. Wang and G. Iliakis, *RPA facilitates rejoining of DNA double-strand breaks in an in vitro assay utilizing genomic DNA as substrate.* International journal of radiation biology, 2001. **77**: 593-607.

162. Brammer, I., M. Zoller and E. Dikomey, *Relationship between cellular radiosensitivity and DNA damage measured by comet assay in human normal, NBS and AT fibroblasts.* International journal of radiation biology, 2001. **77**: 929-938.

163. Wang, H., Z.C. Zeng, T.a. Bui, S.J. DiBiase, W. Qin, et al., *Nonhomologous end-joining of ionizing radiation-induced DNA double-stranded breaks in human tumor cells deficient in BRCA1 or BRCA2.* Cancer research, 2001. **61**: 270-277.

164. Wang, H., Z.C. Zeng, A.R. Perrault, X. Cheng, W. Qin, et al., *Genetic evidence for the involvement of DNA ligase IV in the DNA-PK-dependent pathway of non-homologous end joining in mammalian cells.* Nucleic Acids Res, 2001. **29**(8): 1653-1660.

165. Fouladi, B., C.a. Waldren, B. Rydberg and P.K. Cooper, *Comparison of repair of DNA double-strand breaks in identical sequences in primary human fibroblast and immortal hamster-human hybrid cells harboring a single copy of human chromosome 11.* Radiation Research, 2000. **153**: 795-804.

166. Wachsberger, P.R., W.-h. Li, M. Guo, D. Chen, N. Cheong, et al., *Breaks in Rejoining of DNA Double-Strand Mouse Fibroblasts Ku80-Deficient.* 1999. **407**: 398-407.

167. Dikomey, E. and I. Brammer, *Relationship between cellular radiosensitivity and non-repaired double-strand breaks studied for different growth states, dose rates and plating conditions in a normal human fibroblast line.* International journal of radiation biology, 2000. **76**: 773-781.

168. Foray, N., C.F. Arlett and E.P. Malaise, *Underestimation of the small residual damage when measuring DNA double-strand breaks (DSB): is the repair of radiation-induced DSB complete?* International journal of radiation biology, 1999. **75**: 1589-1595.

169. Frankenburg-Schwager, M., R. Harbich, S. Beckonert and D. Frankenberg, *Half-life values for DNA double-strand break rejoining in yeast can vary by more than an order of magnitude depending on the irradiation conditions.* International journal of radiation biology, 1994. **66**: 543-547.

170. Frankenberg, D., *Survival Curves with Shoulders : Damage Interaction , Unsaturated but Kinetics or Inducible Dose-Dependent Rejoining Repair of DNA Double-Strand Breaks ?* 1994. **100**: 97-100.

171. Frankenberg-Schwager, M., R. Harbich, D. Frankenberg and V. Jain, *2-deoxy-D-glucose inhibits rejoining of radiation-induced DNA double-strand breaks in yeast.* International journal of radiation biology, 1992. **61**: 185-190.

172. Dikomey, E. and J. Franzke, *Effect of heat on induction and repair of DNA strand breaks in X-irradiated CHO cells.* International journal of radiation biology, 1992. **61**: 221-233.

173. Frankenberg-Schwager, M., D. Frankenberg and R. Harbich, *Different oxygen enhancement ratios for induced and unrejoined DNA double-strand breaks in eukaryotic cells.* Radiation Research, 1991. **128**: 243-250.

174. Frankenberg-Schwager, M., D. Frankenberg, R. Harbich and C. Adamczyk, *A comparative study of rejoining of DNA double-strand breaks in yeast irradiated with 3.5 MeV alpha-particles or with 30 MeV electrons.* International journal of radiation biology, 1990. **57**: 1151-1168.

175. Botchway, S.W., D.L. Stevens, M.A. Hill, T.J. Jenner, P.O. Neill, et al., *Induction and Rejoining of DNA Double-Strand Breaks in Chinese with Characteristic Aluminum K Hamster V79-4 Cells Irradiated X Rays and Copper L Ultrasoft.* 1997. **324**: 317-324.

176. Stenerlöw, B., J. Carlsson, E. Blomquist and K. Erixon, *Clonogenic cell survival and rejoining of DNA double-strand breaks: comparisons between three cell lines after photon or He ion irradiation.* International journal of radiation biology, 1994. **65**: 631-639.

177. Ahnström, G., J. Nygren and S. Eriksson, *The effect of dimethyl sulphoxide on the induction and repair of double-strand breaks in human cells after irradiation with gamma-rays and accelerated ions: rapid or slow repair may*

depend on accessibility of breaks in chromatin of different compactness. International journal of radiation biology, 2000. **76**: 533-538.

178. Asaithamby, A., N. Uematsu, A. Chatterjee, M.D. Story, S. Burma, et al., *Repair of HZE-particle-induced DNA double-strand breaks in normal human fibroblasts.* Radiation Research, 2008. **169**: 437-446.

179. Belli, M., R. Cherubini, M. Dalla Vecchia, V. Dini, G. Moschini, et al., *DNA DSB induction and rejoining in V79 cells irradiated with light ions: a constant field gel electrophoresis study.* International journal of radiation biology, 2000. **76**: 1095-1104.

180. Coquerelle, T.M., K.F. Weibezahn and C. Lücke-Huhle, *Rejoining of double strand breaks in normal human and ataxia-telangiectasia fibroblasts after exposure to 60Co gamma-rays, 241Am alpha-particles or bleomycin.* International journal of radiation biology and related studies in physics, chemistry, and medicine, 1987. **51**: 209-218.

181. deLara, C.M., T.J. Jenner, K.M. Townsend, S.J. Marsden and P. O'Neill, *The effect of dimethyl sulfoxide on the induction of DNA double-strand breaks in V79-4 mammalian cells by alpha particles.* Radiation Research, 1995. **144**: 43-49.

182. Foray, N., C. Monroco, B. Marples, J.H. Hendry, B. Fertil, et al., *Repair of radiation-induced DNA double-strand breaks in human fibroblasts is consistent with a continuous spectrum of repair probability.* International journal of radiation biology, 1998. **74**: 551-560.

183. Heilmann, J., H. Rink, G. Taucher-Scholz and G. Kraft, *DNA strand break induction and rejoining and cellular recovery in mammalian cells after heavy-ion irradiation.* Radiation Research, 1993. **135**: 46-55.

184. Höglund, E., E. Blomquist, J. Carlsson and B. Stenerlöw, *DNA damage induced by radiation of different linear energy transfer: initial fragmentation.* International journal of radiation biology, 2000. **76**: 539-547.

185. Höglund, H. and B. Stenerlöw, *Induction and rejoining of DNA double-strand breaks in normal human skin fibroblasts after exposure to radiation of different linear energy transfer: possible roles of track structure and chromatin organization.* Radiation Research, 2001. **155**: 818-825.

186. Kühne, M., K. Rothkamm and M. Löbrich, *No dose-dependence of DNA double-strand break misrejoining following alpha-particle irradiation.* International journal of radiation biology, 2000. **76**: 891-900.

187. Löbrich, M., P.K. Cooper and B. Rydberg, *Joining of correct and incorrect DNA ends at double-strand breaks produced by high-linear energy transfer radiation in human fibroblasts.* Radiation Research, 1998. **150**(6): 619-626.

188. Löbrich, M., B. Rydberg and P.K. Cooper, *DNA double-strand breaks induced by high-energy neon and iron ions in human fibroblasts. II. Probing individual notI fragments by hybridization.* Radiation Research, 1994. **139**: 142-151.

189. Meijer, a.E., a.R.-M. Jernberg, T. Heiden, B. Stenerlöw, L.M. Persson, et al., *Dose and time dependent apoptotic response in a human melanoma cell line exposed to accelerated boron ions at four different LET.* International journal of radiation biology, 2005. **81**: 261-272.

190. Newman, H.C., K.M. Prise, M. Folkard and B.D. Michael, *DNA double-strand break distributions in X-ray and alpha-particle irradiated V79 cells: evidence for non-random breakage.* International journal of radiation biology, 1997. **71**: 347-363.

191. Okayasu, R., *Repair of DNA damage induced by accelerated heavy ions--a mini review.* International journal of cancer. Journal international du cancer, 2012. **130**: 991-1000.

192. Pinto, M., K.M. Prise and B.D. Michael, *Evidence for complexity at the nanometer scale of radiation-induced DNA DSBs as a determinant of rejoining kinetics.* Radiation Research, 2005. **164**: 73-85.

193. Prise, K.M., G. Ahnström, M. Belli, J. Carlsson, D. Frankenberg, et al., *A review of dsb induction data for varying quality radiations.* International journal of radiation biology, 1998. **74**: 173-184.

194. Ritter, S. and M. Durante, *Heavy-ion induced chromosomal aberrations: a review.* Mutation research, 2010. **701**: 38-46.

195. Roots, R., W. Holley, a. Chatterjee, M. Irizarry and G. Kraft, *The formation of strand breaks in DNA after high-LET irradiation: a comparison of data from in vitro and cellular systems.* International journal of radiation biology, 1990. **58**: 55-69.

196. Rydberg, B., M. Löbrich and P.K. Cooper, *DNA double-strand breaks induced by high-energy neon and iron ions in human fibroblasts. I. Pulsed-field gel electrophoresis method.* Radiation Research, 1994. **139**: 133-141.

197. Stenerlöw, B., E. Blomquist, E. Grusell, T. Hartman and J. Carlsson, *Rejoining of DNA double-strand breaks induced by accelerated nitrogen ions.* International journal of radiation biology, 1996. **70**(4): 413-420.

198. Stenerlöw, B., E. Höglund and J. Carlsson, *Induction and rejoining of large DNA fragments after ion irradiation.* Radiation Research, 1999. **151**: 642-648.

199. Stenerlöw, B., E. Höglund, J. Carlsson and E. Blomquist, *Rejoining of DNA fragments produced by radiations of different linear energy transfer.* International journal of radiation biology, 2000. **76**(4): 549-557.

200. Suzuki, M., M. Watanabe, K. Suzuki, K. Nakano and K. Matsui, *Heavy ion-induced chromosome breakage studied by premature chromosome condensation (PCC) in Syrian hamster embryo cells.* International journal of radiation biology, 1992. **62**: 581-586.

201. Tsoulou, E., L. Baggio, R. Cherubini and C.a. Kalfas, *Low-dose hypersensitivity of V79 cells under exposure to gamma-rays and 4He ions of different energies: survival and chromosome aberrations.* International journal of radiation biology, 2001. **77**: 1133-1139.

202. Weber, K.J. and M. Flentje, *Lethality of heavy ion-induced DNA double-strand breaks in mammalian cells.* International journal of radiation biology, 1993. **64**: 169-178.

203. Yokota, Y., S. Yamada, Y. Hase, N. Shikazono, I. Narumi, et al., *Initial Yields of DNA Double-Strand Breaks and DNA Fragmentation Patterns Depend on Linear Energy Transfer in Tobacco BY-2 Protoplasts Irradiated with Helium , Carbon and Neon Ions Linear Energy Transfer in Tobacco BY-2 Protoplasts Irra-.* 2007. **101**: 94-101.

204. Kemp, L.M., S.G. Sedgwick and P.A. Jeggo, *X-ray sensitive mutants of Chinese hamster ovary cells defective in double-strand break rejoining.* Mutat Res, 1984. **132**(5-6): 189-196.

205. Koch, C.J. and A.R. Giandomenico, *The alkaline elution technique for measuring DNA single strand breaks: increased reliability and sensitivity.* Anal Biochem, 1994. **220**(1): 58-65.

206. Löbrich, M., A. Shibata, A. Beucher, A. Fisher, M. Ensminger, et al., *gamma H2AX foci analysis for monitoring DNA double-strand break repair Strengths, limitations and optimization.* Cell Cycle, 2010. **9**(4): 662-669.

207. Iliakis, G., *The anatomy and cell cycle evolution of DNA damage signaling and repair foci.* Cell Cycle, 2010. **9**(3): 444-445.

208. Markova, E., N. Schultz and I.Y. Belyaev, *Kinetics and dose-response of residual 53BP1/gamma-H2AX foci: Co-localization, relationship with DSB repair and clonogenic survival.* International journal of radiation biology, 2007. **83**(5): 319-329.

209. Nakamura, A.J., V.A. Rao, Y. Pommier and W.M. Bonner, *The complexity of phosphorylated H2AX foci formation and DNA repair assembly at DNA double-strand breaks.* Cell Cycle, 2010. **9**(2): 389-397.

210. Paull, T.T., E.P. Rogakou, V. Yamazaki, C.U. Kirchgessner, M. Gellert, et al., *A critical role for histone H2AX in recruitment of repair factors to nuclear foci after DNA damage.* Current Biology, 2000. **10**(15): 886-895.

211. Zlobinskaya, O., G. Dollinger, D. Michalski, V. Hable, C. Greubel, et al., *Induction and repair of DNA double-strand breaks assessed by gamma-H2AX foci after irradiation with pulsed or continuous proton beams.* Radiation and Environmental Biophysics, 2012. **51**(1): 23-32.

212. Tobias, F., D. Lob, N. Lengert, M. Durante, B. Drossel, et al., *Spatiotemporal dynamics of early DNA damage response proteins on complex DNA lesions.* Plos One, 2013. **8**(2): e57953.

213. Hable, V., G.A. Drexler, T. Bruning, C. Burgdorf, C. Greubel, et al., *Recruitment kinetics of DNA repair proteins Mdc1 and Rad52 but not 53BP1 depend on damage complexity.* Plos One, 2012. **7**(7): e41943.

214. Krawczyk, P.M., J. Stap, C. van Oven, R. Hoebe and J.A. Aten, *Clustering of double strand break-containing chromosome domains is not inhibited by inactivation of major repair proteins.* Radiat Prot Dosimetry, 2006. **122**(1-4): 150-153.

215. Krawczyk, P.M., T. Borovski, J. Stap, T. Cijsouw, R. ten Cate, et al., *Chromatin mobility is increased at sites of DNA double-strand breaks.* Journal of Cell Science, 2012. **125**(9): 2127-2133.

216. Du, L.L., T.M. Nakamura and P. Russell, *Histone modification-dependent and -independent pathways for recruitment of checkpoint protein Crb2 to double-strand breaks.* Genes & Development, 2006. **20**(12): 1583-1596.

217. Melander, F., S. Bekker-Jensen, J. Falck, J. Bartek, N. Mailand, et al., *Phosphorylation of SDT repeats in the MDC1 N terminus triggers retention of NBS1 at the DNA damage-modified chromatin.* Journal of Cell Biology, 2008. **181**(2): 213-226.

218. Bekker-Jensen, S. and N. Mailand, *Assembly and function of DNA double-strand break repair foci in mammalian cells.* DNA Repair, 2010. **9**(12): 1219-1228.

219. Mailand, N., S. Bekker-Jensen, H. Faustrup, F. Melander, J. Bartek, et al., *RNF8 ubiquitylates histones at DNA double-strand breaks and promotes assembly of repair proteins.* Cell, 2007. **131**(5): 887-900.

220. Wang, B., K. Hurov, K. Hofmann and S.J. Elledge, *NBA1, a new player in the Brca1 A complex, is required for DNA damage resistance and checkpoint control.* Genes & Development, 2009. **23**(6): 729-739.

221. Costes, S.V., I. Chiolo, J.M. Pluth, M.H. Barcellos-Hoff and B. Jakob, *Spatiotemporal characterization of ionizing radiation induced DNA damage*

foci and their relation to chromatin organization. Mutation Research-Reviews in Mutation Research, 2010. **704**(1-3): 78-87.

222. Belyaev, I.Y., *Radiation-induced DNA repair foci: Spatio-temporal aspects of formation, application for assessment of radiosensitivity and biological dosimetry.* Mutation Research-Reviews in Mutation Research, 2010. **704**(1-3): 132-141.

223. Okayasu, R., M. Okada, A. Okabe, M. Noguchi, K. Takakura, et al., *Repair of DNA damage induced by accelerated heavy ions in mammalian cells proficient and deficient in the non-homologous end-joining pathway.* Radiation Research, 2006. **165**(1): 59-67.

224. Noon, A.T. and A.A. Goodarzi, *53BP1-mediated DNA double strand break repair: Insert bad pun here.* DNA Repair, 2011. **10**(10): 1071-1076.

225. Darzynkiewicz, Z., F. Traganos, H. Zhao, H.D. Halicka, J. Skommer, et al., *Analysis of Individual Molecular Events of DNA Damage Response by Flow- and Image-Assisted Cytometry.* Recent Advances in Cytometry, Part B: Advances in Applications, Fifth Edition, 2011. **103**: 115-147.

226. Goodarzi, A.A. and P.A. Jeggo, *Irradiation induced foci (IRIF) as a biomarker for radiosensitivity.* Mutation Research-Fundamental and Molecular Mechanisms of Mutagenesis, 2012. **736**(1-2): 39-47.

227. Richmond, T.J., *Hot papers - Crystal structure - Crystal structure of the nucleosome core particle at 2.8 angstrom resolution by K. Luger, A.W. Mader, R.K. Richmond, D.F. Sargent, T.J. Richmond - Comments.* Scientist, 1999. **13**(23): 15-15.

228. Luger, K., A.W. Mader, R.K. Richmond, D.F. Sargent and T.J. Richmond, *Crystal structure of the nucleosome core particle at 2.8 A resolution.* Nature, 1997. **389**(6648): 251-260.

229. Davey, C.A., D.F. Sargent, K. Luger, A.W. Maeder and T.J. Richmond, *Solvent mediated interactions in the structure of the nucleosome core particle at 1.9 angstrom resolution.* Journal of Molecular Biology, 2002. **319**(5): 1097-1113.

230. Takahashi, A. and T. Ohnishi, *Does gamma H2AX foci formation depend on the presence of DNA double strand breaks?* Cancer Letters, 2005. **229**(2): 171-179.

231. Rogakou, E.P., D.R. Pilch, A.H. Orr, V.S. Ivanova and W.M. Bonner, *DNA double-stranded breaks induce histone H2AX phosphorylation on serine 139.* Journal of Biological Chemistry, 1998. **273**(10): 5858-5868.

232. Rothkamm, K. and M. Löbrich, *Evidence for a lack of DNA double-strand break repair in human cells exposed to very low x-ray doses.* Proceedings of the National Academy of Sciences of the United States of America, 2003. **100**(9): 5057-5062.

233. Burma, S., B.P. Chen, M. Murphy, A. Kurimasa and D.J. Chen, *ATM phosphorylates histone H2AX in response to DNA double-strand breaks.* Journal of Biological Chemistry, 2001. **276**(45): 42462-42467.

234. Stiff, T., M. O'Driscoll, N. Rief, K. Iwabuchi, M. Löbrich, et al., *ATM and DNA-PK function redundantly to phosphorylate H2AX after exposure to ionizing radiation.* Cancer research, 2004. **64**(7): 2390-2396.

235. Falck, J., J. Coates and S.P. Jackson, *Conserved modes of recruitment of ATM, ATR and DNA-PKcs to sites of DNA damage.* Nature, 2005. **434**(7033): 605-611.

236. Chowdhury, D., M.C. Keogh, H. Ishii, C.L. Peterson, S. Buratowski, et al., *gamma-H2AX dephosphorylation by protein phosphatase 2A facilitates DNA double-strand break repair.* Molecular Cell, 2005. **20**(5): 801-809.

237. Ewald, B., D. Sampath and W. Plunkett, *H2AX phosphorylation marks gemcitabine-induced stalled replication forks and their collapse upon S-phase checkpoint abrogation.* Molecular Cancer Therapeutics, 2007. **6**(4): 1239-1248.

238. Panier, S. and D. Durocher, *Regulatory ubiquitylation in response to DNA double-strand breaks.* DNA Repair, 2009. **8**(4): 436-443.

239. Rothkamm, K. and S. Horn, *gamma-H2AX as protein biomarker for radiation exposure.* Annali Dell Istituto Superiore Di Sanita, 2009. **45**(3): 265-271.

240. Sedelnikova, O.A., E.P. Rogakou, I.G. Panyutin and W.M. Bonner, *Quantitative detection of (125) IdU-induced DNA double-strand breaks with gamma-H2AX antibody.* Radiation Research, 2002. **158**(4): 486-492.

241. Celeste, A., S. Petersen, P.J. Romanienko, O. Fernandez-Capetillo, H.T. Chen, et al., *Genomic instability in mice lacking histone H2AX.* Science, 2002. **296**(5569): 922-927.

242. Yuan, J.S. and J.J. Chen, *MRE11-RAD50-NBS1 Complex Dictates DNA Repair Independent of H2AX.* Journal of Biological Chemistry, 2010. **285**(2): 1097-1104.

243. Celeste, A., O. Fernandez-Capetillo, M.J. Kruhlak, D.R. Pilch, D.W. Staudt, et al., *Histone H2AX phosphorylation is dispensable for the initial recognition of DNA breaks.* Nature Cell Biology, 2003. **5**(7): 675-U651.

244. Xie, A.Y., N. Puget, I. Shim, S. Odate, I. Jarzyna, et al., *Control of sister chromatid recombination by histone H2AX.* Molecular Cell, 2004. **16**(6): 1017-1025.

245. Sonoda, E., G.Y. Zhao, M. Kohzaki, P.K. Dhar, K. Kikuchi, et al., *Collaborative roles of gamma H2AX and the Rad51 paralog Xrcc3 in homologous recombinational repair.* DNA Repair, 2007. **6**(3): 280-292.

246. Boker, W. and G. Iliakis, *Computational methods for analysis of foci: Validation for radiation-induced gamma-H2AX foci in human cells.* Radiation Research, 2006. **165**(1): 113-124.

247. Rothkamm, K., S. Balroop, J. Shekhdar, P. Fernie and V. Goh, *Leukocyte DNA damage after multi-detector row CT: A quantitative biomarker of low-level radiation exposure.* Radiology, 2007. **242**(1): 244-251.

248. Schultz, L.B., N.H. Chehab, A. Malikzay and T.D. Halazonetis, *p53 Binding protein 1 (53BP1) is an early participant in the cellular response to DNA double-strand breaks.* Journal of Cell Biology, 2000. **151**(7): 1381-1390.

249. Sengupta, S., A.I. Robles, S.P. Linke, N.I. Sinogeeva, R. Zhang, et al., *Functional interaction between BLM helicase and 53BP1 in a Chk1-mediated pathway during S-phase arrest.* Journal of Cell Biology, 2004. **166**(6): 801-813.

250. Falk, M., E. Lukasova, B. Gabrielova, V. Ondrej and S. Kozubek, *Chromatin dynamics during DSB repair.* Biochimica Et Biophysica Acta-Molecular Cell Research, 2007. **1773**(10): 1534-1545.

251. Nazarov, O.B., A.N. Smirnova, R.I. Krutilina, M.P. Svetlova, L.V. Solovjeva, et al., *Dephosphorylation of histone gamma-H2AX during repair of DNA double-strand breaks in mammalian cells and its inhibition by calyculin A.* Radiation Research, 2003. **160**(3): 309-317.

252. Hamer, G., H.L. Roepers-Gajadien, A. van Duyn-Goedhart, I.S. Gademan, H.B. Kal, et al., *DNA double-strand breaks and gamma-H2AX signaling in the testis.* Biology of Reproduction, 2003. **68**(2): 628-634.

253. Banath, J.P., S.H. Macphail and P.L. Olive, *Radiation sensitivity, H2AX phosphorylation, and kinetics of repair of DNA strand breaks in irradiated cervical cancer cell lines.* Cancer Res, 2004. **64**(19): 7144-7149.

254. Han, J.X., M.J. Hendzel and J. Allalunis-Turner, *Quantitative analysis reveals asynchronous and more than DSB-associated histone H2AX phosphorylation after exposure to ionizing radiation.* Radiation Research, 2006. **165**(3): 283-292.

255. Ismail, I.H., T.I. Wadhra and O. Hammarsten, *An optimized method for detecting gamma-H2AX in blood cells reveals a significant interindividual variation in the gamma-H2AX response among humans.* Nucleic Acids Research, 2007. **35**(5).

256. Leatherbarrow, E.L., J.V. Harper, F.A. Cucinotta and P. O'Neill, *Induction and quantification of gamma-H2AX foci following low and high LET-irradiation.* International journal of radiation biology, 2006. **82**(2): 111-118.

257. Smallbone, K., E. Simeonidis, N. Swainston and P. Mendes, *Towards a genome-scale kinetic model of cellular metabolism.* Bmc Systems Biology, 2010. **4**.

258. Boldogh, I., D. Milligan, M.S. Lee, H. Bassett, R.S. Lloyd, et al., *hMYH cell cycle-dependent expression, subcellular localization and association with replication foci: evidence suggesting replication-coupled repair of adenine : 8-oxoguanine mispairs.* Nucleic Acids Research, 2001. **29**(13): 2802-2809.

259. Tarsounas, M., D. Davies and S.C. West, *BRCA2-dependent and independent formation of RAD51 nuclear foci.* Oncogene, 2003. **22**(8): 1115-1123.

260. Liu, Y. and N. Maizels, *Coordinated response of mammalian Rad51 and Rad52 to DNA damage.* EMBO Rep, 2000. **1**(1): 85-90.

261. Siaud, N., M.A. Barbera, A. Egashira, I. Lam, N. Christ, et al., *Plasticity of BRCA2 function in homologous recombination: genetic interactions of the PALB2 and DNA binding domains.* PLoS Genet, 2011. **7**(12): e1002409.

262. Yang, H., P.D. Jeffrey, J. Miller, E. Kinnucan, Y. Sun, et al., *BRCA2 function in DNA binding and recombination from a BRCA2-DSS1-ssDNA structure.* Science, 2002. **297**(5588): 1837-1848.

263. Robberecht, C., T. Voet, M.Z. Esteki, B.A. Nowakowska and J.R. Vermeesch, *Nonallelic homologous recombination between retrotransposable elements is a driver of de novo unbalanced translocations.* Genome Research, 2013. **23**(3): 411-418.

264. Tyson, G., F. Spasoro and K.B. Smith, *iFall - A Cell-phone Based Fall Detection and Warning System.* Journal of the American Geriatrics Society, 2010. **58**: 69-70.

265. Tyson, R.A., D.B.A. Epstein, K.I. Anderson and T. Bretschneider, *High Resolution Tracking of Cell Membrane Dynamics in Moving Cells: an Electrifying Approach.* Mathematical Modelling of Natural Phenomena, 2010. **5**(1): 34-55.

266. Zwolak, J., N. Adjerid, E.Z. Bagci, J.J. Tyson and J.C. Sible, *A quantitative model of the effect of unreplicated DNA on cell cycle progression in frog egg extracts.* Journal of Theoretical Biology, 2009. **260**(1): 110-120.

267. Azzoli, C.G., J. Patel, L.M. Krug, V. Miller, S. Subzwari, et al., *Pralatrexate plus vitamin B12 and folic acid supplementation in patients with previously-treated, advanced non-small cell lung cancer: safety and efficacy in a phase 1 trial.* Ejc Supplements, 2009. **7**(2): 530-531.

268. Li, S.H., P. Brazhnik, B. Sobral and J.J. Tyson, *Temporal Controls of the Asymmetric Cell Division Cycle in Caulobacter crescentus.* Plos Computational Biology, 2009. **5**(8).

269. Zhang, T.L., P. Brazhnik and J.J. Tyson, *Computational Analysis of Dynamical Responses to the Intrinsic Pathway of Programmed Cell Death.* Biophysical Journal, 2009. **97**(2): 415-434.

270. Brown, A.B., C. Rudin, N. Rizvi, W. Travis, N. Takebe, et al., *Phase I study of obatoclax mesylate (GX15-070MS), a bcl-2 antagonist, plus topotecan in relapsed small cell lung carcinoma and other solid tumors.* Journal of Clinical Oncology, 2009. **27**(15).

271. Walker, J.R., R.A. Corpina and J. Goldberg, *Structure of the Ku heterodimer bound to DNA and its implications for double-strand break repair.* Nature, 2001. **412**(6847): 607-614.

272. Mimoi, T. and J.A. Hardin, *Mechanism of interaction between Ku protein and DNA.* The Journal of Biological Chemistry, 1986. **261**(22): 10375-10379.

273. Meek, K., V. Dang and S.P. Lees-Miller, *DNA-PK: The Means to Justify the Ends?* Advances in Immunology, 2008. **99**: 33-58.

274. Reynolds, P., J.A. Anderson, J.V. Harper, M.A. Hill, S.W. Botchway, et al., *The dynamics of Ku70/80 and DNA-PKcs at DSBs induced by ionizing radiation is dependent on the complexity of damage.* Nucleic Acids Research, 2012.

275. Jeggo, P. and P. O'Neill, *The Greek Goddess, Artemis, reveals the secrets of her cleavage.* DNA Repair (Amst), 2002. **1**(9): 771-777.

276. Chiu, C.Y., R.B. Cary, D.J. Chen, S.R. Peterson and P.L. Stewart, *Cryo-EM imaging of the catalytic subunit of the DNA-dependent protein kinase.* Journal of Molecular Biology, 1998. **284**(4): 1075-1081.

277. Leuther, K.K., O. Hammarsten, R.D. Kornberg and G. Chu, *Structure of DNA-dependent protein kinase: implications for its regulation by DNA.* EMBO Journal, 1999. **18**(5): 1114-1123.

278. Tashiro, S., J. Walter, A. Shinohara, N. Kamada and T. Cremer, *Rad51 accumulation at sites of DNA damage and in postreplicative chromatin.* Journal of Cell Biology, 2000. **150**(2): 283-291.

279. Tashiro, S., N. Kotomura, A. Shinohara, K. Tanaka, K. Ueda, et al., *S phase specific formation of the human Rad51 protein nuclear foci in lymphocytes.* Oncogene, 1996. **12**(10): 2165-2170.

280. Yamamoto, A., T. Taki, H. Yagi, T. Habu, K. Yoshida, et al., *Cell cycle dependent expression of the mouse Rad51 gene in proliferating cells.* Molecular & General Genetics, 1996. **251**(1): 1-12.

281. Buis, J., T. Stoneham, E. Spehalski and D.O. Ferguson, *Mre11 regulates CtIP-dependent double-strand break repair by interaction with CDK2.* Nature Structural & Molecular Biology, 2012. **19**(2): 246-252.

282. Cheng, Q., N. Barboule, P. Frit, D. Gomez, O. Bombarde, et al., *Ku counteracts mobilization of PARP1 and MRN in chromatin damaged with DNA double-strand breaks.* Nucleic Acids Research, 2011. **39**(22): 9605-9619.

283. Chan, S.H., A.M. Yu and M. Mcvey, *Dual Roles for DNA Polymerase Theta in Alternative End-Joining Repair of Double-Strand Breaks in Drosophila.* Plos Genetics, 2010. **6**(7).

284. Rass, E., A. Grabarz, I. Plo, J. Gautier, P. Bertrand, et al., *Role of Mre11 in chromosomal nonhomologous end joining in mammalian cells.* Nat Struct Mol Biol, 2009. **16**(8): 819-824.

285. Dinkelmann, M., E. Spehalski, T. Stoneham, J. Buis, Y. Wu, et al., *Multiple functions of MRN in end-joining pathways during isotype class switching.* Nat Struct Mol Biol, 2009. **16**(8): 808-813.

286. Audebert, M., B. Salles, M. Weinfeld and P. Calsou, *Involvement of polynucleotide kinase in a poly(ADP-ribose) polymerase-1-dependent DNA double-strand breaks rejoining pathway.* J Mol Biol, 2006. **356**(2): 257-265.

287. Audebert, M., B. Salles and P. Calsou, *Effect of double-strand break DNA sequence on the PARP-1 NHEJ pathway.* Biochem Biophys Res Commun, 2008. **369**(3): 982-988.

288. Liang, L., L. Deng, Y.P. Chen, G.C. Li, C.S. Shao, et al., *Modulation of DNA end joining by nuclear proteins.* Journal of Biological Chemistry, 2005. **280**(36): 31442-31449.

289. Crespan, E., T. Czabany, G. Maga and U. Hubscher, *Microhomology-mediated DNA strand annealing and elongation by human DNA polymerases lambda and beta on normal and repetitive DNA sequences.* Nucleic Acids Research, 2012. **40**(12): 5577-5590.

290. Wang, H., Z.C. Zeng, T.A. Bui, E. Sonoda, M. Takata, et al., *Efficient rejoining of radiation-induced DNA double-strand breaks in vertebrate cells deficient in genes of the RAD52 epistasis group.* Oncogene, 2001. **20**(18): 2212-2224.

291. Simsek, D., E. Brunet, S.Y.W. Wong, S. Katyal, Y. Gao, et al., *DNA Ligase III Promotes Alternative Nonhomologous End-Joining during Chromosomal Translocation Formation.* Plos Genetics, 2011. **7**(6).

292. Aguilera, A. and R. Rothstein, *Molecular genetics of recombination*. Topics in current genetics,. 2007, Berlin ; New York: Springer. xxiv, 524 p.

293. Symington, L.S., *Role of RAD52 epistasis group genes in homologous recombination and double-strand break repair.* Microbiol Mol Biol Rev, 2002. **66**(4): 630-670.

294. Deng, X., A. Prakash, K. Dhar, G.S. Baia, C. Kolar, et al., *Human replication protein A-Rad52-single-stranded DNA complex: stoichiometry and evidence for strand transfer regulation by phosphorylation.* Biochemistry, 2009. **48**(28): 6633-6643.

295. Sharma, S., J.K. Hicks, C.L. Chute, J.R. Brennan, J.Y. Ahn, et al., *REV1 and polymerase zeta facilitate homologous recombination repair.* Nucleic Acids Research, 2012. **40**(2): 682-691.

296. Canman, C.E., *REV1 and DNA Polymerase zeta Facilitate Homologous Recombination Repair*. Environmental and Molecular Mutagenesis, 2010. **51**(7): 703-703.

297. Löbrich, M., B. Rydberg and P.K. Cooper, *Repair of x-ray-induced DNA double-strand breaks in specific Not I restriction fragments in human fibroblasts: Joining of correct and incorrect ends.* Proceedings of the National Academy of Sciences of the United States of America, 1995. **92**(26): 12050-12054.

298. Kuhne, M., E. Riballo, N. Rief, K. Rothkamm, P.A. Jeggo, et al., *A double-strand break repair defect in ATM-deficient cells contributes to radiosensitivity.* Cancer research, 2004. **64**(2): 500-508.

299. Asaithamby, A. and D.J. Chen, *Cellular responses to DNA double-strand breaks after low-dose gamma-irradiation.* Nucleic Acids Research, 2009. **37**(12): 3912-3923.

300. Lindborg, L. and J.E. Grindborg, *Nanodosimetric results and radiotherapy beams: A clinical application?* Radiation Protection Dosimetry, 1997. **70**(1-4): 541-546.

301. Botchway, S.W., D.L. Stevens, M.A. Hill, T.J. Jenner and P. ONeill, *Induction and rejoining of DNA double-strand breaks in Chinese hamster V79-4 cells*

irradiated with characteristic aluminum K and copper L ultrasoft X rays. Radiation Research, 1997. **148**(4): 317-324.

302. de Lara, C.M., M.A. Hill, T.J. Jenner, D. Papworth and P. O'Neill, *Dependence of the yield of DNA double-strand breaks in Chinese hamster V79-4 cells on the photon energy of ultrasoft X rays.* Radiation Research, 2001. **155**(3): 440-448.

303. Emfietzoglou, D., F.A. Cucinotta and H. Nikjoo, *A complete dielectric response model for liquid water: A solution of the Bethe Ridge problem.* Radiation Research, 2005. **164**(2): 202-211.

304. Nikjoo, H., S. Uehara, D. Emfietzoglou and F.A. Cucinotta, *Track-structure codes in radiation research.* Radiation Measurements, 2006. **41**(9-10): 1052-1074.

305. Liamsuwan, T., D. Emfietzoglou, S. Uehara and H. Nikjoo, *Microdosimetry of low-energy electrons.* International journal of radiation biology, 2012. **88**(12): 899-907.

306. Emfietzoglou, D., I. Kyriakou, I. Abril, R. Garcia-Molina, I.D. Petsalakis, et al., *Electron inelastic mean free paths in biological matter based on dielectric theory and local-field corrections.* Nuclear Instruments & Methods in Physics Research Section B-Beam Interactions with Materials and Atoms, 2009. **267**(1): 45-52.

307. Emfietzoglou, D., R. Garcia-Molina, I. Kyriakou, I. Abril and H. Nikjoo, *A dielectric response study of the electronic stopping power of liquid water for energetic protons and a new I-value for water.* Physics in Medicine and Biology, 2009. **54**(11): 3451-3472.

308. Nikjoo, H., D.T. Goodhead, D.E. Charlton and H.G. Paretzke, *Energy deposition in small cylindrical targets by ultrasoft x-rays.* Phys Med Biol, 1989. **34**(6): 691-705.

309. Uehara, S., H. Nikjoo and D.T. Goodhead, *Cross-Sections for Water-Vapor for the Monte-Carlo Electron Track Structure Code from 10-Ev to the Mev Region.* Physics in Medicine and Biology, 1993. **38**(12): 1841-1858.

310. Emfietzoglou, D. and H. Nikjoo, *The effect of model approximations on single-collision distributions of low-energy electrons in liquid water.* Radiation Research, 2005. **163**(1): 98-111.

311. Nikjoo, H., D. Emfietzoglou and D.E. Charlton, *The Auger effect in physical and biological research.* International journal of radiation biology, 2008. **84**(12): 1011-1026.

312. Roots, R. and S. Okada, *Estimation of life times and diffusion distances of radicals involved in X-ray-induced DNA strand breaks or killing of mammalian cells.* Radiation Research, 1975. **64**(2): 306-320.

313. Chapman, J.D. and C.J. Gillespie, *Radiation-induced events and their time scale in mammalian cells.* Adv. Radiat. Biol, 1981. **9**(143-198): 54.

314. Charlton, D. and J. Humm, *A method of calculating initial DNA strand breakage following the decay of incorporated 125I.* International journal of radiation biology, 1988. **53**(3): 353-365.

315. Martin, R.F. and W.A. Haseltine, *Range of radiochemical damage to DNA with decay of iodine-125.* Science, 1981. **213**(4510): 896-898.

316. Nikjoo, H., P. ONeill, D.T. Goodhead and M. Terrissol, *Computational modelling of low-energy electron-induced DNA damage by early physical and chemical events.* International journal of radiation biology, 1997. **71**(5): 467-483.

317. Blocher, D., *In Chef Electrophoresis a Linear Induction of Dsb Corresponds to a Nonlinear Fraction of Extracted DNA with Dose.* International journal of radiation biology, 1990. **57**(1): 7-12.

318. Nikjoo, H., P. Girard, D.E. Charlton, K.G. Hofer and C.A. Laughton, *Auger electrons - A nanoprobe for structural, molecular and cellular processes.* Radiation Protection Dosimetry, 2006. **122**(1-4): 72-79.

319. Watanabe, R. and H. Nikjoo, *Modelling the effect of incorporated halogenated pyrimidine on radiation-induced DNA strand breaks.* International journal of radiation biology, 2002. **78**(11): 953-966.

320. Umrania, Y., H. Nikjoo and J.M. Goodfellow, *A Knowledge-Based Model of DNA Hydration.* International journal of radiation biology, 1995. **67**(2): 145-152.

321. Röntgen, W.C., *Über eine neue Art von Strahlen. Vorläufige (1) Mitteilung.* Sirzungsberichte das Physikalisch-Medizinischen Gesellschaft, 1895: 138-148.

322. Thacker, J., *Radiation-induced mutation in mammalian cells at low doses and dose rates.* Advances in radiation biology, 1992. **16**: 77-124.

323. Natarajan, A., A. Balajee, J. Boei, S. Chatterjee, F. Darroudi, et al., *Recent developments in the assessment of chromosomal damage.* International journal of radiation biology, 1994. **66**(5): 615-623.

324. Cade, S., *Radiation induced cancer in man.* Br J Radiol, 1957. **30**(356): 393-402.

325. Bryant, H.E., N. Schultz, H.D. Thomas, K.M. Parker, D. Flower, et al., *Specific killing of BRCA2-deficient tumours with inhibitors of poly(ADP-ribose) polymerase.* Nature, 2005. **434**(7035): 913-917.

326. Brahme, A., *Accurate description of the cell survival and biological effect at low and high doses and LET's.* Journal of Radiation Research, 2011. **52**(4): 389-407.

327. Helleday, T., E. Petermann, C. Lundin, B. Hodgson and R.A. Sharma, *DNA repair pathways as targets for cancer therapy.* Nat Rev Cancer, 2008. **8**(3): 193-204.

328. Bristow, R.G., *Introduction: DNA Repair and Radiotherapy Targeting: An Overview.* Seminars in Radiation Oncology, 2010. **20**(4): 215-216.

329. Bristow, R.G., H. Ozcelik, F. Jalali, N. Chan and D. Vesprini, *Homologous recombination and prostate cancer: A model for novel DNA repair targets and therapies.* Radiotherapy and Oncology, 2007. **83**(3): 220-230.

330. Thoms, J. and R.G. Bristow, *DNA Repair Targeting and Radiotherapy: A Focus on the Therapeutic Ratio.* Seminars in Radiation Oncology, 2010. **20**(4): 217-222.

331. Welcsh, P.L. and M.C. King, *BRCA1 and BRCA2 and the genetics of breast and ovarian cancer.* Human Molecular Genetics, 2001. **10**(7): 705-713.

332. Pellegata, N.S. and G.N. Ranzani, *The significance of p53 mutations in human cancers.* European Journal of Histochemistry, 1996. **40**(4): 273-282.

333. Hollstein, M., D. Sidransky, B. Vogelstein and C.C. Harris, *P53 Mutations in Human Cancers.* Science, 1991. **253**(5015): 49-53.

334. Reynolds, P., J.A. Anderson, J.V. Harper, M.A. Hill, S.W. Botchway, et al., *The dynamics of Ku70/80 and DNA-PKcs at DSBs induced by ionizing radiation is dependent on the complexity of damage.* Nucleic Acids Res, 2012. **40**(21): 10821-10831.

335. Nikjoo, H., S. Uehara, D. Emfietzoglou and F. Cucinotta, *Track-structure codes in radiation research.* Radiation Measurements, 2006. **41**(9): 1052-1074.

336. Meijer, A.E., A.R.M. Jernberg, T. Heiden, B. Stenerlöw, L.M. Persson, et al., *Dose and time dependent apoptotic response in a human melanoma cell line exposed to accelerated boron ions at four different LET.* International journal of radiation biology, 2005. **81**(4): 261-272.